Photobiomodulation and Stem Cell Differentiation: Application to Modulate Adipogenesis Through Cellular and Nuclear Morphology

by

Andrew Redmond McColloch

DISSERTATION

Submitted in partial fulfillment of the requirements

for the degree of Doctor of Philosophy at

The University of Texas at Arlington

May 2020

Arlington, Texas

Supervising Committee:

Michael Cho, Supervising Professor

Hanli Liu

Alan Bowling

Cheng-Jen Chuong

Mark Pellegrino

ABSTRACT

Photobiomodulation and Stem Cell Differentiation: Application to Modulate Adipogenesis Through Cellular and Nuclear Morphology

Andrew Redmond McColloch

The University of Texas at Arlington, 2020

Supervising Professor: Michael Cho

Mesenchymal stem cells (MSCs) are of great interest in regenerative medicine due to their capability to self-renew and differentiate to various lineages. Typically, differentiation to specific cell types has relied on the use of growth factors and other reagents to provide an environment conducive to the desired cell type. More recently, orthogonal cues other than chemical factors have been elucidated to regulate the lineage commitment. For example, the cell shape, cellular mechanics and substrate stiffness have been found to play a role in determining the fate of MSCs. However, it remains still elusive how the morphological and mechanical changes in the nucleus are involved in directing MSCs to the intended lineage. Using immunolabeling and computer-assisted image analysis, the first aim is designed to elucidate changes in the nucleus during differentiation to the fat-storing adipocytes.

Recent studies suggest that low level light exposure can serve as yet another non-biological factor that can modulate the MSC differentiation. Referred to as photobiomodulation (PBM), it describes the influence of light irradiation on biological tissues and has been shown to affect a variety of cells. Laser light in the near infrared spectrum (NIR, 780 – 2500 nm) in particular has been shown to directly affect heme-containing proteins, changing their level of activity. NIR light has been used in the medical field for analyses of cerebral blood flow. Recently, new evidence suggest light exposure can alter stem cell differentiation, potentially by interacting directly with the heme-containing protein of oxidative phosphorylation, cytochrome C. The second aim of the thesis is to apply NIR light exposure (1064 nm) to the cells undergoing adipogenic differentiation and determine the effect of PBM on differentiated adipocytes.

Obesity, often caused by enlarged hypertrophic adipocytes, carries a multitude of physiological risks including diabetes and heart disease. Interestingly, clinical trials of photobiomodulation on obese participants has shown significant weight loss, suggesting PBM may hinder lipid accumulation and regulate adipocyte maturation. However, such a hypothesis remains to be validated, and the potential mechanisms need be understood. In addition, to establish possible clinical efficacy, the effects of PBM must be quantitatively determined in an *in vitro* obesity model. The third aim is to characterize the model and apply NIR exposure (1064 nm) to examine a reduction in the lipid accumulation and conformational and functional restoration of hypertrophic adipocytes.

COPYRIGHT

ACKNOWLEDGEMENTS

I would like to thank the following people who made this work possible:

To Drs. Alfred and Janet Potvin for providing the funding for the research;

To my supervising professor, Dr. Michael Cho for his guidance and enthusiasm, as well as challenging me to think critically and to find solutions to tough problems;

To my collaborators, Drs. Alan Bowling and Hanli Liu as well as the members of their labs, Manoochehr Rabiei, Hashini Wanniarachchi, and Drs. Xinlong Wang and Anqi Wu, for their assistance and being available and understanding when I needed it;

To my committee members, Drs. Alan Bowling, Hanli Liu, Cheng-Jen Chuong, and Mark Pellegrino for their time and expertise;

And to my lab members, Edidiong Inyang, Caleb Liebman, and Dr. Bo Chen for their friendship, guidance, and willingness to brainstorm new ideas.

DEDICATION

I dedicate this work to all those who helped me along the way:

To my family, who gifted me with unwavering support and instilled in me a passion for science;

To Parisa, who without you this would not be possible, or at least completely different;

To my friends, who were always there to lean on through tough times;

To Missile, for being the best friend I could ask for;

And to SARS-CoV-2, for making this last semester memorable.

Table of Contents

Photobiomodulation and Stem Cell Differentiation: Application to Modulate Adipogenesis Through Cellular and Nuclear Morphology i

ABSTRACT ii

COPYRIGHT iv

ACKNOWLEDGEMENTS v

DEDICATION vi

TABLE OF FIGURES ix

CHAPTER 1: 1

GENERAL INTRODUCTION 1

References 8

CHAPTER 2: 11

Correlation between Nuclear Morphology and Adipogenic Differentiation: Application of a Combined Experimental and Computational Modeling Approach 11

Abstract 12

Introduction 13

Results 15

Discussion 28

Methods 33

References 42

CHAPTER 3: 48

Altered Adipogenesis of Human Mesenchymal Stem Cells by Photobiomodulation Using 1064 nm Laser Light 48

Abstract 49

Introduction 51

Materials and Methods 54

Results 59

Discussion 69

Conclusion 77

References 78

CHAPTER 4: 86

Photobiomodulation with NIR Laser Light Reduces Lipid Levels and Restores Glucose Transport Function of Hypertrophic Adipocytes in an *in vitro* Model of Obesity 86

Abstract 87
Introduction 88
Materials and Methods 90
Results 93
Discussion 101
References 108
CHAPTER 5: 112
GENERAL CONCLUSIONS 112
References 122

TABLE OF FIGURES

Figure 2. 1. Adipogenic differentiation over 15 days. MSCs underwent differentiation toward adipocytes in AD medium. Fluorescent markers observed are DAPI (blue) and LipidTOX (green). Images shown depict days 1 (A), 5 (B), 9 (C), and 15 (D). Scale bar = 50 µm (A through D). In addition, high magnification (90x) images of the nuclei and lipid droplets in hMSC during adipogenic differentiation acquired at 1 (E) and 7 (F) days. Scale bar = 10 µm (E and F). 16

Figure 2. 2. Python-generated images depicting masks for computer-assisted analysis of morphological and fluorescent data. (A) Original composite 3-color fluorescent microscope image- nuclei (blue), lipid (green), and LMNA (red). (B) Nuclei segmented and the size and shape determined after K-means clustering. Lipid droplets (C) and LNMA expression (D) segmented and separated from the original image. Images were taken from the same location after 9 days of differentiation using a 20X microscope objective. Scale bars = 50 µm 18

Figure 2. 3. Correlation between the nucleus size and lipid deposition. Nuclei area, as assessed by the DAPI fluorescence, decreased over time, and the lipid production increased exponentially. A reduction in the nucleus size was evident by day 5, while lipid increased most significantly after day 9. Data presented as mean ± SEM from 10 independent experiments averaging over 600 cells per each experiment. 20

Figure 2. 4. Comparison of adipogenic differentiation of hMSCs plated on glass (A, control), Jasplakinolide-treated (B) and seeded on micro-contact printed surface (C). Cells treated with the actin polymerizing agent demonstrated significantly larger nuclear area vs. control (D). Cells attached to the patterned substrates showed similar nuclear area, but with an increased aspect ratio (E). Nuclei in blue color and lipid expression in green color. Data represent mean ± SEM of 3 independent experiments. Scale bars = 50 µm. In addition, (F) and (G) show high magnification (90x) images of treated cells with jasplakinolide at day 1 and 7 of differentiation, respectively. In the jasplakinolide-treated cells, the size of nuclei was larger with a much diminished lipid accumulation. Scale bars = 10 µm. 22

Figure 2. 5. LMNA expression and distribution. (A) Fluorescent images of LMNA at different days of adipogenic differentiation. Images recorded using a 60X magnification objective. Scale bar = 5 µm. (B) The LMNA expression increases early during differentiation, while nuclear morphology (roundness) is reduced. (C) Relative fold change of adipocyte maturation gene PPARγ and nuclear envelope gene LMNA. Data represent mean ± SEM of 3 independent experiments. 24

Figure 2. 6. (A) Schematic of nucleus with actin filaments, membrane, cytoplasm, and nuclear components. (B) Frame stills from modeling simulation of nuclear shape during differentiation. The initial number of actin springs represented by the red lines is assumed to be 16. The cytoskeletal tension is released during maturation, allowing elastic LMNA to conform to a more compact shape. Interior beads represent repositioning of the nuclear components while extended red lines represent actin filaments dissociating from the nucleus over time. Axes indicate nuclear dimension in μm. 26

Figure 2. 7. (A) Model-generated results of nuclear size demonstrating consistency with experimental data (blue curve with error bars) over 5 separate simulations. (B) Mathematical calculation of changes in the nuclear membrane tension (nN) as actin filaments reorganize and disappear. Results from 5 separate simulations are shown. Simulations are a result of increasing n from Equation 1. It was found that n = 4 (shown in yellow) most closely followed experimental data. 27

Figure 3. 1. Average temperature rise of adipogenic differentiation media in 35 mm petri dish during exposure to 1064 nm laser at varying laser powers. Temperature was recorded at one minute intervals using an Omega HH42A thermistor. Data represent mean ± SEM of 3 independent experiments. Since the laser beam size was fixed at 13.6 cm2, the 1 W exposure corresponds to 0.074 W/cm2. The red line indicates a threshold temperature increase of 1° C. 59

Figure 3. 2. Multi-channel fluorescence image demonstrating lipid production (green) and nuclear size (blue). Image were recorded after 9 days of differentiation using a 40x microscope objective. (A) Fluorescence intensity of lipid detection dye LipidTOX Green at increasing fluence of 1064 nm PBM for 2 min/day after 7 days of adipogenic differentiation. (B) Data presented as mean ± SEM, n=5. Bar = 25 μm. * indicates $p < 0.05$, ** $p > 0.05$. 61

Figure 3. 3. Example images of change in nuclear shape from MSCs unexposed to adipogenic induction medium or laser irradiation (A), seven days after adipogenic induction (B), and 26.4 J/cm2 laser exposure 2 min/day after 7 days of differentiation (C). Average nuclei area of control and laser-irradiated groups with increasing fluence. Samples taken after 7 days of adipogenic differentiation (D). Scale bar = 15 μm. Data presented as mean ± SEM, n=3. * $p < 0.05$, ** $p > 0.05$. 62

Figure 3. 4. Comparison of lipid production determined by LipidTOX fluorescence intensity during adipogenic differentiation (A). Nuclear area in pixels of PBM and control groups (B). Laser-irradiated (PBM) group was exposed to a fluence of 17.6 J/cm2 2 min/day for 9 days. Data presented as mean ± SEM, n=3. 63

Figure 3. 5. Triglyceride fluorescence intensity determined by Triglyceride Assay Kit (Abcam) in stem cell conditioned media through 15 days of adipogenic differentiation. Fluence = 17.6 J/cm^2. Data presented as mean ± SEM, n=3. No statistically significant differences were observed. 64

Figure 3. 6. Relative expression of RNA production of adipogenic and ROS-sequestering genes. PBM group exposed to a fluence of 17.6J/cm2 2 min/day for 10 days. Normalized to GAPDH, data presented as mean ± SEM, n=3. 65

Figure 3. 7. ATP quantification of MSCs determined by luciferase luminescence via CellTiter-Glo Assay (Promega). Cells irradiated for 2 minutes, incubated for 15 minutes, and then ATP was quantified using a plate reader. Data presented as mean ± SEM, n=5. * $p < 0.05$, ** $p > 0.05$ 66

Figure 3. 8. MitoSOX staining of MSCs during adipogenic differentiation taken at different days. During days 1, 5, and 9 without exposure MitoSOX staining begins lower, but increases as differentiation continues (A-C). Cells exposed to laser irradiation at a fluence of 17.6 J/cm2 2 min/day every day show an overall lower amount of mitochondrial superoxide formation as differentiation proceeds (D-F). Scale bar = 50 µm. Quantification of MitoSOX fluorescence over differentiation shown in (G). Data presented as mean ± SEM, n=3. * $p < 0.05$, ** $p > 0.05$. 67

Figure 3. 9. Comparison of lipid production determined by LipidTOX fluorescence intensity over 9 days of differentiation. hMSCs were exposed to 2 mM of the known catalase inhibitor 3-AT added in ADM media. Control group (no PBM) was also treated with the inhibitor, while the laser-irradiated (PBM) group was exposed to a fluence of 17.6 J/cm2 2 min/day every day. Data presented as mean ± SEM, n=3. No statistically significant difference was observed. 69

Figure 4. 1. Adipose-derived stem cells 15 days after being induced toward adipocytes. ADSCs challenged with 500 µM Palmitic Acid displayed greater lipid quantity and larger droplets (B) compared to control (A). Images taken at 20X. Scale bar = 50 µm. 93

Figure 4. 2. Lipid content of ADSCs undergoing adipogenic differentiation under normal (ADM) and hypertrophic (PA) conditions. ADSCs exposed to palmitic acid demonstrated significantly greater amounts of lipid during later differentiation stages. Mean ± SEM, n=3. 94

Figure 4. 3. Fluorescent quantification of glucose analog 2-NBDG corresponding to levels of glucose differentiation ADSCs uptake. Glucose uptake increases during differentiation for both normal and hypertrophic groups. However, ADSCs exposed to palmitic acid demonstrate lower glucose uptake at all points over differentiation. Mean ± SEM, n=3. 95

Figure 4. 4. Fluorescent quantification of the major adipocyte glucose transporter GLUT4. Normal differentiation shows an increase in GLUT4 expression, while cells induced to hypertrophy show a decreasing trend. Mean ± SEM, n=3. 96

Figure 4. 5. Adipose-derived stem cells 15 days after being induced toward adipocytes (A). ADSCs induced to hypertrophy using 500 µM Palmitic Acid (B). ADSCs induced to hypertrophy and exposed to 17.6 J/cm^2 PBM for 7 days (C). Images taken at 40X. Scale bar = 25 µm. 98

Figure 4. 6. Lipid content of ADSCs undergoing adipogenic differentiation. Hypertrophic ADSCs (PA) display significantly greater amounts of lipid compared to normal (ADM) and laser irradiated (PA-PBM) groups. Hypertrophic cells exposed to laser (PA-PBM) produced slightly more lipid than ADM, and significantly less than PA. Mean ± SEM, n=3. 99

Figure 4. 7. 2-NBDG fluorescence comparing glucose uptake at baseline (BL) through to end-stage (D15) adipogenic differentiation. Application of PBM shows an overall trend similar to hypertrophic cells. At the final day, glucose fluorescence in PA PBM was significantly greater than PA, although still less than that of normal differentiation. Mean ± SEM, n=3. 100

Figure 4. 8. Fluorescence quantification of GLUT4 levels in ADSCs undergoing adipogenic differentiation. Normal adipogenesis (ADM) show an increase in GLUT4 levels over time, while cells induced to hypertrophy (PA) show a decrease in protein expression. Hypertrophic cells exposed to laser irradiation (PA PBM) show an initial decrease, followed by an increase and return to baseline values. Mean ± SEM, n=3. 101

CHAPTER 1:
GENERAL INTRODUCTION

Stem cells are cells with the capacity to differentiate to multiple cell types and are of great interest to cellular and tissue engineering due to their abundant supply of lineage-specific cell types[1]. Stem cells exist in a hierarchy, known as potency, of number of potential lineages they are able to become. Potency of stem cells exist in the range: totipotent, pluripotent, multipotent, and unipotent[2]. A totipotent stem cell can be induced to any other cell type (e.g. a zygote in early embryonic development), while a unipotent cell can only become one terminally differentiated cell (e.g. myogenic progenitor to skeletal muscle). Typically, stem cells in adult tissues are multipotent: able to differentiate to several, but not all, cell types.

Adult stem cells have historically been differentiated through addition of chemical induction factors. These reagents have been well established to reliably produce the desired cell type at maximum efficiency[3]. More recently however, researchers have elucidated the cellular response to physical cues as a method of reliable lineage-specific differentiation. Physical cues that mimic the host environment generate cells of that type. For example, stem cells grown on hard substrates more reliably differentiate toward osteocytes, while those on soft surfaces are induced to adipocytes[4,5]. The characteristics of the physical environment, as well as chemical, is imperative to the differentiation success of stem cells.

However, while several groups have examined the physical environment and its effect on the cytoskeletal network, few have investigated the morphological characteristics of the nucleus. During differentiation, cells transform to a unique cell type. This requires massive re-working of the cell's internal protein structure, which starts with activation of new transcription of DNA. The nucleus is also the largest and stiffest organelle in the cell, whose bulk mechanical properties contribute considerably to the overall cell shape[6]. Additionally, the cytoskeleton interacts directly with the nucleus through a series of linker proteins that have been shown to mediate inter-nuclear movement[7].

Recently, work has been done investigating alternative physical methods to induce differentiation. These methods directly or indirectly alter a variety of cellular processes, which in turn change the face of genetic communication. One such novel method is the use of light irradiation. Photobiomodulation (PBM), also known as low-level light therapy (LLLT), describes the influence of light on biological tissues[8]. Typically, PBM utilizes the near-infrared spectrum (NIR) existing between wavelengths 780 – 2500 nm, due to the absorbance of heme-containing molecules such as hemoglobin or cytochrome c oxidase in this wavelength range[9]. The use of 1064 nm laser light is of significant interest to us because as of yet this wavelength has not been prominently investigated in the application of stem cell differentiation and adipogenesis.

Most researchers describe the mechanism of PBM as acting primarily at the site of the mitochondria. Cytochrome c oxidase (CCO), a copper- and heme- containing protein at the final stage of the electron transport chain, acts as a photon acceptor from NIR light.

CCO has various absorption peaks in the NIR region, and researchers have utilized many to investigate potential wavelength-dependent phenomena[10-12]. Once CCO accepts a photon, the inhibitory molecule nitrous oxide (NO) is dissociated leading to enhanced flux through the electron transport chain (ETC)[8]. Increased levels of ETC activity result in several downstream effects including transient reactive oxygen species (ROS) production, elevated levels of ATP, as well as the anti-inflammatory actions of free NO. Mitochondrial superoxide ROS is a highly charged molecule which can generate DNA damage and influence cell survival[13]. Because of this, the cell retains several mitigation processes to limit the degree of ROS influence in cellular activity[14]. ROS is naturally produced with enhanced ETC flux as electrons “leak” from the system[15]. This transient superoxide increase is followed by an activation of ROS-sequestering events, including transcriptional activation of ROS-eliminating enzymes.

For stem cell differentiation, energy dynamics and ROS levels are important factors in lineage specificity. As stem cells differentiate, they shift from primarily glycolysis to oxidative phosphorylation for energy production[16]. High levels of ROS have been demonstrated to direct stem cells away from osteocytes and towards an adipocyte lineage[17]. Osteo- and adipo-genic lineage differentiation exist as opposites to each other, requiring inverse factors and transcriptional regulation[18]. Several groups have shown the influence of PBM on osteogenic differentiation, demonstrating an increase in calcium production in the irradiated groups[11,12]. However, the potential effects of light irradiation on stem cells undergoing adipogenic differentiation have yet to be fully elucidated. With

PBM having been shown to enhance osteogenesis, it is therefore reasonable to presume the opposite will be true for adipogenesis.

Adipose cells are the main component of fat tissue in the body. Fat tissue can be separated into two main categories: white fat and brown fat. White fat is the main energy storage in the body and is the site of many complications due to obesity[19]. Obesity and metabolic disease have situated themselves as one of the largest public health concerns, with complications arising from diabetes, cancer, and heart disease[20]. A regimen of regular exercise and a healthy diet exists as a proven treatment for obesity, however individuals continue to seek out other methods for fat reduction. Surgical methods such as liposuction and gastric band are expensive, invasive procedures requiring days to weeks of recovery and potential for complications. Because of this, researchers have developed safe and effective methods of non-invasive fat removal. Laser therapy has itself been utilized as a method for body contouring and spot fat reduction, offering promising reductions in spot fat reduction of the waist, arms, and hips[21]. However, this overview fails to understand the mechanism behind the fat reduction and whether the complications of obesity are mitigated. However, the mechanisms behind the fat reduction remain elusive.

Inherent in obesity is a dysfunction in adipocyte physiology, categorized as cell number increase (hyperplasia) and cell size increase (hypertrophy)[22]. As lipid levels increase, adipocytes swell to contain the material. Several downstream effects of obesity (insulin resistance, inflammation, etc.) can be ascribed to the dysfunctional size and operations

of hypertrophic adipocytes[23]. Enlarged, dysregulated adipocytes promote inflammatory cytokines, release damaging free fatty acids, and increase levels of intracellular ROS[24]. Additionally, hypertrophic adipocytes have been shown to promote hypoxia and can lead to a reduction in insulin sensitivity, the main progression toward diabetes[25].

Photobiomodulation, as described here, may be a benefit to hypertrophic adipocytes by reducing lipid content and inflammation. As described before, PBM can help reduce overall lipid content, potentially leading to a reduction in adipocyte hypertrophy. PBM has also been used to enhance healing in models of diabetic-related wounds[26]. However, little research has been performed on the adipocytes themselves. Mechanistically, the influence of NIR PBM on stem cells differentiating toward adipocytes, as well as on a hypertrophic obesity model, has yet to be elucidated. Additionally, how this novel physical factor impacts, either directly or indirectly, the physiology of the stem cell nucleus is of specific interest.

To this end, a research strategy has been developed to modulate stem cell differentiation through novel physical methods and investigate the influence of these methods on nuclear mechanics and lipid physiology. To determine these processes, three aims was developed and experiments were designed. Among these aims were individual sub-aims developed to focus the research and complete all stated goals.

Aim 1: To quantify the Alterations in Nuclear Morphology of MSCs during Adipogenic Differentiation

- **1(A):** To chemically induce MSCs toward the adipocyte lineage, track their maturation using fluorescent microscopy, and generate an automated algorithm to process fluorescent nuclei images and provide quantitative analyses of nuclear morphology over time
- **1(B):** To determine the interplay of nuclear lamina protein lamin a/c and cytoskeletal actin organization on nuclear shape
- **1(C):** To validate a simulation model of nuclear remodeling that can reproduce and predict the observed changes during adipogenic differentiation

Aim 2: To determine the Influence of 1064nm NIR Laser Light on MSC Differentiation, as well as its Effect on Nuclear Morphology and Production of ATP and ROS

- **2(A):** To characterize the effect of 1064 nm photobiomodulation on stem cell differentiation to adipocytes
- **2(B):** To determine the influence of ROS and ATP generation from PBM on stem cell differentiation
- **2(C):** To examine PBM effect on nuclear reorganization during differentiation

Aim 3: To utilize NIR Laser Light to Restore Form and Function of Hypertrophic Adipocytes in an *in vitro* Obesity Model

- **3(A):** To generate and characterize and *in vitro* obesity model using stem cells differentiated to adipocytes and induced to hypertrophy
- **3(B):** To quantify the effect of NIR irradiation on lipid levels and droplet size of hypertrophic adipocytes

- **3(C):** To determine the potential restorative function of NIR light through conformational (cell/nuclear shape) and functional (protein levels/cell metabolism) states

References

1. Minguell, J. J., A. Erices, and P. Conget. 2001. "Mesenchymal stem cells." *Experimental biology and medicine (Maywood, N.J.)* 226: 507–20. doi:10.1177/153537020122600603.

2. Singh, Vimal K., Abhishek Saini, Manisha Kalsan, Neeraj Kumar, and Ramesh Chandra. 2016. "Describing the Stem Cell Potency: The Various Methods of Functional Assessment and In silico Diagnostics." *Frontiers in Cell and Developmental Biology* 4: 134. doi:10.3389/fcell.2016.00134.

3. Chamberlain, Giselle, James Fox, Brian Ashton, and Jim Middleton. 2007. "Concise Review: Mesenchymal Stem Cells: Their Phenotype, Differentiation Capacity, Immunological Features, and Potential for Homing." *Stem Cells* 25: 2739–2749. doi:10.1634/stemcells.2007-0197.

4. Engler, Adam J., Shamik Sen, H. Lee Sweeney, and Dennis E. Discher. 2006. "Matrix Elasticity Directs Stem Cell Lineage Specification." *Cell* 126: 677–689. doi:10.1016/j.cell.2006.06.044.

5. Zhao, Wen, Xiaowei Li, Xiaoyan Liu, Ning Zhang, and Xuejun Wen. 2014. "Effects of substrate stiffness on adipogenic and osteogenic differentiation of human mesenchymal stem cells." *Materials science & engineering. C, Materials for biological applications* 40: 316–23. doi:10.1016/j.msec.2014.03.048.

6. Caille, Nathalie, Olivier Thoumine, Yanik Tardy, and Jean-Jacques Meister. 2002. "Contribution of the nucleus to the mechanical properties of endothelial cells." *Journal of biomechanics* 35: 177–87.

7. Lee, Yin Loon, and Brian Burke. 2017. "LINC complexes and nuclear positioning." *Seminars in Cell & Developmental Biology* 82: 67–76. doi:10.1016/j.semcdb.2017.11.008.

8. Freitas, Lucas Freitas de, and Michael R. Hamblin. 2016. "Proposed Mechanisms of Photobiomodulation or Low-Level Light Therapy." *IEEE journal of selected topics in quantum electronics : a publication of the IEEE Lasers and Electro-optics Society* 22: 348–364. doi:10.1109/jstqe.2016.2561201.

9. Karu, Tiina I. 2014. "Cellular and Molecular Mechanisms of Photobiomodulation (Low-Power Laser Therapy)." *IEEE Journal of Selected Topics in Quantum Electronics* 20: 143–148. doi:10.1109/jstqe.2013.2273411.

10. Wang, Yuguang, Ying-Ying Huang, Yong Wang, Peijun Lyu, and Michael R. Hamblin. 2016. "Photobiomodulation (blue and green light) encourages osteoblastic-differentiation of human adipose-derived stem cells: role of intracellular calcium and light-gated ion channels." *Scientific reports* 6: 33719. doi:10.1038/srep33719.

11. Wang, Yuguang, Ying-Ying Huang, Yong Wang, Peijun Lyu, and Michael R. Hamblin. 2016. "Photobiomodulation of human adipose-derived stem cells using 810nm and 980nm lasers operates via different mechanisms of action." *Biochimica et biophysica acta* 1861: 441–449. doi:10.1016/j.bbagen.2016.10.008.

12. Tani, Alessia, Flaminia Chellini, Marco Giannelli, Daniele Nosi, Sandra Zecchi-Orlandini, and Chiara Sassoli. 2018. "Red (635 nm), Near-Infrared (808 nm) and Violet-Blue (405 nm) Photobiomodulation Potentiality on Human Osteoblasts and Mesenchymal Stromal Cells: A Morphological and Molecular In Vitro Study." *International Journal of Molecular Sciences* 19: 1946. doi:10.3390/ijms19071946.

13. Brieger, Katharine, Stefania Schiavone, Francis J. Miller Jr., and Karl-Heinz Krause. 2012. "Reactive oxygen species: from health to disease." *Swiss Medical Weekly* 142. doi:10.4414/smw.2012.13659.

14. Ighodaro, O. M., and O. A. Akinloye. 2018. "First line defence antioxidants-superoxide dismutase (SOD), catalase (CAT) and glutathione peroxidase (GPX): Their fundamental role in the entire antioxidant defence grid." *Alexandria Journal of Medicine* 54: 287–293. doi:10.1016/j.ajme.2017.09.001.

15. Selivanov, Vitaly A., Tatyana V. Votyakova, Violetta N. Pivtoraiko, Jennifer Zeak, Tatiana Sukhomlin, Massimo Trucco, Josep Roca, and Marta Cascante. 2011. "Reactive oxygen species production by forward and reverse electron fluxes in the mitochondrial respiratory chain." *PLoS computational biology* 7: e1001115. doi:10.1371/journal.pcbi.1001115.

16. Chen, Chien-Tsun, Yu-Ru V. Shih, Tom K. Kuo, Oscar K. Lee, and Yau-Huei Wei. 2008. "Coordinated changes of mitochondrial biogenesis and antioxidant enzymes during osteogenic differentiation of human mesenchymal stem cells." *Stem cells (Dayton, Ohio)* 26: 960–8. doi:10.1634/stemcells.2007-0509.

17. Almeida, Maria, Li Han, Marta Martin-Millan, Charles A. O'Brien, and Stavros C. Manolagas. 2007. "Oxidative Stress Antagonizes Wnt Signaling in Osteoblast Precursors by Diverting β-Catenin from T Cell Factor- to Forkhead Box O-mediated Transcription." *Journal of Biological Chemistry* 282: 27298–27305. doi:10.1074/jbc.m702811200.

18. Lin, Chia-Hua, Nan-Ting Li, Hui-Shan Cheng, and Men-Luh Yen. 2017. "Oxidative stress induces imbalance of adipogenic/osteoblastic lineage commitment in mesenchymal stem cells through decreasing SIRT1 functions." *Journal of cellular and molecular medicine* 22: 786–796. doi:10.1111/jcmm.13356.

19. Cummins, Timothy D., Candice R. Holden, Brian E. Sansbury, Andrew A. Gibb, Jasmit Shah, Nagma Zafar, Yunan Tang, et al. 2014. "Metabolic remodeling of white adipose tissue in obesity." *American Journal of Physiology-Endocrinology and Metabolism* 307: E262–E277. doi:10.1152/ajpendo.00271.2013.

20. Kopelman, Peter G. 2000. "Obesity as a medical problem." *Nature* 404: 635–643. doi:10.1038/35007508.

21. Caruso-Davis, Mary K., Thomas S. Guillot, Vinod K. Podichetty, Nazar Mashtalir, Nikhil V. Dhurandhar, Olga Dubuisson, Ying Yu, and Frank L. Greenway. 2011. "Efficacy of low-level laser therapy for body contouring and spot fat reduction." *Obesity surgery* 21: 722–9. doi:10.1007/s11695-010-0126-y.

22. Jo, Junghyo, Oksana Gavrilova, Stephanie Pack, William Jou, Shawn Mullen, Anne E. Sumner, Samuel W. Cushman, and Vipul Periwal. 2009. "Hypertrophy and/or Hyperplasia: Dynamics of Adipose Tissue Growth." *PLoS Computational Biology* 5: e1000324. doi:10.1371/journal.pcbi.1000324.

23. Muir, Lindsey A., Christopher K. Neeley, Kevin A. Meyer, Nicki A. Baker, Alice M. Brosius, Alexandra R. Washabaugh, Oliver A. Varban, et al. 2016. "Adipose tissue fibrosis, hypertrophy, and hyperplasia: Correlations with diabetes in human obesity." *Obesity* 24: 597–605. doi:10.1002/oby.21377.

24. Furukawa, Shigetada, Takuya Fujita, Michio Shimabukuro, Masanori Iwaki, Yukio Yamada, Yoshimitsu Nakajima, Osamu Nakayama, Makoto Makishima, Morihiro Matsuda, and Iichiro Shimomura. 2004. "Increased oxidative stress in obesity and its impact on metabolic syndrome." *Journal of Clinical Investigation* 114: 1752–1761. doi:10.1172/jci21625.

25. Shoelson, Steven E., Laura Herrero, and Afia Naaz. 2007. "Obesity, Inflammation, and Insulin Resistance." *Gastroenterology* 132: 2169–2180. doi:10.1053/j.gastro.2007.03.059.

26. Ruh, Anelice Calixto, Lúcio Frigo, Marcos Fernando Xisto Braga Cavalcanti, Paulo Svidnicki, Viviane Nogaroto Vicari, Rodrigo Alvaro Brandão Lopes-Martins, Ernesto Cesar Pinto Leal Junior, et al. 2018. "Laser photobiomodulation in pressure ulcer healing of human diabetic patients: gene expression analysis of inflammatory biochemical markers." *Lasers in Medical Science* 33: 165–171. doi:10.1007/s10103-017-2384-6.

CHAPTER 2:

Correlation between Nuclear Morphology and Adipogenic Differentiation: Application of a Combined Experimental and Computational Modeling Approach

Andrew McColloch, Manoochehr Rabiei, Parisa Rabbani,

Alan Bowling, and Michael Cho

Material From:

McColloch, A., Rabiei, M., Rabbani, P. *et al* (2019).

Correlation between Nuclear Morphology and Adipogenic Differentiation: Application of a Combined Experimental and Computational Modeling Approach. *Sci Rep* **9,** 16381

https://doi.org/10.1038/s41598-019-52926-8.

Abstract

Stem cells undergo drastic morphological alterations during differentiation. While extensive studies have been performed to examine the cytoskeletal remodeling, there is a growing interest to determine the morphological, structural and functional changes of the nucleus. The current study is therefore aimed at quantifying the extent of remodeling of the nuclear morphology of human mesenchymal stem cells during biochemically-induced adipogenic differentiation. Results show the size of nuclei decreased exponentially over time as the lipid accumulation is up-regulated. Increases in the lipid accumulation appear to lag the nuclear reorganization, suggesting the nuclear deformation is a prerequisite to adipocyte maturation. Furthermore, the lamin A/C expression was increased and redistributed to the nuclear periphery along with a subsequent increase in the nuclear aspect ratio. To further assess the role of the nucleus, a nuclear morphology with a high aspect ratio was achieved using microcontact-printed substrate. The cells with an elongated nuclear shape did not efficiently undergo adipogenesis, suggesting the cellular and nuclear processes associated with stem cell differentiation at the early stage of adipogenesis cause a change in the nuclear morphology and cannot be abrogated by the morphological cues. In addition, a novel computational biomechanical model was generated to simulate the nuclear shape change during differentiation and predict the forces acting upon the nucleus. This effort led to the development of computational scaling approach to simulate the experimentally observed adipogenic processes over 15 days in less than 1.5 hours.

Introduction

Adult mesenchymal stem cells (MSCs) are of great interest in tissue engineering and in clinical applications due to their capability to differentiate into multiple lineages including bone, adipose, and cartilage.[1] This differentiation potential is unique in stem cells and highly sought after as a method of regenerating the damaged or lost tissue. Typically, MSC differentiation is induced by the lineage-specific chemical stimuli, with the ratio of growth factors optimized for the desired tissue.[2] In addition, multiple laboratories have investigated the influence of cellular morphology and substrate mechanical properties on MSC differentiation.[3-6]

While important strides have been made in elucidating the influence of the cytoskeletal mechanical properties on MSC differentiation, few have examined the effects of the nucleus. The nucleus is the stiffest organelle in the cell and is also responsible for cell mechanics.[7] Additionally, the nucleus houses the cell's genetic code in the form of mobile chromatin structures, which shift as cell morphology changes. For example, it has been previously shown that DNA is wound into chromatin territories, with specific areas corresponding to specific genes.[8-10] The localization of genes within the nucleus is not random and have been demonstrated to be related to gene activation,[11,12] suggesting the reorganization of the nucleus is a prerequisite to initiate the reprogramming to a different cell lineage.[13]

Nuclear mechanical characteristics can be classified as viscoelastic, with two main contributors: DNA wound into chromatin, and the nuclear envelope proteins lamin A and C (LMNA).[14] LMNA is the major structural protein in the nuclear envelope and is thought to be responsible for nuclear shape and chromosome positioning.[15] Defects in the LMNA gene have been associated with various human diseases known as laminopathies with

several symptoms including progeria, muscular dystrophy, and cardiomyopathy.[16] Several laminopathies primarily affect mesenchymal tissues, including mesenchymal stromal cells, and can result in enhanced cellular senescence and altered differentiation potential.[17,18]

Several strides have been made in revealing the effect of nuclear shape change and lamin reorganization during cellular differentiation, including the influence of lamin A/C. For example, Verstraeten et al. demonstrated the changes in the nuclear lamin network during adipogenesis of mouse 3T3-L1 pre-adipocytes.[19] LMNA was shown to move from internuclear structures to the nuclear rim as adipogenesis continued. Interestingly, it was discovered that the fraction of cells expressing lamin increased during differentiation, a phenomenon also seen in human embryonic stem cells where B-type lamins are dominant in an undifferentiated state with eventual lamin A/C activation occurring during differentiation.[20] Furthermore, a point mutation in LMNA resulting in a common laminopathy disorder (p. R482W) has been shown to inhibit adipogenesis by de-regulating anti-adipogenic gene enhancers through an epigenetic mechanism.[21] LMNA has additionally been shown to be influenced by the mechanical properties of the substrate, with soft matrices reducing overall lamin levels.[22] Together, these bring a focus to the role of LMNA in adipogenic differentiation and its influence on controlling the underlying chromatin structure.

Potentially, repositioning of the chromatin structure necessary for lineage specificity of stem cells occurs via LMNA reorganization during stem cell differentiation, resulting in specific gene activation for lineage-directed differentiation. It is reasonable to postulate that DNA could be morphologically manipulated for such genetic activation. This

morphology change, therefore, would be driven by LMNA and result in nuclear shape change. In this paper we monitored and quantified several morphological features of human MSC nuclei over time along with the expression of LMNA and correlated them with adipogenic differentiation markers. We also constructed a 2D numerical simulation model to elucidate the mechanical coupling of F-actins to the nucleus that appears to regulate changes in the shape and size of the nucleus. The high-speed simulation was made possible through a multiscale approach that significantly reduced the computational cost (< 1.5 hrs) while probing the nuclear membrane properties such as its stiffness. Experimental measurements of such nuclear biomechanics with certainty remain yet to be established.

Results

MSCs were seeded onto glass coverslips and induced to differentiate to adipocytes using previously described factors contained in the Adipogenic Differentiation (AD) medium. The extent of adipogenic differentiation was monitored and imaged using LipidTOX staining to visualize the accumulated lipids. Stem cells undergoing adipogenic differentiation at day 1 showed essentially no detectable accumulation of lipids (Fig. 1A). Lipid accumulation became increasingly visible at day 5 (Fig. 1B) and at day 9 (Fig. 1C). By day 15, the stem cells incubated with the AD medium demonstrated a high level of LipidTOX staining (Fig. 1D). The nuclei were also stained and imaged using DAPI. It is interesting to note that there still is a fraction of cells that showed no lipid accumulation even at day 15. To better visualize adipogenesis, images were acquired using a higher magnification microscope objective (90x) at day 1 (Fig. 1E) and day 7 (Fig. 1F). A few interesting observations should be noted. First, the lipid droplets were shown to be non-uniform. Second, the varying size and shape of nuclei were visible at day 7. There

appears to be a correlation between the nuclear morphology and the level of lipid accumulation.

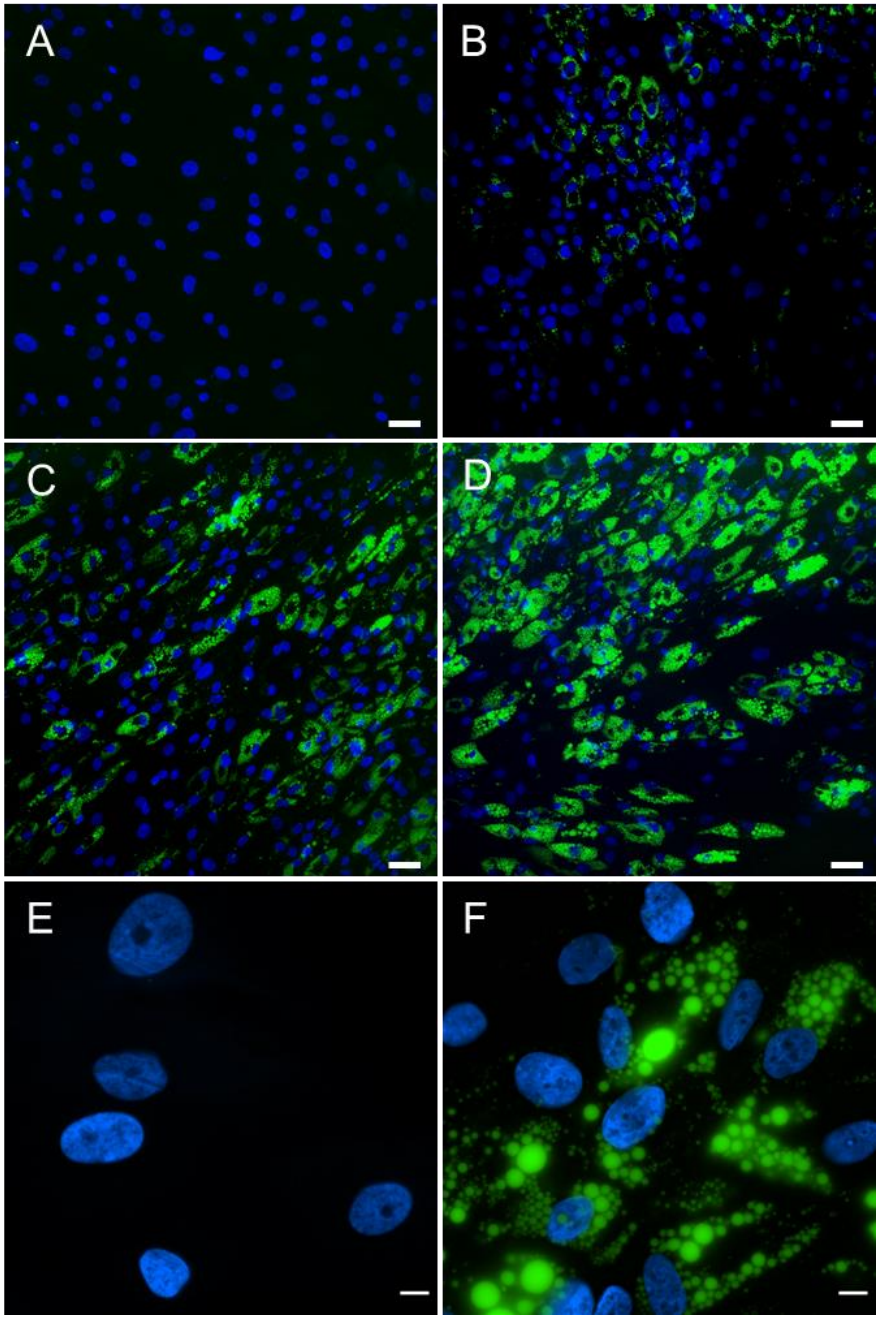

Figure 2. 1. *Adipogenic differentiation over 15 days. MSCs underwent differentiation toward adipocytes in AD medium. Fluorescent markers observed are DAPI (blue) and LipidTOX (green). Images shown depict days 1 (A), 5 (B), 9 (C), and 15 (D). Scale bar = 50 µm (A through D). In addition, high magnification (90x) images of the nuclei and lipid droplets in hMSC during adipogenic differentiation acquired at 1 (E) and 7 (F) days. Scale bar = 10 µm (E and F).*

To further examine and determine such a correlation between the nuclear morphology and the extent of adipogenesis, we developed a custom-built code to rapidly and accurately analyze a large number of stem cells undergoing adipogenesis. Following image acquisition, fluorescent images were processed using code written in Python for the nuclei morphology, lipid production, and lamin A/C (LMNA) intensity. To increase statistical significance, a 20x microscope objective was used to capture between 75 and 100 cells in a single field of view. For example, one set of images taken at day 9 was further processed and analyzed (Fig. 2). Nuclei were segmented via the unsupervised learning algorithm K-means clustering, a method commonly utilized for cell segmentation.[23] Three-color fluorescent images were first merged (Fig. 2A), and signal from DAPI staining and background were separated, clustered nuclei were delineated, and finally morphological characteristics were ascertained (Fig. 2B). Additionally, lipid accumulation via LipidTOX fluorescence and LMNA expression were also separated and analyzed by utilizing masks of the different fluorescent channels (Fig. 2C and 2D, respectively).

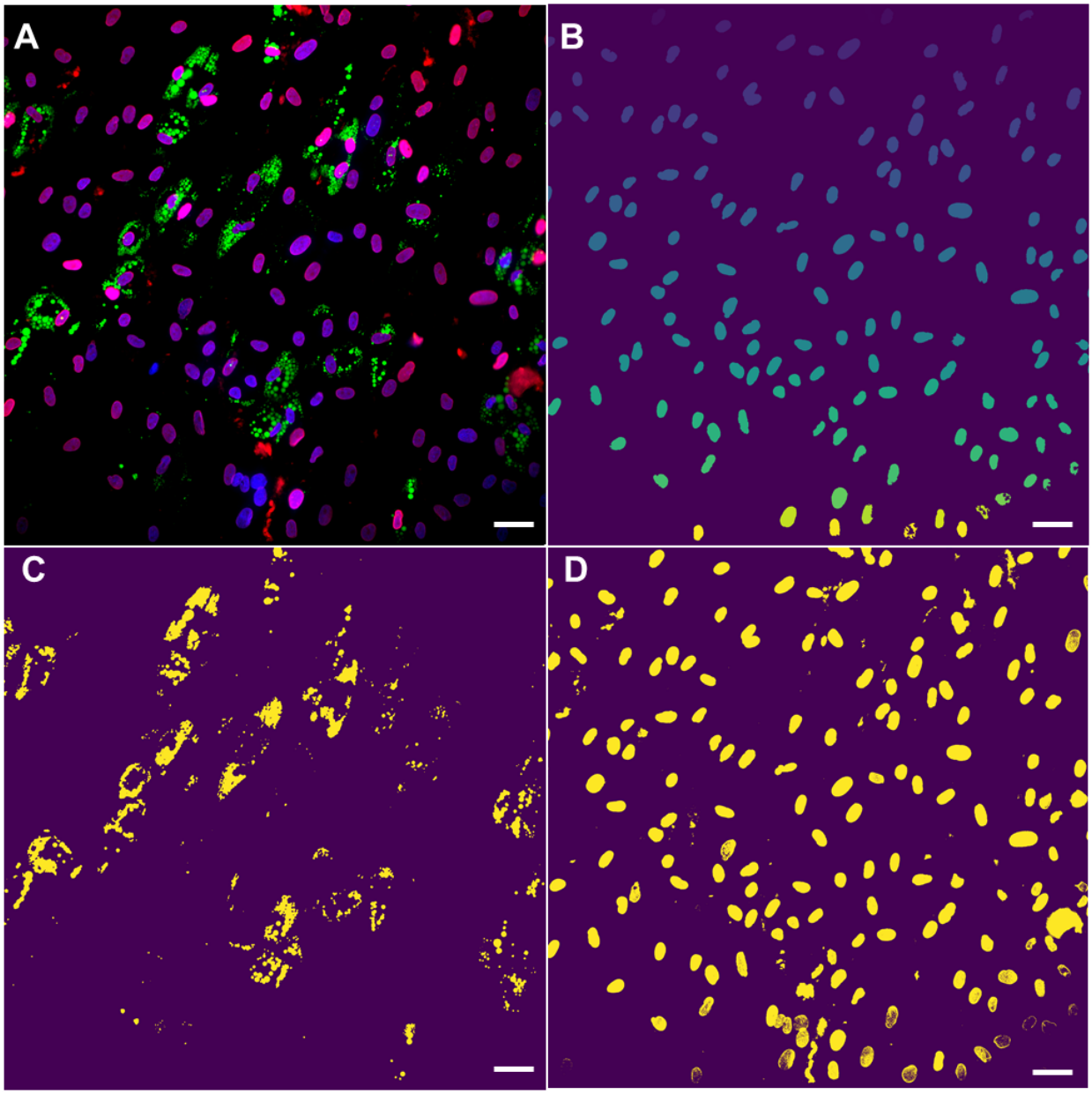

Figure 2. 2. *Python-generated images depicting masks for computer-assisted analysis of morphological and fluorescent data. (A) Original composite 3-color fluorescent microscope image- nuclei (blue), lipid (green), and LMNA (red). (B) Nuclei segmented and the size and shape determined after K-means clustering. Lipid droplets (C) and LNMA expression (D) segmented and separated from the original image. Images were taken from the same location after 9 days of differentiation using a 20X microscope objective. Scale bars = 50 µm*

The images processed by the custom-build code allowed for easy but more accurate quantification of the nuclear morphological parameters such as the nuclear size, aspect ratio and roundness. A significant decrease (~ 70%) in the nucleus size (pixels^2) was observed within the first 5 days of adipogenesis (Fig. 3). The subsequent and further

reduction in the nucleus size was not as pronounced in the next 10 days of adipogenesis. The accumulation of lipid droplets was monitored at the same time and fluorescently measured to assess the extent of adipogenesis. The buildup of lipid droplets over 15 days appeared to have increased exponentially. However, unlike the changes we observed in the nuclear size, the lipid production was substantially increased after 9 days of adipogenic differentiation and appeared to lag behind the remodeling of nuclei. More than 80% of lipid deposition occurred following the most significant decrease in the nuclear area at day 5. The implication here may be that the nuclear remodeling and morphological modulation precede adipogenesis and therefore could be a prerequisite for the intended differentiation.

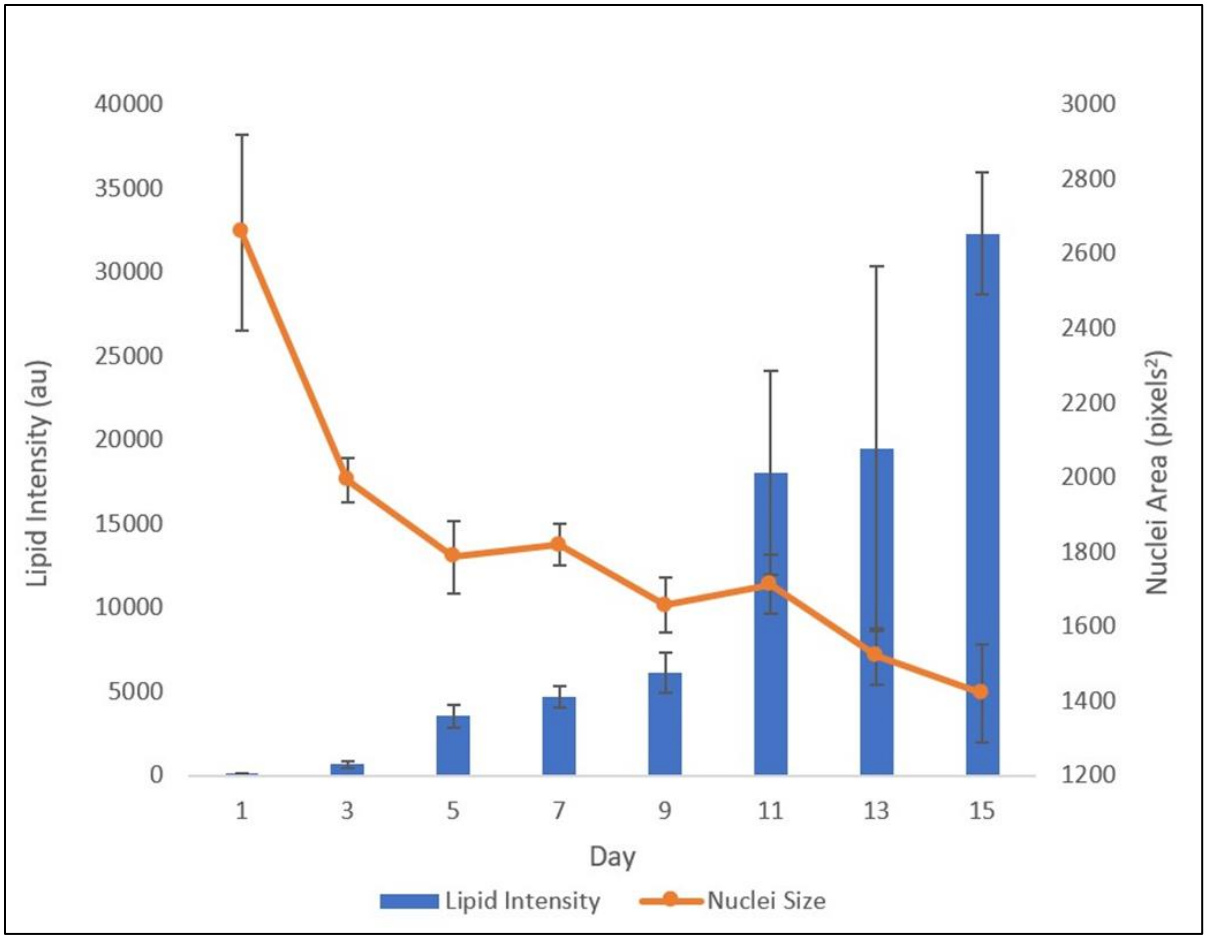

Figure 2. 3. *Correlation between the nucleus size and lipid deposition. Nuclei area, as assessed by the DAPI fluorescence, decreased over time, and the lipid production increased exponentially. A reduction in the nucleus size was evident by day 5, while lipid increased most significantly after day 9. Data presented as mean ± SEM from 10 independent experiments averaging over 600 cells per each experiment.*

Since changes in the nuclei are likely mediated by reorganization of the cytoskeleton,[24-26] two different methods were applied to influence the cytoskeleton and thereby alter the size and shape of the nucleus. First, the cells were treated with a pharmacological agent (jasplakinolde) to stabilize the actin structure that presumably resisted changes in the nucleus. Second, the cells were seeded onto a fibronectin-coated and microcontact-printed substrate to suppress adipogenesis. Fluorescent images at day 7 of adipogenesis show that both the jasplakinolde treatment and forced elongated cell seeding led to suppression or delay of the intended differentiation (Fig. 4A to 4C).

Quantitative analysis of the nuclear morphology following the two treatments revealed that adipogenesis can be hindered by either keeping the nuclear size artificially large (Fig. 4D; jasplakinolde treatment) or by increasing the nuclear aspect ratio (Fig. 4E; elongated cell seeding). To better visualize the effect of actin cytoskeleton, images were acquired using a 90x magnification objective following the jasplakinolde treatment (Fig. 4F at day 1 and Fig. 4G at day 7). The results are consistent that the artificially stabilized actin cytoskeleton hindered the intended differentiation. Moreover, to address potential impact of altered cell proliferation among treated and control groups, an MTT assay was performed. After seven days of differentiation, no significant differences were observed between groups (data available but not shown).

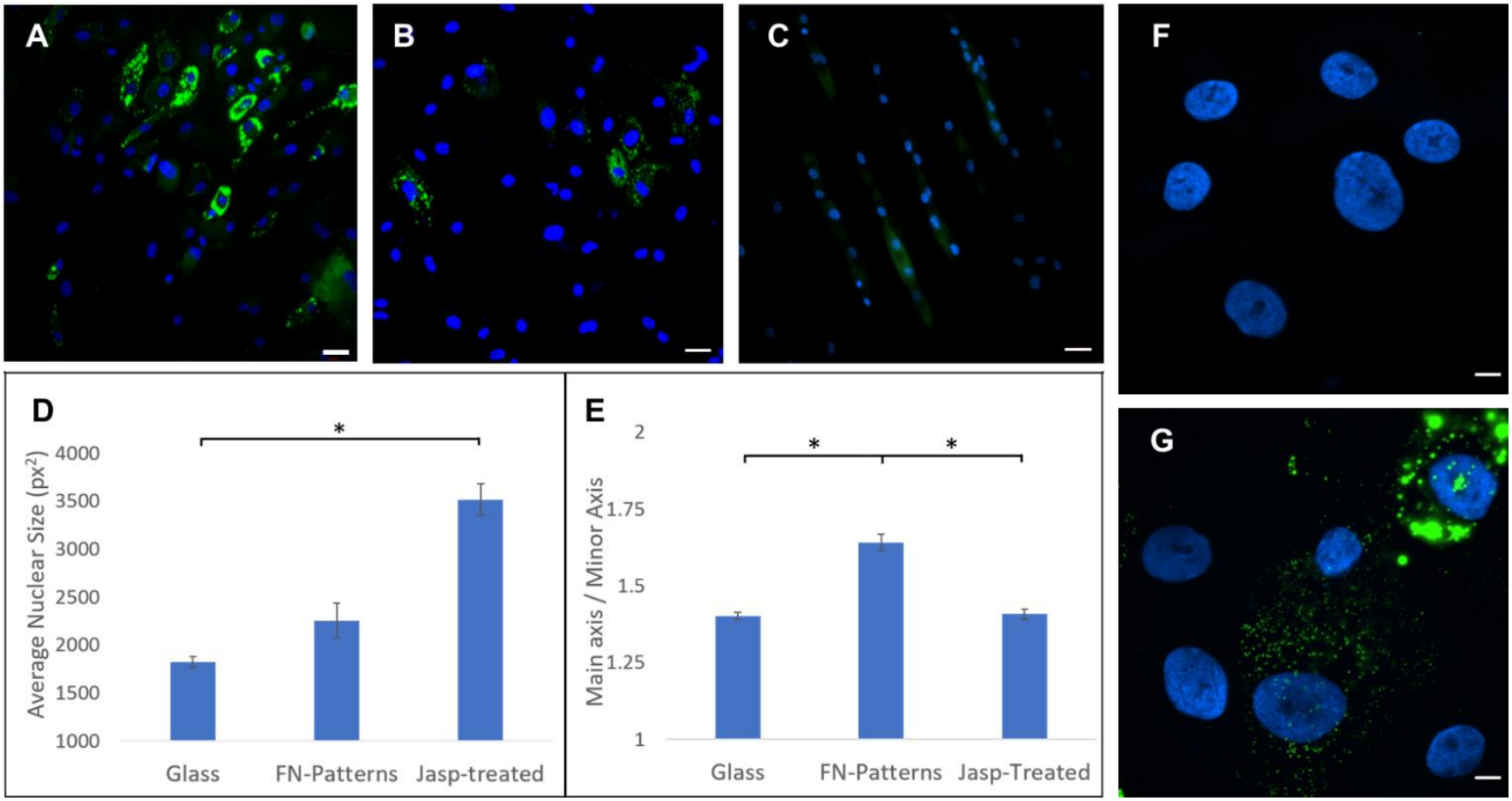

Figure 2. 4. *Comparison of adipogenic differentiation of hMSCs plated on glass (A, control), Jasplakinolide-treated (B) and seeded on micro-contact printed surface (C). Cells treated with the actin polymerizing agent demonstrated significantly larger nuclear area vs. control (D). Cells attached to the patterned substrates showed similar nuclear area, but with an increased aspect ratio (E). Nuclei in blue color and lipid expression in green color. Data represent mean ± SEM of 3 independent experiments. Scale bars = 50 µm. In addition, (F) and (G) show high magnification (90x) images of treated cells with jasplakinolide at day 1 and 7 of differentiation, respectively. In the jasplakinolide-treated cells, the size of nuclei was larger with a much diminished lipid accumulation. Scale bars = 10 µm.*

To further probe the influence of nuclear morphology on adipogenic differentiation, we monitored and quantified the intensity and distribution of a major nuclear envelope protein, LMNA. Using fluorescently conjugated antibody, the LMNA expression was shown to increase during differentiation as the nuclear remodeling occurred (Fig. 5A). The LMNA was observed to redistribute over time and became more prevalent along the periphery of the nuclei along with a reduction in punctate structures of the nuclear interior. As another measure of the nuclear morphology, the roundness was monitored and measured. The nuclear roundness, which is inverse of the aspect ratio, was linearly decreased over the 15 days of differentiation (Fig. 5B). Conversely, the LMNA fluorescence intensity sharply increased from day 3 to day 7 and then remained relatively unchanged. To probe the gene expression of LMNA during adipogenesis, total RNA was extracted at day 5 of differentiation, which corresponds to the day of the most significant decrease in nuclear area (see Fig. 3). The adipose gene peroxisome proliferator-activated receptor gamma (PPARγ) was used as a positive control due to its recognized upregulation (~ 35-fold) during adipogenesis[27]. Notably, LMNA mRNA production increased more than 4-fold compared to control (Fig. 5C). Taken together, the LMNA is up-regulated and also spatially redistributed to the nuclear membrane over time.

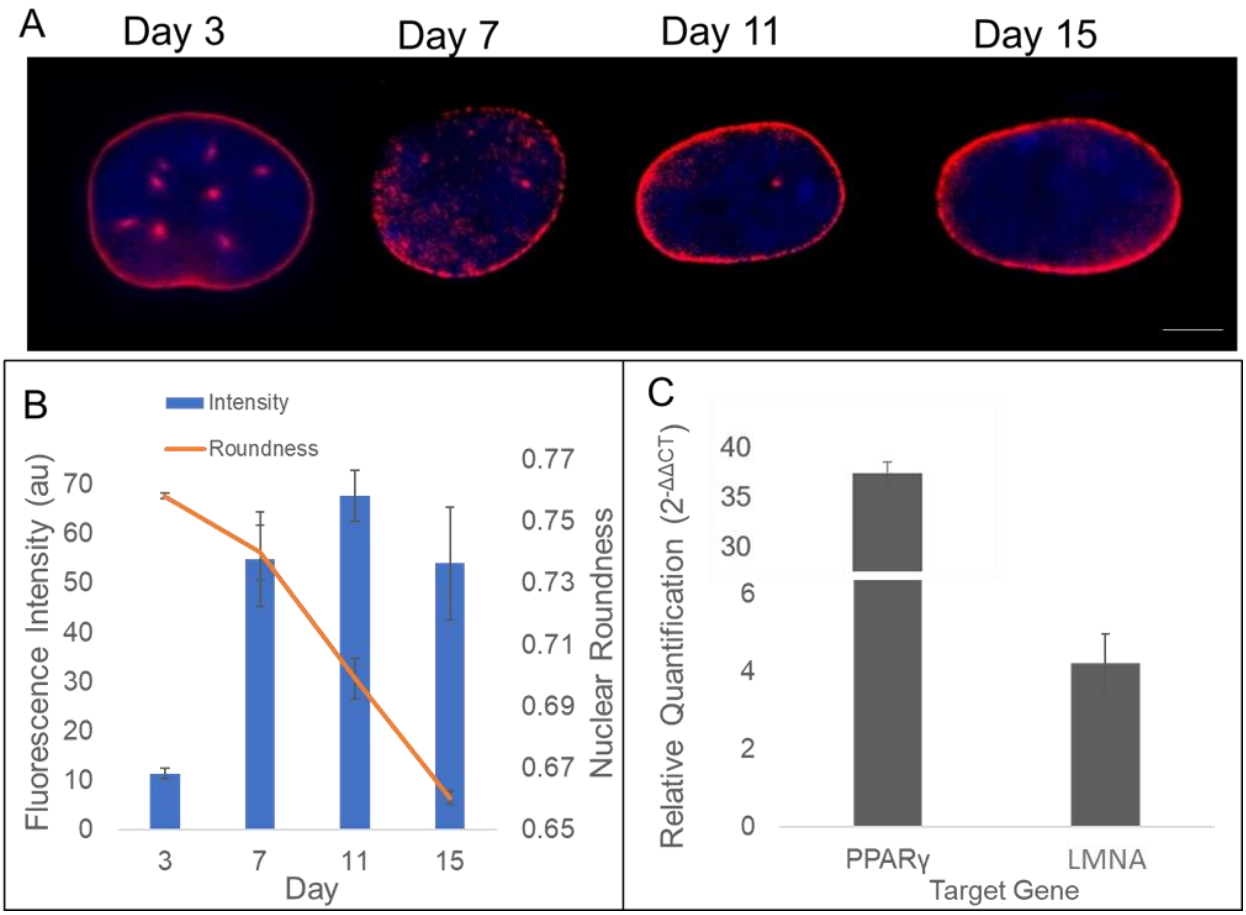

Figure 2. 5. *LMNA expression and distribution. (A) Fluorescent images of LMNA at different days of adipogenic differentiation. Images recorded using a 60X magnification objective. Scale bar = 5 µm. (B) The LMNA expression increases early during differentiation, while nuclear morphology (roundness) is reduced. (C) Relative fold change of adipocyte maturation gene PPARγ and nuclear envelope gene LMNA. Data represent mean ± SEM of 3 independent experiments.*

Numerical simulation was next utilized to further understand the dynamics of nuclear remodeling. Because experimental measurements of the nuclear biomechanics with certainty are lacking during adipogenesis, the results from numerical simulation can provide important and quantitative mechanical environment in the nucleus. For simplicity and to significantly reduce computational time, the nucleus is assumed to be filled with beads that represent the nuclear components such as chromosomes and other structures. To model the cytoskeletal forces and their change, the actin filaments are

attached to the nuclear membrane and allowed to dissociate from it over time (Fig. 6A). It is reasonable to assume that actin stress fibers keep the nucleus membrane under tension[28-30]. As differentiation proceeds and actins are rearranged, this tension is released, and therefore the nucleus undergoes morphological changes. After actin is depolymerized, the lipid droplets are formed that exert additional force on the nucleus. Several frame stills of the simulation were captured and shown to depict the actin tension over time as the actin tension was reduced while the lipid droplets accumulated (Fig. 6B). To validate the model, at least 5 simulations were carried out and the results were compared to the experimental data (Fig. 7A). The simulation model was able to faithfully reproduce the experimental data, demonstrating a good agreement. Using the model, the forces acting on the nucleus as a function of time may be simulated and predicted (Fig. 7B). For example, the initial nuclear membrane tension is found to be ~ 20 nN and decreases rapidly to zero as the actin cytoskeleton is reorganized during the first 7 days of differentiation. The membrane tension is then observed to rise to ~ 8 nN, because of the interaction between internal and external forces acting on the nuclear membrane. The

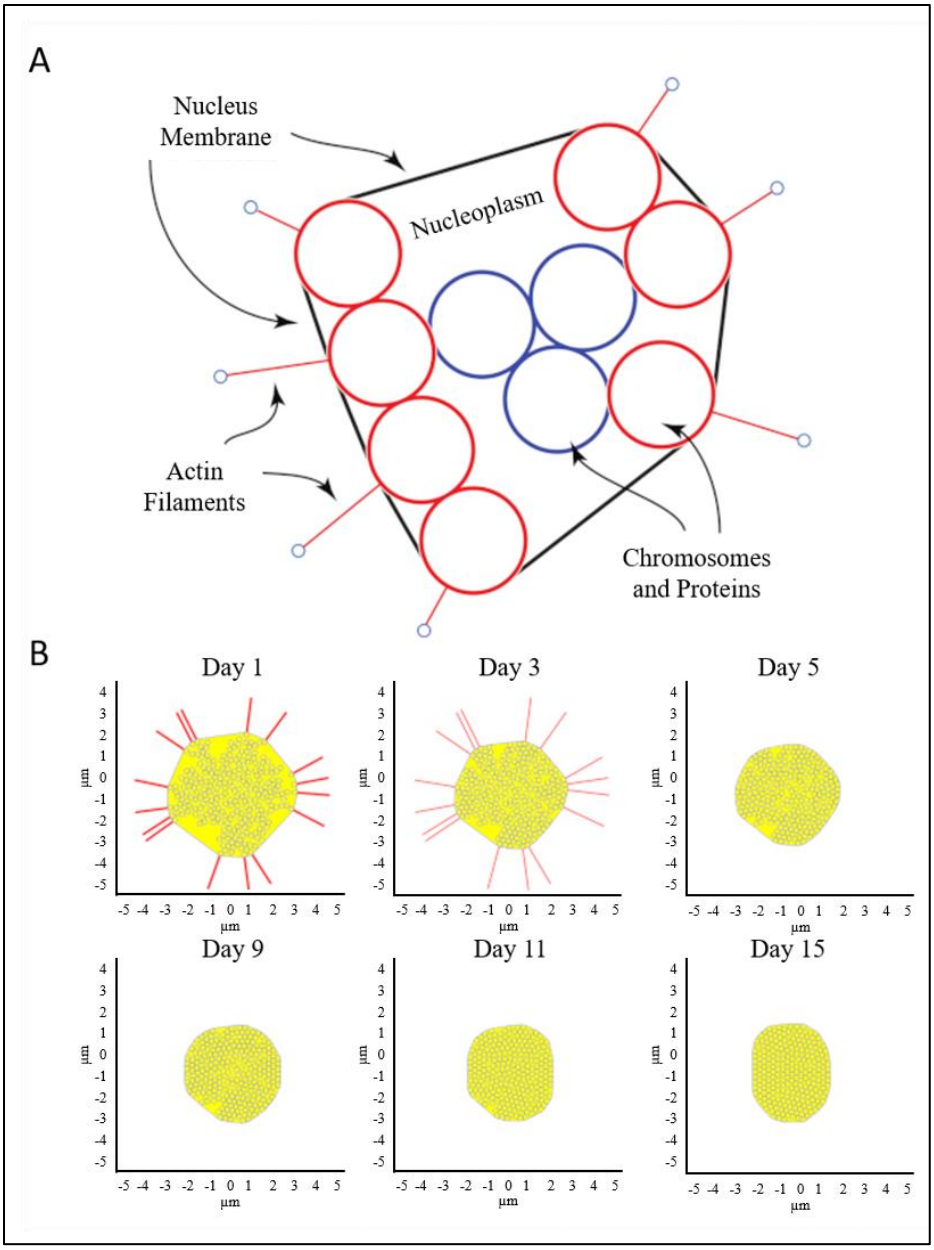

Figure 2. 6. *(A) Schematic of nucleus with actin filaments, membrane, cytoplasm, and nuclear components. (B) Frame stills from modeling simulation of nuclear shape during differentiation. The initial number of actin springs represented by the red lines is assumed to be 16. The cytoskeletal tension is released during maturation, allowing elastic LMNA to conform to a more compact shape. Interior beads represent repositioning of the nuclear components while extended red lines represent actin filaments dissociating from the nucleus over time. Axes indicate nuclear dimension in µm.*

external forces are caused by lipid accumulation, which squeeze the nucleus causing contraction. The internal forces are caused by resistance to compaction by the protein and chromosome structures within the nucleus.

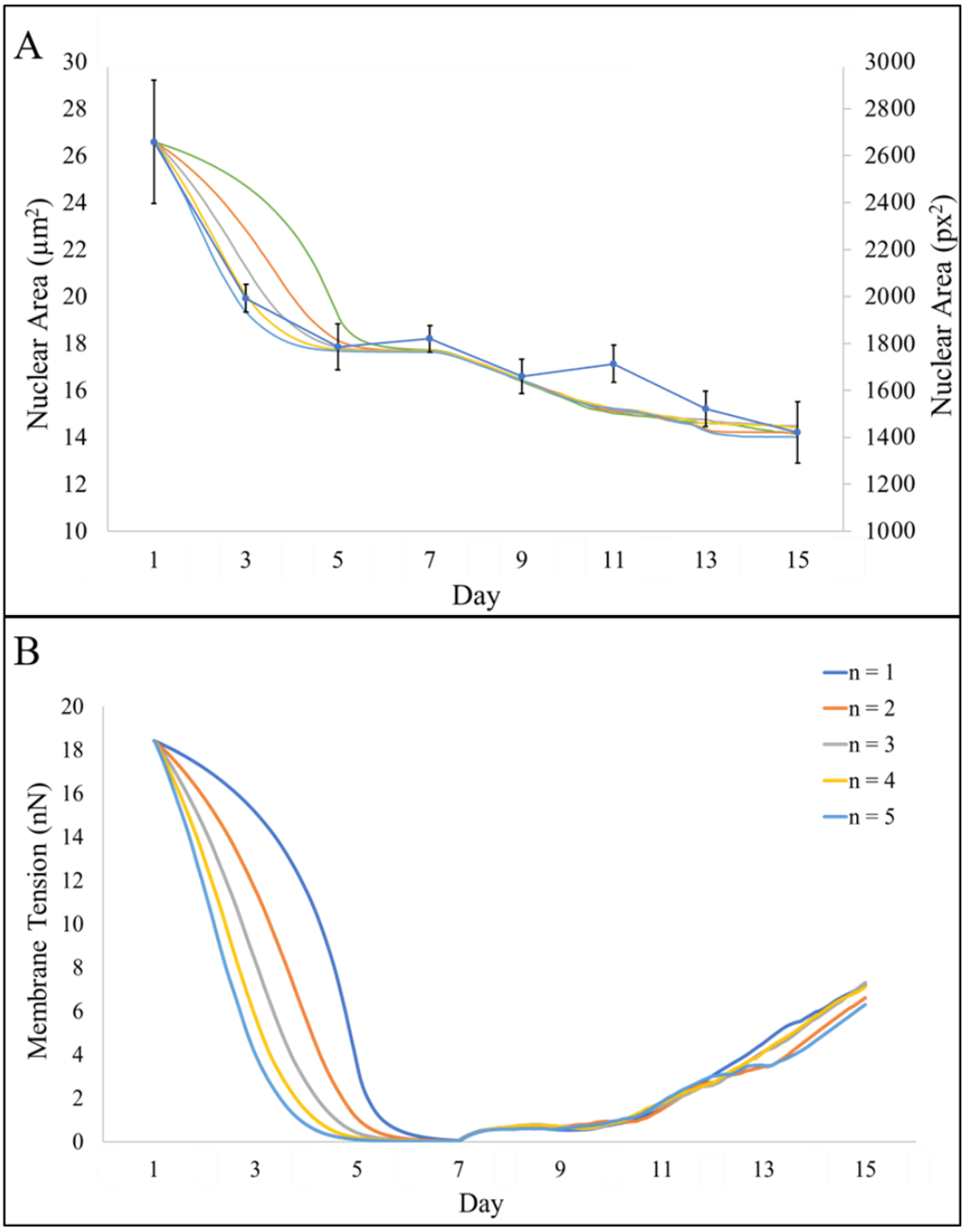

Figure 2. 7. *(A) Model-generated results of nuclear size demonstrating consistency with experimental data (blue curve with error bars) over 5 separate simulations. (B) Mathematical calculation of changes in the nuclear membrane tension (nN) as actin filaments reorganize and disappear. Results from 5 separate simulations are shown. Simulations are a result of increasing n from Equation 1. It was found that n = 4 (shown in yellow) most closely followed experimental data.*

Discussion

As stem cells progress to fully differentiated lineages, they undergo several morphological changes. These changes occur both in the cytoskeleton as well as the nucleus. Several previous researchers have examined the actin remodeling that takes place during adipogenesis. Titushkin et al., described the rearranging of actin filaments to the cell perimeter and eventual depolymerization as maturation continued.[31] Others include the influence of substrate stiffness and its response to actin organization on differentiation potential. Indeed, a modified substrate enhances the differentiation efficiency of MSCs to specific cell types.[3-5] However, studies on remodeling of the nucleus are scarce.

The nucleus contributes to the overall mechanical properties of the cell by being one of the largest and stiffest organelles.[7] The nucleus is also the repository for the cell's genetic code, which must be manipulated for gene activation. As demonstrated in Figure 3, the nucleus decreases in size over time during differentiation to mature adipocytes. Interestingly, the nuclear size reduction occurs mostly by day 5, with 70% of reduction occurring by this time point. The nuclear shrinkage precedes the exponential growth of fat deposition – a marker of mature adipocytes – suggesting the nuclear reorganization must occur prior to activation of the intricate machinery that promotes mature adipocytes. This is consistent with the findings that hMSC adipogenic differentiation occurs in two distinct parts; (1) lineage direction into pre-adipocytes and (2) adipocyte maturation.[32-35] Moreover, along with a reduction in nuclear size, we also observe a change in overall morphology of nucleus as adipogenesis continues. Differentiation brings about an increase in the aspect ratio (e.g., reciprocal decrease in roundness) of the nucleus. We compared the timing of the nuclear shape change with that of the expression of the

nuclear structural protein lamin A/C and found an inverse relationship. The LMNA protein expression appeared to increase as the nuclear morphology was altered to an increased aspect ratio (Fig. 5). Additionally, RT-qPCR experiments demonstrated a larger than 4-fold increase in production of LMNA mRNA when compared to control. LMNA exists as a network of intermediate filaments to provide structure and support for the nuclear envelope.[36] As a major driver of nuclear configuration, it stands to reason that an upregulation of LMNA may actively manipulate the nuclear shape. Indeed, LMNA structures have been shown to directly control chromosome positioning,[37] which in turn result in gene activation.[38] Fluorescent images of LMNA suggest a redistribution, as well as upregulation, of LMNA as adipogenesis continues. LMNA reorients along the nuclear periphery accompanied by a reduction in internuclear punctuates. This redistribution follows in line with published results which demonstrated a reorganization of the lamin network from internuclear structures during early differentiation to localization along the nuclear rim.[19] However, similar groups investigating nuclear structural rearrangement show an inverse phenomenon in expression levels of LMNA. Here, we demonstrate LMNA levels redistribute and increase in expression, while several researchers describe an overexpression of lamin as inhibiting adipocyte differentiation and lipid synthesis.[20,21] Verstraeten et al., also described an overall loss of lamin proteins after 18 days of adipocyte differentiation when compared to non-differentiated preadipocytes.[19] One potential explanation to this observation is the length of differentiation performed in regards to cell type. Several examples explained above made use of the commonly studied mouse 3T3-L1 preadipocyte cell line, which can attain a fully differentiated state in as little as 10 days.[39] Human mesenchymal stem cells derived from bone marrow are

however not primed for adipocyte differentiation and may therefore require longer differentiation times to observe the full effect. Indeed, we did observe a change in expression and localization of LMNA similar to that of early differentiation, with potential to continue over several weeks.

The size and shape alterations of the nucleus during differentiation are quantifiable and can be used as inputs to develop a model of nuclear morphology over time. A multibody model depicting forces generated on the nucleus was developed. The model took into account the actin filaments reorganizing and dissociating from the nucleus during adipogenic differentiation. This cytoskeletal rearrangement is theorized to reduce tension on the nuclear membrane, allowing the nucleus to reduce in size. Over several simulations, the model demonstrated similar area reduction and accurately predicted the experimental data (see Fig. 7A). Since the mechanical properties of actin filaments are known, the model can also be used to predict the membrane tension. As a result of nucleus becoming smaller, the nuclear components (represented by spherical particles in Fig. 6) must be reorganized to better fit the contracting nucleus. Such nuclear reorganization may induce potential chromosome rearrangement. Chromosome territories have been described as the compartmentalization of DNA in the nucleus, and evidence suggests these high-order arrangements influence gene expression.[40,41] As MSCs reprogram toward a specified lineage, corresponding gene regulation must occur to enhance the physiology of the lineage-specific cell. It is noteworthy to point out Kuroda et al. measured the positioning of two chromosomes (12 and 16) during adipogenic differentiation as a non-random event, indicating a directed influence on gene expression.[42] The stiffness of the stem cell nucleus membrane cannot be found in

literature with any certainty. However, the static and dynamic balance of forces in the simulation can be used to calculate the membrane stiffness. In the simulation, the initial configuration of the nucleus is generated randomly. The model is given time to settle and achieve a static force balance. Because the stiffness of the actin filaments is known in literature, $K_{actin} = 0.0437\ N/m$[43], we can use it to find the nuclear membrane stiffness. Using multiple nucleus configurations, this stiffness was found to be $K_{membrane} \approx 0.0055 \pm 0.0005\ N/m$, which is approximately an order of magnitude smaller than K_{actin}. The value calculated for the presented simulation is $K_{membrane} = 0.0051\ N/m$.

Depolymerization of actin filaments' effect on the nucleus is hypothesized to function as a reduction of stiffness over time with the formula:

$$K_{Depolymerization} = K_{Actin} \times (1 - \frac{t}{t_{Depolymerization}})^n \quad (1)$$

where KDepolymerization is the equivalent stiffness of the actin filament during depolymerization process, t is time elapsed from the start of the depolymerization process, $t_{Depolymerization} = 4\ days$ denotes the total depolymerization process time, and n determines the rate of depolymerization. Larger values of n indicate a more rapid depolymerization at the start of process. It was found that n = 4 yielded the best match to the experimental observations, suggesting a very rapid dissociation at the start and slowing down over time.

To further investigate changes in the nuclear shape as a prerequisite for adipogenesis, we utilized microcontact printing of fibronectin to pattern hMSC nuclei into high aspect ratios at the time of cell seeding. This protocol achieved the cell morphology similar to that of microchannels, in which the stretched cell morphology squeezed the nucleus, reducing its roundness (see Fig. 4). As differentiation proceeded on the

patterned surfaces, adipogenesis was hindered when compared to that on glass substrate. One possible explanation of the observed results is that the initial overall cell shape and microfilament network is integral to the differentiation potential of MSCs. Alternatively, when the actin polymerizing is stabilized by jasplakinolide, an enhancement of microfilament organization also reduced adipogenesis. Our findings suggest that the mechanical cues modulate the intended differentiation, and the specific cell shapes lend themselves to downstream terminally differentiated cell types (e.g., spindle shape of fibroblast).[44] The influence of several growth factors on gene regulation has also been described,[45,46] as well as that of substrate mechanical properties.[47,48] This chemical and physical direction of genetic regulation may therefore guide the nuclear shape. In this case, the nuclear shape is a result of – rather than a requirement for – gene regulation, and therefore cannot be forced to encourage differentiation. Forcing the nuclei into a confined shape may prove deleterious to the processes of nuclear remodeling, which should be completed step-wise. The differentiation of MSCs into fully mature adipocytes appear to occur in stages, and stem cells cannot leap previous stages to reach the end more quickly.

In conclusion, we provide evidence for the nuclear reorganization of human MSCs during adipogenic differentiation. We described a significant reduction in the nuclear area along with an increase in the aspect ratio over time. Lamin A/C, the major structural network in the nucleus, is reorganized and upregulated along with this change in shape, suggesting a direct relationship between the LMNA and nuclear morphology. To further elucidate the influence of nuclear shape on differentiation, MSCs with high nuclear aspect ratios were differentiated on microcontact printed patterns. The patterns failed to enhance

differentiation, providing evidence for the directed genetic reorganization of stem cells as differentiation continues into distinct, terminally differentiated cell types. Finally, numerical simulations were successfully developed to predict dynamical changes of the nuclei as hMSCs are directed to differentiate to adipocytes.

Methods

Cell Culture

MSCs were purchased from Lonza and expanded on tissue culture plates in growth medium (PT-3001, Lonza) until confluence. Once confluent, stem cells were detached from culture plates with 0.5% Trypsin-EDTA and seeded onto glass coverslips at a density of 2.5×10^4 *cells/cm*^{2}.

Adipogenic Differentiation

To induce differentiation toward adipocytes, cells were grown in adipogenic differentiation (AD) medium as described previously[10]. AD medium consisted of: High-Glucose Dulbecco's Modified Eagle Medium (DMEM), 10% fetal bovine serum (FBS), 1% penicillin-streptomycin, 1 *μM* dexamethasone, 200 *μM* indomethacin, 10 *μg/mL* insulin, and 0.5 mM 3-isobutyl-1-methylxanthine (IBMX).

MSCs underwent differentiation for 15 days, with samples being removed for analysis every other day. Samples were fixed in 4 paraformaldehyde for 20 minutes and stained for fluorescence microscopy. Cells were then mounted on to microscope slides and analyzed for nuclei morphology and lipid production.

To examine the influence of actin reorganization on nuclear properties, the actin polymerizing drug jasplakinolide (Santa Cruz Biotech) was used as previously described[49]. MSCs undergoing differentiation were treated with 0.01 *μM* Jasplakinolide in the AD medium, similarly replenished every other day for 15 days.

To confirm any differences in nuclear shape or lipid production are a result of treatment and not cell proliferation dependent, an MTT assay was performed (Sigma). MSCs were seeded on 96-well plates at the density described previously. Cell proliferation of treated cells and control cells were examined following days 1 and 7 of differentiation. Similarly, to prevent cell cycle dependency on differentiating cells of both control and treated groups, cycle synchronization was performed and examined. Cell cycles were synchronized in the G_1/G_0 phase using the starvation method as previously described[50]. Briefly, after seeding cells onto coverslips and before differentiation media was added, cells were supplied with growth medium without serum or growth factors for 20h. Following this incubation period, cells were supplied adipogenic medium as specified by treatment group.

Microcontact-printed Surface Preparation

To probe whether nuclei shape before differentiation influences the speed and efficiency of maturation, a microcontact-printing technique was performed. Stamping patterns were designed in AutoCAD (Autodesk, San Rafael, CA) and embedded onto a silicon wafer by MuWells (San Diego, CA). Linear patterns were fabricated with a width of 20 *μm* and a depth of 5 *μm*. Polydimethylsiloxane (PDMS) molds were generated with raised design features by mixing 10:1 (w/w) elastomer: crosslinker and pouring onto the silicon wafer. Molds were cured overnight at 60°until hardened. Stamping of fibronectin patterns was performed as described by established protocol[51]. Briefly, PDMS molds were cleaned thoroughly with ethanol, dried with compressed air, and the surfaces containing the stamp features were treated with plasma to promote protein attachment. 50 *μg/mL* of rhodamine-conjugated fibronectin (Cytoskeleton, Denver, CO) was added to the surface of the molds and allowed to bind for 30 minutes. Following binding, the molds

were washed with PBS three times and deionized water once. Quickly after washing, the molds were flipped onto 35 mm cell culture dishes and the protein monolayer was allowed to transfer for 5 minutes. After transfer, PDMS molds were carefully peeled off and the dishes were washed with PBS and blocked with 1% F-127 for 30 minutes to prevent cell attachment to the non-stamped surfaces. Excess F-127 was removed with additional washing with PBS and the dishes were incubated overnight in PBS.

Fluorescence Microscopy

Fluorescent microscopy images were taken on a Nikon Eclipse E800 (Melville, NY) at time points of every other day during differentiation. Fluorescent detection included staining for chromatin (NucBlue R37605, Thermofisher) for 15 minutes and lipid deposition (LipidTOX Green H34475, Thermofisher) for 30 minutes. Additionally, immunostaining was performed to observe the nuclear envelope protein, lamin A/C (LMNA). Briefly, cells were fixed in 4 paraformaldehyde for 20 minutes, permeabilized in 0.2% Triton X-100 (Sigma) for 15 minutes and blocked with 3 bovine serum albumin for 30 minutes. Cells were incubated with Alexa-Fluo 594-conjugated anti-LMNA antibodies produced in rabbit (ab215324, Abcam) for 1 h. LMNA antibodies and LipidTOX were diluted in phosphate buffered saline (PBS) at ratios of 1:500 and 1:200, respectively.

RNA Extraction and reverse transcription-quantitative polymerase chain reaction (RT-qPCR)

Gene profiling after 5 days of adipogenesis in experimental (AD) and control (AC) mediums was performed by reverse transcription-quantitative polymerase chain reaction (RT-qPCR). Briefly, RNA was extracted from cells following the protocol from the Quick RNA mini prep kit (Zymo Research, Irvine, CA). Isolated RNA was transcribed to cDNA using the AzuraQuant cDNA synthesis kit (Azura Genomics, Raynham, MA) according to

the manufacturer's protocol. Quantitative PCR was performed on a 7500 Fast Real-Time PCR System (Applied Biosystems, Foster City, CA) using AzuraQuant Green Fast qPCR Master Mix HiRox. Primers were purchased from Real Time Primers (Elkins Park, PA) and included adipose maturation gene Human peroxisome proliferator-activated receptor gamma (PPARγ) and nuclear membrane protein Human Lamin A/C (LMNA). GAPDH served as the internal reference to normalize the level of gene expression across all samples. Forward and reverse sequence information is recorded in Table 2.1. Fold changes in gene expression for experimental groups were analyzed relative to untreated controls using the double-delta cycle threshold (2-ΔΔCT) method[52].

Target Gene	Forward Primer	Reverse Primer
PPARγ	5'- GTG CGT GAG GAG TTT AAG GA -3'	5'- GTG CGT GAG GAG TTT AAG GA -3'
LMNA	5'- GTG CGT GAG GAG TTT AAG GA -3'	5'- GTG CGT GAG GAG TTT AAG GA -3'
GAPDH	5'- GAG TCA ACG GAT TTG GTC GT -3'	5'- TTG ATT TTG GAG GGA TCT CG -3'

Table 2. 1. *Forward and reverse primers used for RT-qPCR gene analysis.*

Imaging and Statistical Analysis

Image analysis was done through the fully automated pipeline to compute three major properties: lipid intensity, lamin intensity, and nuclei area. As a preprocessing step all images were normalized by subtraction of the average from all and division by the standard deviation.

Nuclei were segmented by K-means clustering which is an unsupervised learning algorithm popularly used for cell segmentation[23]. There are two classes considered for this step: 1) nuclei, 2) background. After segmentation, the morphology operation is implemented to separate the attached nuclei and removing any remainder of background noise, afterwards detected segments are labeled individually. Labeling the segmented particles gives the number of detected nuclei and makes it possible to extract

morphological properties of each particle (nucleus), for this study the area of each nucleus is the focus.

To get the lipid and lamin intensities from the fluorescent images, it's necessary to remove the background noise. For this purpose, images are filtered by the Gaussian kernel leading to a Gaussian blurred image. A fraction of the Gaussian blurred image is subtracted from the original image as background noise. For background removal there are two parameters that can be modified as needed, the coefficient for Gaussian blurred image and the sigma for the Gaussian filter. All non-zero pixels after background removal are considered as fat or lamin, respectively. To make sure the intensity measure for images from different runs are unified, all the images are normalized by dividing by the maximum pixel value and multiplying with 255, basically they are converted into 8bit images. Then the intensity per cell is computed by total intensity divided, summation of all pixel values, by the number of cells for each image.

The image analysis pipeline is written in Python 3.5 and open source image analysis libraries OpenCV, Scikit-learn and Scikit-Image has been used. Nuclear morphological characteristics were also determined using ImageJ software for comparison purpose. Statistical analysis was performed in Excel (Microsoft, Redmond, WA). Comparison between groups was performed using ANOVA (single factor) with a significance threshold of $p < 0.05$.

Dynamic Model and Simulation

To further elucidate the mechanical forces experienced by the nuclei during adipogenesis, we developed a two-dimensional model of forces acting upon the nucleus as differentiation continues. A model of the nucleus was simulated in MATLAB2018a (MathWorks, Natick, MA). The simulation was generated with the following assumptions:

1) actin filaments keep the nucleus membrane under tension, and 2) this tension dissipates over time due to actin depolymerization and rearrangement, and rearrangement of nucleus' contents during differentiation. Subsequently, the production of lipids inside the cell drives the later compaction of the nucleus.

The system was modeled as one stem cell nucleus in two dimensions, as shown in Figure 6. The nucleus membrane is modeled as one continuous spring under tension. All of the nuclear components are modeled as rigid spherical particles. Nucleoplasm is modeled as a liquid exerting drag forces on the rigid particles, effectively damping the particles' movement. The cytoskeletal forces are represented by actin filaments attached to the nuclear membrane. The actin filaments are modeled as springs keeping the membrane under tension. The number of attached actins (i.e., 16) is modeled to be equal to the number of beads in the periphery of nucleus as shown in Figure 6B. The effects of rearrangement and depolymerization of the cytoskeletal structure are modeled as the reduction in actin filaments stiffness over time. The rate is governed by the Equation 1. The actin stiffness reaches the value of zero after the 5^{th} day. The nucleus is disconnected from the cytoskeleton at this point. The effect of lipid accumulation is modeled as external forces acting on the nucleus.

Given the known values of actin filament stiffness and nucleus area we can estimate the stiffness of the nucleus membrane. This is based on the static and dynamic balance of forces between the membrane and actin filaments before differentiation. Additionally, observing the change in membrane area versus nuclear membrane tension, we can determine the rate of actin rearrangement and depolymerization. Finally we can

estimate the amount of force lipid accumulation exerts on the nucleus based on the change in the nucleus area in the later stages.

The dynamic model consists of 250 rigid spherical particles inside the nucleus representing the chromosomes and proteins. Using the nucleus density and allowing for the mass of the nucleoplasm, the mass of each particle is calculated to be $m = 21.8672 \times 10^{-18} kg = 21.8672\, fg$ with a radius of $r = 123.1\, nm$. A total of six forces act on the particles. Contact, viscous damping, and the random forces associated with Brownian motion act on all particles, while the actin, membrane and external forces act only on the particles in the periphery of the nucleus. Applying Newton's second law to a representative particle yields,

$$m\,\ddot{\boldsymbol{x}} + \beta\,\dot{\boldsymbol{x}} = \sum \boldsymbol{F} \tag{2}$$

where $\boldsymbol{x}$ contains the generalized coordinates, and $\ddot{\boldsymbol{x}}$ and $\dot{\boldsymbol{x}}$ are generalized acceleration and velocity. The mass of one particle is m. The term $\beta = 1.39 \times 10^{-8}\, kg/s$ is the coefficient of viscous friction for nucleoplasm. The sum of all other forces is $\sum \boldsymbol{F}$ which includes contact forces, random forces associated with Brownian motion, membrane tension forces, Actin forces, and external forces resulting from lipid accumulation.

The simulation of nucleus contraction using Equation 2 in molecular dynamics simulations is prohibitively expensive computationally. The forces involved are many orders of magnitude larger than the masses. That will cause large accelerations that drastically increase computational time. This is a common issue with all molecular dynamics simulations. For Equation 2, it will take one minute of CPU time to model one nanosecond of real time. Because the contraction of the nucleus was observed over 15

days, it is infeasible to obtain a simulation by simply applying standard numerical integration techniques to Equation 2, as in molecular dynamics simulation.

In this work, a scaling approach is used, which is based on the method of multiple scales (MMS)[53]. The premise is that large accelerations produce high frequency vibrations, on the order of 1/picoseconds, which have diminishing effects on the long term system behavior, on the order of days and weeks. Thus, the model can be scaled to remove the high frequency component of the motion when it is desired to observe the system behavior over longer time periods. The MMS uses an asymptotic expansion to decompose Equation 1 into different time scales, T_i, based on $T_i = e^i\, t$, where e is a small number obtained from the model characteristics. Examination of the e^0 term, the *zero order perturbation*[54], suggests a cancellation of the generalized active forces in the model. These cancelled forces can be removed from the dynamic model by scaling the generalized active forces. In this case, two scaling factors are needed because of the imbalances between viscous damping and the remaining forces. These dimensionless scaling factors are $a_2 \approx O(\beta/K_{actin})$ and $b_2 \approx O(m/\beta)$.

The resulting scaled dynamic model has the form:

$$m\,\ddot{\boldsymbol{x}} + a_2\,\beta\,\dot{\boldsymbol{x}} = (a_2 b_2)\,\sum \boldsymbol{F} \tag{3}$$

where the dimensionless scaling factors are $a_2 = 3.2 \times 10^{-10}$, and $b_2 = 1.6 \times 10^{-12}$. The unit system is, time in $10^3 s = 1\ ks$, mass in $10^{-18} kg = 1\ fg$, and length in $1\ \mu m$. All of the terms in Equation 3 are in proportion in the selected unit system. Therefore, the system can be simulated in exceptionally fast time. Total CPU time is $4738.3\ s \approx 1.5\ hours$ for 15 days of observation. This represents a computation time reduction on the order of 10^{14}; the computational time for a standard numerical integration would be

beyond hundreds of years. This drastic reduction in computational time allows an exploration of the physical properties of the nucleus such as the membrane stiffness and the actin depolymerization rate described in Equation 1. The value of the parameters used in the simulation are included in Table 2.2. Details of the computer simulation are more thoroughly discussed elsewhere[55].

Parameter	Definition	Value	Change
ρ	Nuclear density	$1400\ kg.m^{-3}$ [56]	constant
η	nucleoplasm viscosity	$6\ \times 10^{-3}\ kg.m^{-1}.s^{-1}$ [57]	constant
kB	Boltzmann constant	$1.380 \times 10^{-23} J.K^{-1}$	constant
T	temperature	$310.15\ K$	constant
ka	actin stiffness	$0.0437\ kg.s^{-2}$ [43]	Changes with the eqn. 1

Table 2. 2. *Additional parameters in computer simulation.*

References

1. Minguell, J., Erices, A. & Conget, P. Mesenchymal stem cells. *Exp. Biol. Med*. **226**(6), 507–520 (2001).

2. Chamberlain, G., Fox, J., Ashton, B. & Middleton, J. Concise review: Mesenchymal stem cells: Their phenotype, differentiation capacity, immunological features, and potential for homing. *Stem Cells.* **25**(11), 2739–2749, DOI: 10.1634/stemcells.2007-0197 (2007).

3. Engler, A. J., Sen, S., Sweeney, L. H. & Discher, D. E. Matrix elasticity directs stem cell lineage specification. *Cell*. **126**(4), 126, 677–689, DOI: 10.1016/j.cell.2006.06.044 (2006).

4. Zhao, W., Li, X., Liu, X., Zhang, N. & Wen, X. Effects of substrate stiffness on adipogenic and osteogenic differentiation of human mesenchymal stem cells. *Mater Sci Eng: C.***40**, 316–323, DOI: 10.1016/j.msec.2014.03.048 (2014).

5. Mao, A. S., Shin, J. & Mooney, D. J. Effects of substrate stiffness and cell-cell contact on mesenchymal stem cell differentiation. *Biomaterials.* **98**, 184–191, DOI: 10.1016/j.biomaterials.2016.05.004 (2016).

6. Kilian, K. A., Bugarija, B., Lahn, B. T. & Mrksich, M. Geometric cues for directing the differentiation of mesenchymal stem cells. *Proc. Natl. Acad. Sci.* **107**, 4872–4877, DOI: 10.1073/pnas.0903269107 (2010).

7. Caille, N., Thoumine, O., Tardy, Y. & Meister, J. Contribution of the nucleus to the mechanical properties of endothelial cells. *J. Biomech.* **35**, 177–87 (2002).

8. Boyle, S., Gilchrist, S., Bridger, J.M., Mahy, N.L., Ellis, J.A. and Bickmore, W.A. The spatial organization of human chromosomes within the nuclei of normal and emerin-mutant cells. *Human Molec. Genetics*. **10**(3), 211-220 (2001).

9. Cremer, T., Cremer, M., Dietzel, S., Müller, S., Solovei, I. and Fakan, S. Chromosome territories–a functional nuclear landscape. *Curr. Opinion Cell Biol*. **18**(3), 307-316 (2006).

10. Meaburn, K. J., & Misteli, T. Cell biology: chromosome territories. *Nature*. **445**(7126), 379 (2007).

11. Egecioglu, D. & Brickner, J. H. Gene positioning and expression. *Curr. Opinion Cell Biol.* **23**(3), 338–345 (2011).

12. Stachecka, J., Nowacka-Woszuk, J., Kolodziejski, P., & Szczerbal, I. The importance of the nuclear positioning of the PPARG gene for its expression during porcine in vitro adipogenesis. *Chromosome Res.* **27**(3), 271–284 (2019).

13. Dixon, J. R. et al. Chromatin architecture reorganization during stem cell differentiation. *Nature.* **518**, 331, DOI:10.1038/nature14222 (2015).

14. Heo, S., Cosgrove, B. D., Dai, E. N. & Mauck, R. L. Mechano-Adaptation of the stem cell nucleus. *Nucleus* **9**, 09-19, DOI: 10.1080/19491034.2017.1371398 (2017).

15. Gruenbaum, Y. & Foisner, R. Lamins: nuclear intermediate filament proteins with fundamental functions in nuclear mechanics and genome regulation. *Annu. Rev. Biochem*. **84**, 131–64, DOI: 10.1146/annurev-biochem-060614-034115 (2015).

16. Rankin, & Ellard. The laminopathies: a clinical review. *Clinical Genetics*. **70**(4), 261–274, doi:10.1111/j.1399-0004.2006.00677.x (2006).

17. Maraldi, N., Lattanzi, G., Capanni, C., Columbaro, M., Mattioli, E., Sabatelli, P., Manzoli, F. Laminopathies: A chromatin affair. *Adv. Enzyme Regulation*. **46**(1), 33–49, doi:10.1016/j.advenzreg.2006.01.001 (2006).

18. Scaffidi, P., & Misteli, T. Lamin A-dependent misregulation of adult stem cells associated with accelerated ageing. *Nature Cell Biology*, **10**(4), DOI: ncb1708. doi:10.1038/ncb1708 (2008).

19. Verstraeten, V., Renes, J., Ramaekers, F., Kamps, M., Kuijpers, H., Verheyen, F., Broers, J. Reorganization of the nuclear lamina and cytoskeleton in adipogenesis. *Histochem. Cell Biol.* **135**(3), 251–261, doi:10.1007/s00418-011-0792-4 (2011).

20. Constantinescu, D., Gray, H., Sammak, P., Schatten, G., & Csoka, A. Lamin A/C expression Is a marker of mouse and human embryonic stem cell differentiation. *Stem Cells.* **24**(1), 177–185, doi:10.1634/stemcells.2004-0159 (2006).

21. Oldenburg, A., Briand, N., Sørensen, A., Cahyani, I., Shah, A., Moskaug, J., & Collas, P. A lipodystrophy-causing lamin A mutant alters conformation and epigenetic regulation of the anti-adipogenic MIR335 locus. *J. Cell Biol*. **216**(9), doi:10.1083/jcb.201701043 (2017).

22. Swift, J. et al. Nuclear Lamin-A scales with tissue stiffness and enhances matrix-directed differentiation. *Science*. **341**(6149), 1240104. doi:10.1126/science.1240104 (2013).

23. Sarrafzadeh, O. & Dehnavi, A. Nucleus and cytoplasm segmentation in microscopic images using k-means clustering and region growing. *Adv. Biomed. Res.* **4** (2015).

24. Wang, Y., Nagarajan, M., Uhler, C., & Shivashankar, G. V. Orientation and repositioning of chromosomes correlate with cell geometry–dependent gene expression. *Molec. Biol. Cell.* **28**(14), 1997-2009. (2017).

25. Makhija, E., Jokhun, D. S., & Shivashankar, G. V. Nuclear deformability and telomere dynamics are regulated by cell geometric constraints. *Proc. Natl. Acad. Sci.*, **113**(1), E32-E40. (2016).

26. Ramdas, N. M., & Shivashankar, G. V. Cytoskeletal control of nuclear morphology and chromatin organization. *J. Molec. Biol.* **427**(3), 695-706. (2015).

27. Rosen, E. D., Walkey, C. J., Puigserver, P., & Spiegelman, B. M. Transcriptional regulation of adipogenesis. *Genes Dev..* **14**(11), 1293-1307. (2000).

28. Driscoll, T. P., Cosgrove, B. D., Heo, S. J., Shurden, Z. E., & Mauck, R. L. Cytoskeletal to nuclear strain transfer regulates YAP signaling in mesenchymal stem cells. *Biophys. J.* **108**(12), 2783-2793. (2015).

29. Maniotis, A. J., Chen, C. S., & Ingber, D. E. Demonstration of mechanical connections between integrins, cytoskeletal filaments, and nucleoplasm that stabilize nuclear structure. *Proc. Natl. Acad. Sci.* **94**(3), 849-854. (1997).

30. Kim, D. H., & Wirtz, D. Cytoskeletal tension induces the polarized architecture of the nucleus. *Biomaterials*. **48**, 161-172. (2015).

31. Titushkin, I., Sun, S., Paul, A. & Cho, M. Control of adipogenesis by ezrin, radixin and moesin-dependent biomechanics remodeling. *J. Biomech.* **46**, 521–526, DOI: 10.1016/j.jbiomech.2012.09.027 (2013).

32. José, M. & José, F. Adipocyte Differentiation in *Adipose Tissue Biology* (ed. Symonds, M. E.), 17-38 (Springer 2012).

33. van den Dungen, M. W., Murk, A. J., Kok, D. E. & Steegenga, W. T. Comprehensive DNA methylation and gene expression profiling in differentiating human adipocytes. *J. Cell Biochem*. **117**, 2707–2718, DOI: 10.1002/jcb.25568 (2016).

34. Carnevalli, L. S. et al. S6k1 plays a critical role in early adipocyte differentiation. *Dev. Cell.* **18**, 763–774, DOI: 10.1016/j.devcel.2010.02.018 (2010).

35. Menssen, A. et al. Differential gene expression profiling of human bone marrow-derived mesenchymal stem cells during adipogenic development. *BMC Genomics.* **12**, 461, DOI: 10.1186/1471-2164-12-461 (2011).

36. Goldman, R. D., Gruenbaum, Y., Moir, R. D., Shumaker, D. K. & Spann, T. P. Nuclear lamins: building blocks of nuclear architecture. *Genes Dev*. **16**, 533–547, DOI: 10.1101/gad.960502 (2002).

37. Guelen, L. et al. Domain organization of human chromosomes revealed by mapping of nuclear lamina interactions. *Nature.* **453**, 948, DOI: 10.1038/nature06947 (2008).

38. Kosak, S. T. et al. Coordinate gene regulation during hematopoiesis is related to genomic organization. *PLoS. Biol*. **5**, e309, DOI: 10.1371/journal.pbio.0050309 (2007).

39. Zebisch, K., Voigt, V., Wabitsch, M., & Brandsch, M. Protocol for effective differentiation of 3T3-L1 cells to adipocytes. *Anal. Biochem.* **425**(1), 88–90. doi:10.1016/j.ab.2012.03.005 (2012).

40. Lanctôt, C., Cheutin, T., Cremer, M., Cavalli, G. & Cremer, T. Dynamic genome architecture in the nuclear space: regulation of gene expression in three dimensions. *Nat. Rev. Genet.* **8**, 104–115, DOI: 10.1038/nrg2041 (2007).

41. Nguyen, H. Q. & Bosco, G. Gene positioning effects on expression in eukaryotes. *Ann. Rev. Genet.* **49**, 1–20, DOI: 10.1146/annurev-genet-112414-055008 (2015).

42. Kuroda, M. et al. Alteration of chromosome positioning during adipocyte differentiation. *J. Cell Sci.* **117**, 5897–5903, DOI: 10.1242/jcs.01508 (2004).

43. Kojima, H., Ishijima, A. & Yanagida, T. Direct measurement of stiffness of single actin filaments with and without tropomyosin by in vitro nanomanipulation. *Proc. Natl. Acad. Sci.* **91**, 12962–12966 (1994).

44. Gao, L., McBeath, R. & Chen, C. S. Stem cell shape regulates a chondrogenic versus myogenic fate through rac1 and n-cadherin. *Stem Cells.* **28**, 564–572, DOI: 10.1002/stem.308 (2010).

45. Mikami, Y., Lee, M., Irie, S. & Honda, M. J. Dexamethasone modulates osteogenesis and adipogenesis with regulation of osterix expression in rat calvaria-derived cells. *J. Cell Physiol.* **226**, 739–748, DOI: 10.1002/jcp.22392 (2011).

46. Aghajanian, P., Hall, S., Wongworawat, M. D. & Mohan, S. The roles and mechanisms of actions of vitamin c in bone: New developments. *J. Bone Min. Res.* **30**, 1945–1955, DOI: 10.1002/jbmr.2709 (2015).

47. Nakazawa, N., Sathe, A. R., Shivashankar, G. & Sheetz, M. P. Matrix mechanics controls FHL2 movement to the nucleus to activate p21 expression. *Proc Natl. Acad. Sci.* **113**, E6813–E6822, DOI: 10.1073/pnas.1608210113 (2016).

48. Hu, X., Margadant, F., Yao, M. & Sheetz, M. Molecular stretching modulates mechanosensing pathways. *Protein Sci.* **26**, 1337–1351, DOI: 10.1002/pro.3188 (2017).

49. Müller, P., Langenbach, A., Kaminski, A. & Rychly, J. Modulating the actin cytoskeleton affects mechanically induced signal transduction and differentiation in mesenchymal stem cells. *PLoS ONE.* **8**, e71283, DOI: 10.1371/journal.pone.0071283 (2013).

50. Chen, M. et al. Serum Starvation Induced Cell Cycle Synchronization Facilitates Human Somatic Cells Reprogramming. *PLoS ONE*. **7**(4), e28203. doi:10.1371/journal.pone.0028203 (2012).

51. Hind, L. E., Mackay, J. L., Cox, D. & Hammer, D. A. Two-dimensional motility of a macrophage cell line on microcontactprinted fibronectin. *Cytoskeleton.* **71**, 542–554, DOI: 10.1002/cm.21191 (2014).

52. Livak, K. J., & Schmittgen, T. D. Analysis of relative gene expression data using real-time quantitative PCR and the 2− ΔΔCT method. *Methods*. **25**(4), 402-408. (2001).

53. Haghshenas-Jaryani, M. & Bowling, A. Modeling flexibility in myosin v using a multiscale articulated multi-rigid body approach. ASME J. *Comput. Nonlinear Dyn*. **10**, 011015 (2015).

54. Nayfeh, A. H. Perturbation Methods (John Wiley & Sons 2008).

55. Rabiei, M., McColloch, A. R., Rabbani, S. P., Cho, M., & Bowling, A., Long term dynamic simulation of a stem cell nucleus. ASME J. *Comput. Nonlinear Dyn*. Manuscript submitted for publication (2019).

56. Schürmann, M., Scholze, J., Müller, P., Guck, J., & Chan, C. J. Cell nuclei have lower refractive index and mass density than cytoplasm. *J. Biophotonics*. **9**(10), 1068-1076. (2016).

57. Liang, L., Wang, X., Da, X., Chen, T., & Chen, W. R. Noninvasive determination of cell nucleoplasmic viscosity by fluorescence correlation spectroscopy. *J. Biomed. Optics*. **14**(2), 024013 (2009).

CHAPTER 3:

Altered Adipogenesis of Human Mesenchymal Stem Cells by Photobiomodulation Using 1064 nm Laser Light

Andrew McColloch, Caleb Liebman, Hanli Liu, and Michael Cho

Material From:

McColloch, A., Liebman, C., Liu, H., Cho, M. (2020).

Altered Adipogenesis of Human Mesenchymal Stem Cells by Photobiomodulation Using 1064 nm Laser Light. *Lasers in Surgery and Medicine*. 10.1002/lsm.23278.

Abstract

Background and Objective: Photobiomodulation (PBM) describes the influence of light irradiation on biological tissues. Laser light in the near infrared spectrum (NIR) has been shown to mitigate pain, reduce inflammation, and promote wound healing. The cellular mechanism that mediates PBM's effects is generally accepted to be at the site of the mitochondria, leading to an increased flux through the electron transport chain and ATP production. Moreover, PBM has been demonstrated to reduce oxidative stress through an increased production of reactive oxygen species (ROS)-sequestering enzymes. The aim of the study is to determine whether these PBM-induced effects expedite or interfere with intended stem cell differentiation to the adipogenic lineage.

Materials and Methods: To determine the effects of 1064 nm laser light on human mesenchymal stem cells undergoing adipogenic differentiation, ATP and ROS levels, lipid content, and adipogenic gene production were quantified. Cells were irradiated with three different fluences (8.8, 17.6 and 26.4 J/cm^2) over the course of the experiments.

Results: At a low fluence (8.8 J/cm^2) the ATP increase was essentially negligible, whereas a higher fluence induced a significant increase. In the laser-stimulated cells, PBM over time decreased the ROS level compared to the non-treated control group and significantly reduced the extent of adipogenesis. A reduction in the ROS level was correlated with a diminished lipid accumulation, reduced production of adipose-specific genetic markers and delayed the chemically intended adipogenesis.

Conclusion: In summary, we characterized the use of NIR light exposure to modulate hMSC differentiation. Both the ATP and ROS levels in hMSCs responded to different energy densities. The current study is expected to contribute significantly to the growing

field of PBM as well as stem cell tissue engineering by demonstrating the wavelength-dependent responses of hMSC differentiation.

Introduction

Adult mesenchymal stem cells (MSCs) are of interest to bioengineering due to their unique capability of differentiation to multiple cell types including bone, adipose, and cartilage.[1] Historically, MSC differentiation is induced by chemical means – that is growth factors and other stimuli are added to culture media in an effort to provide an environment conducive to the desired cell type.[2] More recently, orthogonal cues other than chemical factors have been elucidated to regulate the lineage commitment. For example, the cell shape, cellular mechanics, and substrate stiffness have been found to play a role in determining the fate of MSCs.[3-6]

In addition to mechanical properties, additional cues have been brought forward which demonstrate an influence in the MSC fate. One such factor is photo-stimulation by laser irradiance.[7] Photobiomodulation (PBM), as it has come to be known, includes the influence of low-level laser therapy in the form of near-infrared light on biological tissues.[8] Infrared light occupies the electromagnetic wavelength band from 700 nm to 1 mm, with near infrared (NIR) existing between 780 – 2500 nm.[9,10] The NIR wavelength is of particular interest to the medical field due to its absorbance by proteins containing heme groups such as hemoglobin and the cytochrome c oxidase (CCO).[11-13] NIR light has been already used in the medical field for pain attenuation, promotion of wound healing, and tracking cerebral blood flow.[14-16]

The generally accepted mechanism of PBM has been described to be at the site of the mitochondria. The copper- and heme-containing cores of cytochrome c oxidase, the terminal protein of the electron transport chain, accept a photon leading to the dissociation

of inhibitory nitric oxide (NO).[8,11] With the removal of NO, flux through the electron transport chain is enhanced and several downstream effects are produced such as increased ATP production, enhanced ROS signaling, and NO-induced anti-inflammatory events.[17] CCO activity is directly tied to flux through the electron transport chain.[18] Increasing flux through the electron transport chain provides an increase in ATP generation as well as a transient increase in reactive oxygen species (ROS) production as electrons “leak” from the system.[19,20] This ROS increase is followed by activation of several ROS sequestering mechanisms including transcriptional activation of ROS-mitigating enzymes, leading to an overall reduction in oxidative stress over time.[21-23]

In stem cell differentiation, energy dynamics have been shown to play a role in lineage direction. As stem cells differentiate, they shift in energy production from predominantly glycolysis to oxidative phosphorylation.[24-25] In addition, high levels of ROS have been implicated in directing differentiation towards adipocytes.[26] Therefore, high oxidative phosphorylation and low ROS brought about by laser irradiation potentially inhibit differentiation of MSCs toward an adipocyte lineage and, conversely, may enhance osteogenic differentiation and bone formation. Indeed adipo- and osteo-genic differentiations exist as opposites to one another, with specific factors requiring inverse regulations for the different lineages.[27] In regard to bone formation, several groups have shown the influence of laser light on osteogenic differentiation. For example, Tani et al. demonstrated the use of 635 and 808 nm light on calcium deposition of MSCs undergoing osteogenic differentiation.[28] Wang et al., displayed similar trends in calcium production while using 420 and 540 nm wavelengths.[29] Although the influence of laser light on bone

formation has been described in some details, potential effects on MSCs undergoing adipogenic differentiation remain to be further elucidated and confirmed.

Previous studies with PBM and stem cells focus on shorter wavelengths of light (650 – 900 nm) to influence differentiation. At longer wavelengths NIR may offer insights into the mechanisms that are wavelength-dependent. At shorter wavelengths, PBM influences the CCO protein more directly, due to its optimal absorption spectra between 620 and 820 nm.[13] As wavelength increases, the absorption coefficient of water increases, leading to the potential for a rise in temperature. Temperature change has been implicated in several cellular processes and is even suggested as a method of action for PBM to direct calcium signaling within the cell.[30] While 1064 nm specifically has been utilized in diabetic wound healing applications,[31] transcranial clinical trials,[32] and esthetic dentistry,[33] its influence on adult mesenchymal stem cells and the potential to influence adipogenic differentiation remain to be determined. Because the current literature on stem cell differentiation in response to longer wavelength light is scarce, we utilized a 1064 nm laser to determine the potential modulation of adipogenesis by quantitatively measuring the adipogenic markers, morphological nuclear reorganization, and postulated a working model. Our results suggest the 1064 nm PBM does not completely inhibit the intended adipogenesis but rather significantly diminishes the extent of adipogenic differentiation.

Materials and Methods

Cell Culture

Human MSCs were commercially purchased (PT-2501, Lonza, MD) and expanded on tissue culture plates in growth medium (PT-3001, Lonza) until confluence. Human MSCs were harvested from the bone marrow of a female patient of 25 years old. Once confluent, stem cells were detached from culture plates with 0.5% Trypsin-EDTA and seeded onto glass coverslips in 35 mm culture dishes at a density of 2.5 x 10^4 cells/cm^2. The media was changed every other day and the samples were visually inspected for media contamination.

Laser Setup

A collimated laser (Cell Gen Therapeutics, Dallas, TX; model CG-5000) was used to expose hMSCs to 1064 nm IR light. In order to ensure all exposure was consistent, the laser was calibrated using a power meter (ThorLabs, Newton, NJ; model D10MM). For laser stimulation, cells were removed from the incubator and placed on a stage 5 cm directly under the laser aperture. The entire glass coverslip on which hMSCs were seeded was exposed to laser light at different intensities for 2 minutes and immediately returned to the incubator. Laser fluence was calculated as follows:

$$Fluence\ (J/cm^2) = \frac{W \times t}{A}$$

Where *W* is the laser intensity, *t* is exposure time in seconds, and *A* is the beam size (13.6 cm^2). Exposure intensities were 1, 2, and 3 W for 2 minutes, which correspond to the fluence of 8.8, 17.6, and 26.4 J/cm^2, respectively. Following each PBM treatment, the

cells were allowed to rest for 24 hours prior to image recording and other measurements. The 2 min laser exposure time was chosen based on the published data that typically 2 to 12 min laser exposure times have been used for in vivo.[16,29,34-37] Since in vitro experiments are not hindered by laser power attenuation and tissue penetration limitation, the 2 min exposure per day was maintained throughout this study and also to minimize potential thermal effects. It is therefore important to determine changes in temperature during laser exposure. The water absorption spectrum indicates a relatively high absorption coefficient at 1064 nm. An equal volume of the culture media (1.5 mL) was added to 35 mm culture dishes and exposed to laser light at various intensities. Temperature change was measured by an OMEGA digital thermistor (Spectris, Egham, UK; model HH42A).

Stem Cell Differentiation

To induce differentiation toward adipocytes, cells were grown in adipogenic differentiation (AD) medium as described previously.[38] The medium consisted of: High-Glucose Dulbecco's Modified Eagle Medium (DMEM), 15% fetal bovine serum (FBS), 1% penicillin-streptomycin (PS), 1 µM dexamethasone, 200 µM indomethacin, 10 µg/mL insulin, and 0.5 mM 3-isobutyl-1-methylxanthine (IBMX).

Fluorescence Microscopy

Human MSCs underwent differentiation for up to 15 days, with samples being removed for analysis every other day. Samples were fixed in 4% paraformaldehyde for 20 minutes, permeabilized with 0.2% Triton X-100 (Sigma Aldrich, St.Louis, MO) and stained for

adipocyte lineage markers and features. Briefly, cells treated with AD medium were stained for lipid production using LipidTOX Green (Thermofisher, Waltham, MA). In addition, differentiating hMSCs were stained for nuclear morphology using NucBlue chromatin stain (Thermofisher). Differentiation efficiency was determined using fluorescence microscopy, including production of lipid droplets and gene expressions as adipogenic lineage-specific markers. Multichannel images were taken using a Nikon Eclipse E800 microscope (Melville, NY). Fluorescent images were analyzed as previously described utilizing a proprietary pipeline built in Python to automatically analyze fluorescent images, including production of lipid droplets and nuclear size and morphology changes.[39] Briefly, lipid images were filtered by Gaussian kernel, and a portion of the Gaussian-blurred image is removed from the original as background. After background removal, all foreground pixels after background removal are considered as lipid. To ensure unified intensity from separate runs, all images are normalized. For nuclei images, the nuclei were segmented by K-means clustering, an unsupervised learning algorithm commonly used for cell segmentation.[40] Finally, lipid intensity per cell was determined by dividing intensity values by number of nuclei.

ATP Quantification

To determine the effect on cell energy dynamics, ATP levels were quantified via CellTiter-Glo Assay (Promega). Undifferentiated MSCs were seeded onto 96-well plates at 8000 cells/well. Cells were irradiated with increasing fluence levels (0, 8.8, and 26.4 J/cm^2), incubated for 15 minutes, and ATP levels were quantified via luminescence using a microplate reader.

ROS Production

To quantify the effect of laser stimulation on production of reactive oxygen species, live-cell fluorescent microscopy was carried out. At several timepoints during differentiation, samples were removed from differentiation media and stained for mitochondrial superoxide levels. Briefly, cells were washed 3X in PBS and stained using MitoSOX Red mitochondrial superoxide indicator (Thermofisher) diluted in PBS. ROS levels were evaluated using fluorescence intensity.

Catalase Enzyme Blocking by 3-AT

To confirm the method of action of PBM treatment in regard to mitochondrial superoxide levels, the experiment was repeated in the presence of catalase enzyme inhibitor 3-Amino-1,2,4-triazole (3-AT). 3-AT acts as a competitive inhibitor of catalase by covalently bonding to the active center, preventing the enzyme's mechanism of action of converting hydrogen peroxide (H_2O_2) to water and oxygen.[41] Briefly, cells were exposed to 3-AT added to AD media at a concentration of 2 mM. Human MSCs were differentiated in the presence of 3-AT for 9 days with and observed for lipid production.

Triglyceride Assay

Triglyceride levels in stem cell-conditioned media were analyzed for potential lipid leakage across the adipocyte membrane using a fluorometric Triglyceride Assay Kit (Abcam) following manufacturer's instructions. Briefly, at scheduled media changes during differentiation, culture media was removed and stored at -20 °C. 50 µL of sample

was loaded in triplicate to 96-well plates, to which 2 µL Lipase was added. Samples were mixed for 20 minutes while a reaction mix of Assay Buffer, Triglyceride Probe, and Enzyme Mix was prepared using volumes of 47.6 µL, 0.4 µL, and 2 µL, respectively. 50 µL reaction mix was added to sample wells and incubated at room temperature for 60 minutes. Fluorescence was measured using 535/587 nm (ex/em).

RNA Extraction and Reverse Transcriptase Polymerase Chain Reaction (RT-PCR)

Gene profiling of adipogenesis in experimental (AD) and control media was performed by reverse transcription polymerase chain reaction (RT-PCR). Briefly, RNA was extracted from cells following the protocol from the Quick RNA mini prep kit (Zymo Research, Irvine, CA). Isolated RNA was transcribed to cDNA using the AzuraQuant cDNA synthesis kit (Azura Genomics, Raynham, MA) according to the manufacturer's protocol. Quantitative PCR was performed on a 7500 Fast Real-Time PCR System (Applied Biosystems, Foster City, CA) using AzuraQuant Green Fast qPCR Master Mix HiRox. Primers were purchased from Real Time Primers (Elkins Park, PA) and included adipose maturation gene Human peroxisome proliferator-activated receptor gamma (PPARγ) and free radical sequestering enzyme superoxide dismutase 2 (SOD2). GAPDH served as the internal reference to normalize the level of gene expression across all samples. Fold changes in gene expression for experimental groups were analyzed relative to untreated controls using the double-delta cycle threshold ($2^{-\Delta\Delta CT}$) method.[42]

Statistical Analysis

Data are presented as mean ± SEM and compared using a two-factor ANOVA followed by Tukey's test for post hoc analysis. $p < 0.05$ or > 0.05 were indicated with a single (*) or double asterisks (**), respectively.

Results

Temperature Rise

Changes in temperature were determined to rule out possible thermal effects. A thermistor was used to measure temperature rise in the differentiation media. Media temperature was recorded before a laser irradiation and then following preselected

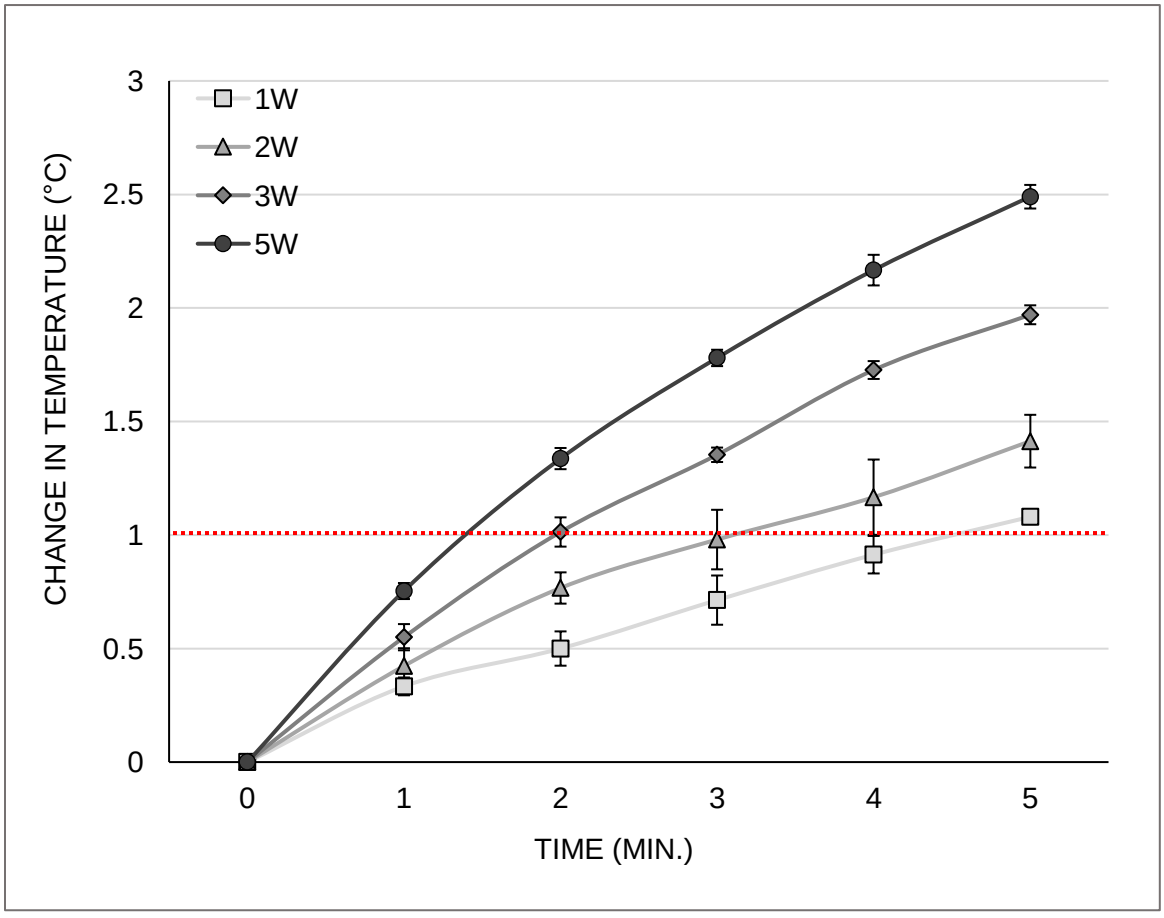

Figure 3. 1. *Average temperature rise of adipogenic differentiation media in 35 mm petri dish during exposure to 1064 nm laser at varying laser powers. Temperature was recorded at one minute intervals using an Omega HH42A thermistor. Data represent mean ± SEM of 3 independent experiments. Since the laser beam size was fixed at 13.6 cm2, the 1 W exposure corresponds to 0.074 W/cm2. The red line indicates a threshold temperature increase of 1° C.*

exposure conditions such as varying laser intensity and exposure duration. Temperature rise was then continuously monitored under different PBM exposure conditions (Fig. 1). This important experiment provided guidance of the range of PBM parameters chosen for this current study. At the exposure duration of 2 min, applying the 1064 nm laser in the range of 1 to 3 W changed the temperature no more than 1 °C, well below the threshold required to influence stem cell differentiation.[43,44] As expected, higher laser powers (e.g., 5 W) did induce appreciable changes of > 1 ^{o}C, which suggests potential thermal effects may not be readily neglected at higher laser powers. All experiments were performed using 2 min exposure.

Fluorescence Microscopy and Imaging Analysis

Human MSCs were seeded onto glass coverslips and directed towards the adipogenic lineage using an adipogenic cocktail as described in the Method section. Cells were then exposed to 1064 nm laser light and examined for modulated stem cell differentiation. The extent of differentiation efficiency was determined by production of lipid droplets. As a positive control experiment, stem cells undergoing adipogenesis using the adipogenic cocktail demonstratively exhibited an abundance of lipid expression (Fig. 2A). Following a 2 min/day laser irradiation for 7 consecutive days, all fluence values tested (8.8, 17.6, and 26.4 J/cm^2) demonstrated a lower lipid production compared to control. Quantitative analysis showed that the lipid droplet production was significantly reduced by the laser exposure, and that the highest fluence we applied (26.4 J/cm^2) caused ~ 50% reduction in the lipid droplets (Fig. 2B).

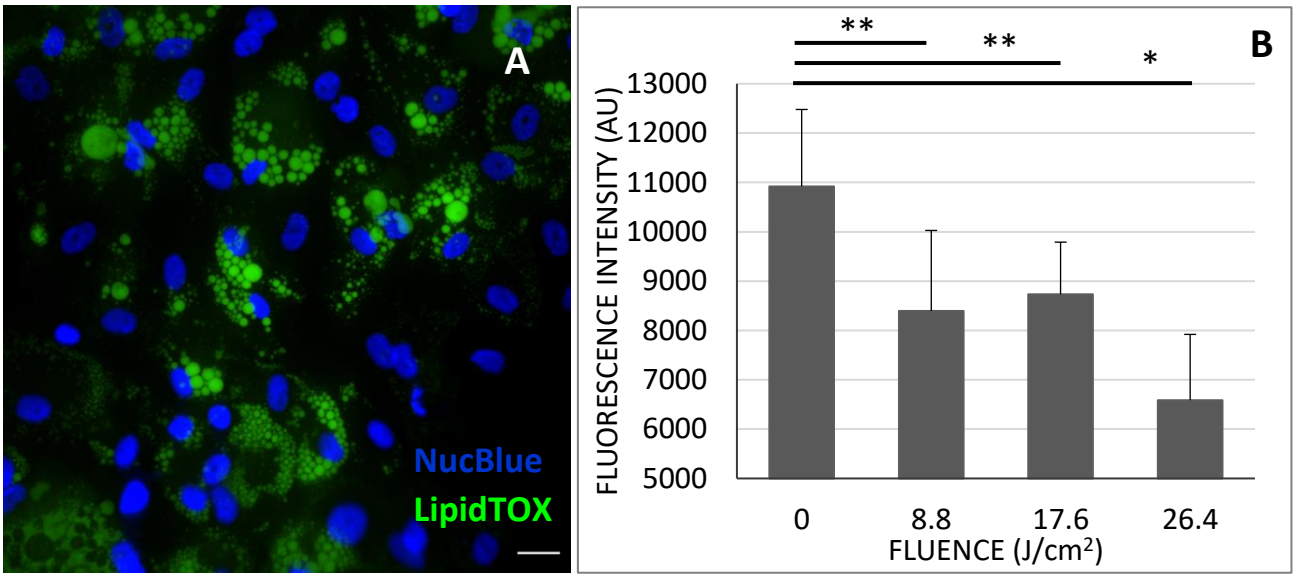

Figure 3. 2. *Multi-channel fluorescence image demonstrating lipid production (green) and nuclear size (blue). Image were recorded after 9 days of differentiation using a 40x microscope objective. (A) Fluorescence intensity of lipid detection dye LipidTOX Green at increasing fluence of 1064 nm PBM for 2 min/day after 7 days of adipogenic differentiation. (B) Data presented as mean ± SEM, n=5. Bar = 25 µm. * indicates $p < 0.05$, ** $p > 0.05$.*

We have recently reported that the extent of adipogenic differentiation was regulated by the nuclear size and shape. In fact, an inverse relationship was established between the nuclear size and adipogenesis.[39] These morphological features were also monitored in response to PBM. As shown in Figure 3A, at day 7 the normally differentiating hMSCs showed the nuclei that are smaller in size in comparison to those treated with PBM (17.6 and 26.4 J/cm^2; Fig. 3B). Quantitative analysis indeed confirmed the visual observation that, while a lower fluence did not alter the nuclear size, higher fluences caused the cells to retain a larger nuclear area (Fig. 3C). The inverse relationship we reported previously appears to be applicable in response to selected PBM. This result also provided a clear rationale that the subsequent experiments should be performed using a fluence of either 17.6 or 26.4 J/cm^2, as these fluences demonstrated a robust reduction in lipid droplets as well as large nuclear size, both of which serve to indicate diminished adipogenesis. These

two fluences have also been shown to minimize unwanted effects such as temperature rise (see Fig. 1).

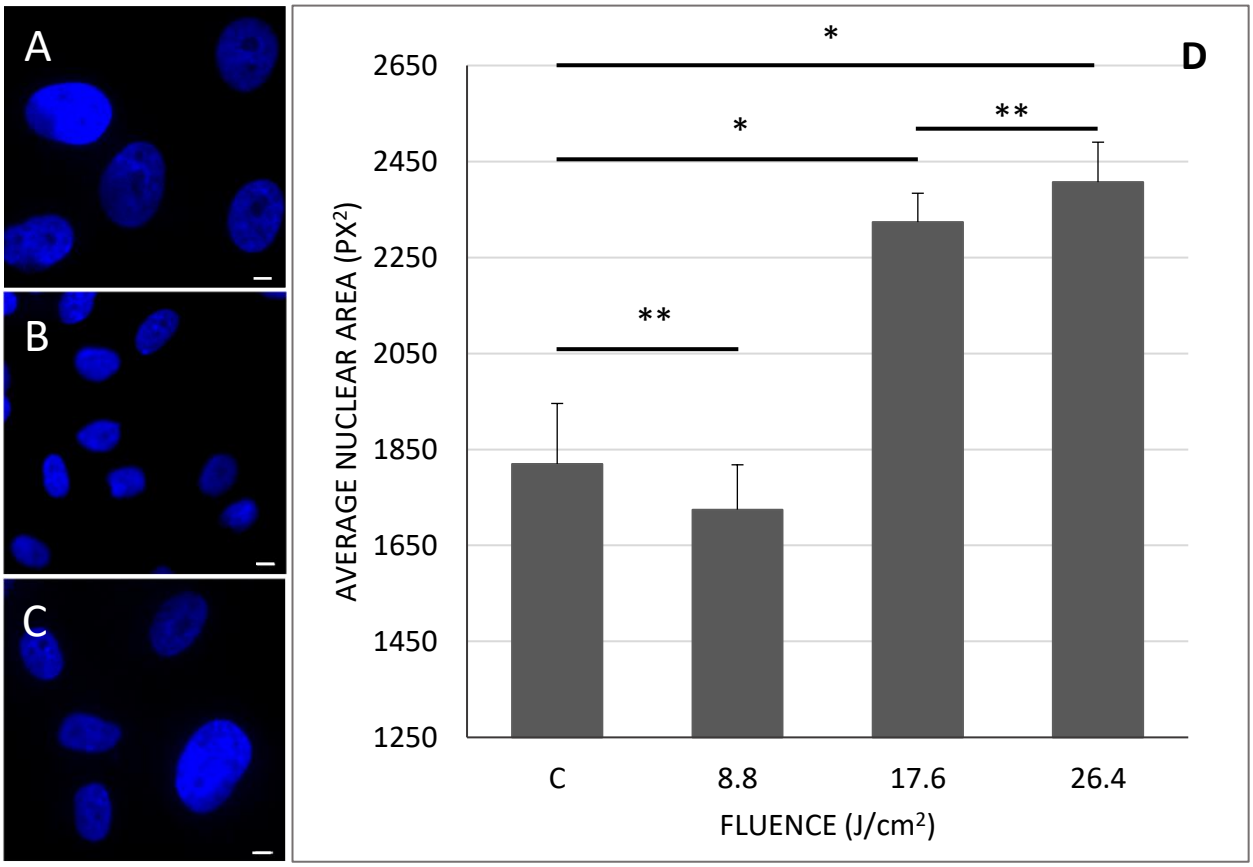

Figure 3. 3. *Example images of change in nuclear shape from MSCs unexposed to adipogenic induction medium or laser irradiation (A), seven days after adipogenic induction (B), and 26.4 J/cm² laser exposure 2 min/day after 7 days of differentiation (C). Average nuclei area of control and laser-irradiated groups with increasing fluence. Samples taken after 7 days of adipogenic differentiation (D). Scale bar = 15 µm. Data presented as mean ± SEM, n=3. * p < 0.05, ** p > 0.05.*

Time-dependent lipid production was recorded over the course of differentiation up to 9 days between control and PBM-exposed stem cells. Human MSCs exposed to PBM did not show an immediate increase in the lipid droplet level. However, by day 7 of the PBM treatment (17.6 J/cm^2), the hindered adipogenesis was evident (Fig. 4A). The time-dependent changes in the nucleus size was also monitored and correlated. It is interesting to note that the PBM-treated hMSCs maintained a relatively constant nuclear size over

the observation period of 9 days. In contrast, the control cells not exposed to PBM exhibited rapid changes by day 5 (Fig. 4B).

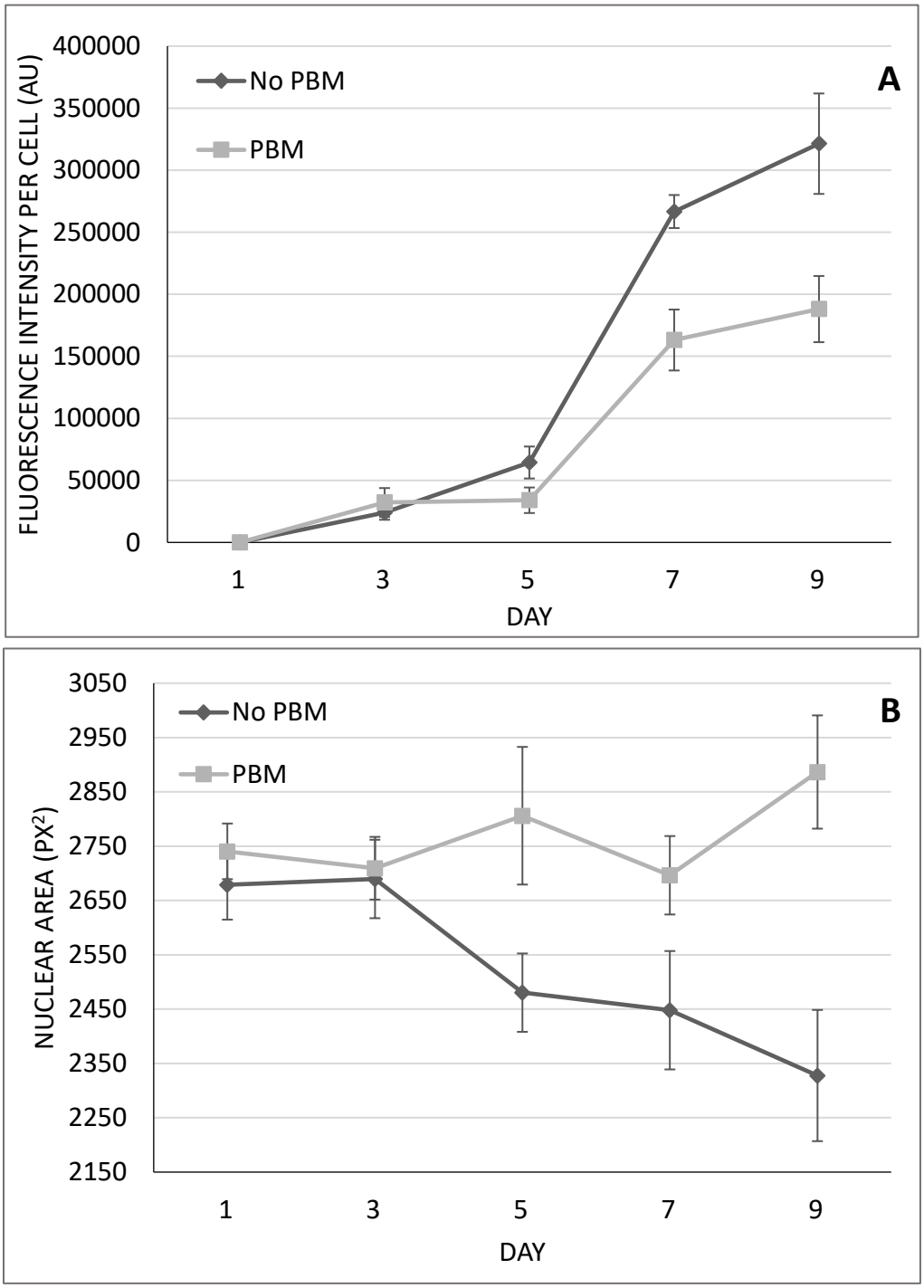

Figure 3. 4. *Comparison of lipid production determined by LipidTOX fluorescence intensity during adipogenic differentiation (A). Nuclear area in pixels of PBM and control groups (B). Laser-irradiated (PBM) group was exposed to a fluence of 17.6 J/cm² 2 min/day for 9 days. Data presented as mean ± SEM, n=3.*

These results indicate that there is (1) an inverse relationship between the extent of adipogenesis and the nuclear remodeling, and (2) PBM inhibits such nuclear remodeling that is required for and likely precedes adipogenesis. Lack of an upregulation of the lipid droplets in response to PBM could be attributed to the lipids potentially leaking out of the cells. We therefore performed negative control experiments in which the supernatants were collected and the level of triglyceride in the stem cell conditioned media was measured (Fig. 5). PBM treatment did not alter the triglyceride measurements over 15 days of adipogenesis, confirming the lipid droplet production was indeed decreased in response to PBM.

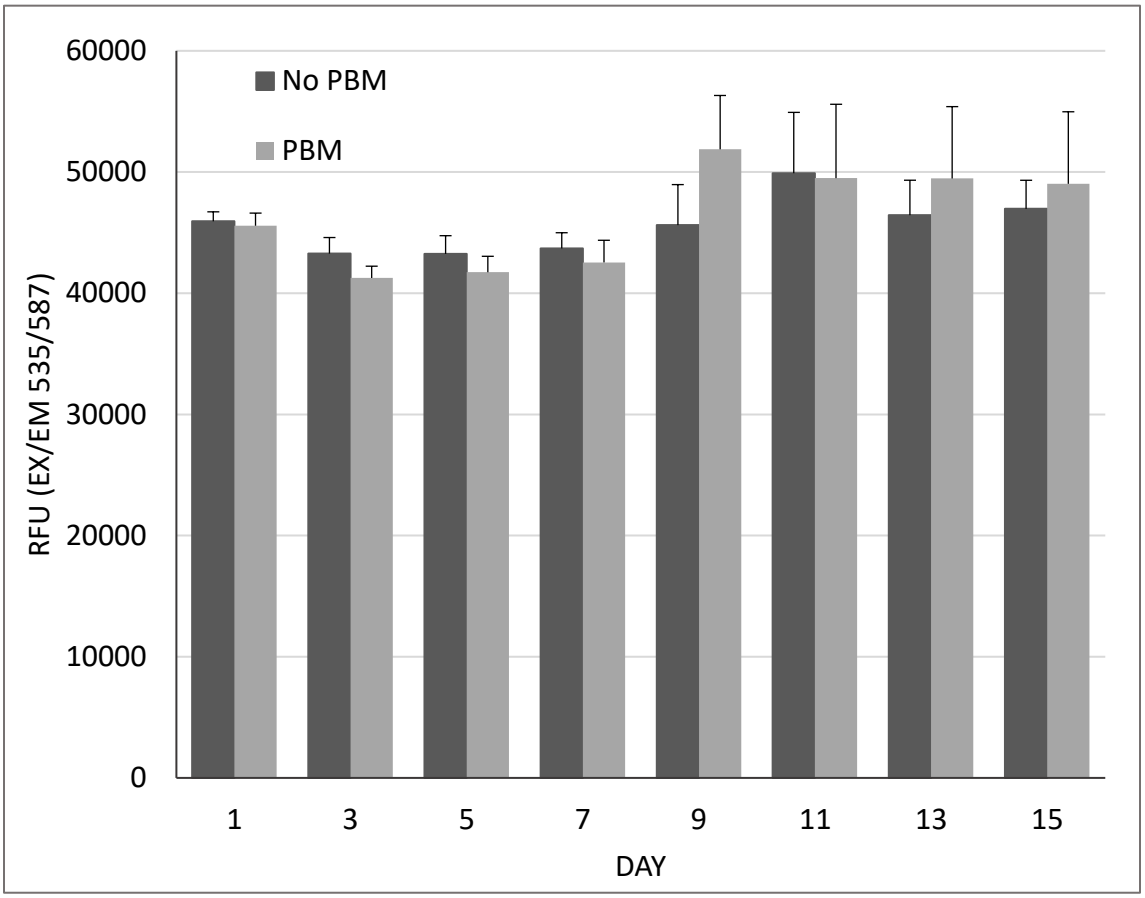

Figure 3. 5. *Triglyceride fluorescence intensity determined by Triglyceride Assay Kit (Abcam) in stem cell conditioned media through 15 days of adipogenic differentiation. Fluence = 17.6 J/cm^2. Data presented as mean ± SEM, n=3. No statistically significant differences were observed.*

2.3 RT-PCR

RT-PCR was used to determine the genetic profiles of the influence of PBM (1064 nm laser) while undergoing adipogenic differentiation. Interestingly, after 10 days of adipogenic differentiation, the major adipogenic markers such as PPARγ were significantly reduced in hMSCs exposed to 17.6 J/cm^2 (Fig. 6). Additionally, the expression of a ROS-associated enzyme gene (SOD2) was also examined. The SOD2 gene was upregulated ~ 20-fold, which suggests an increase in ROS-sequestering transcription.

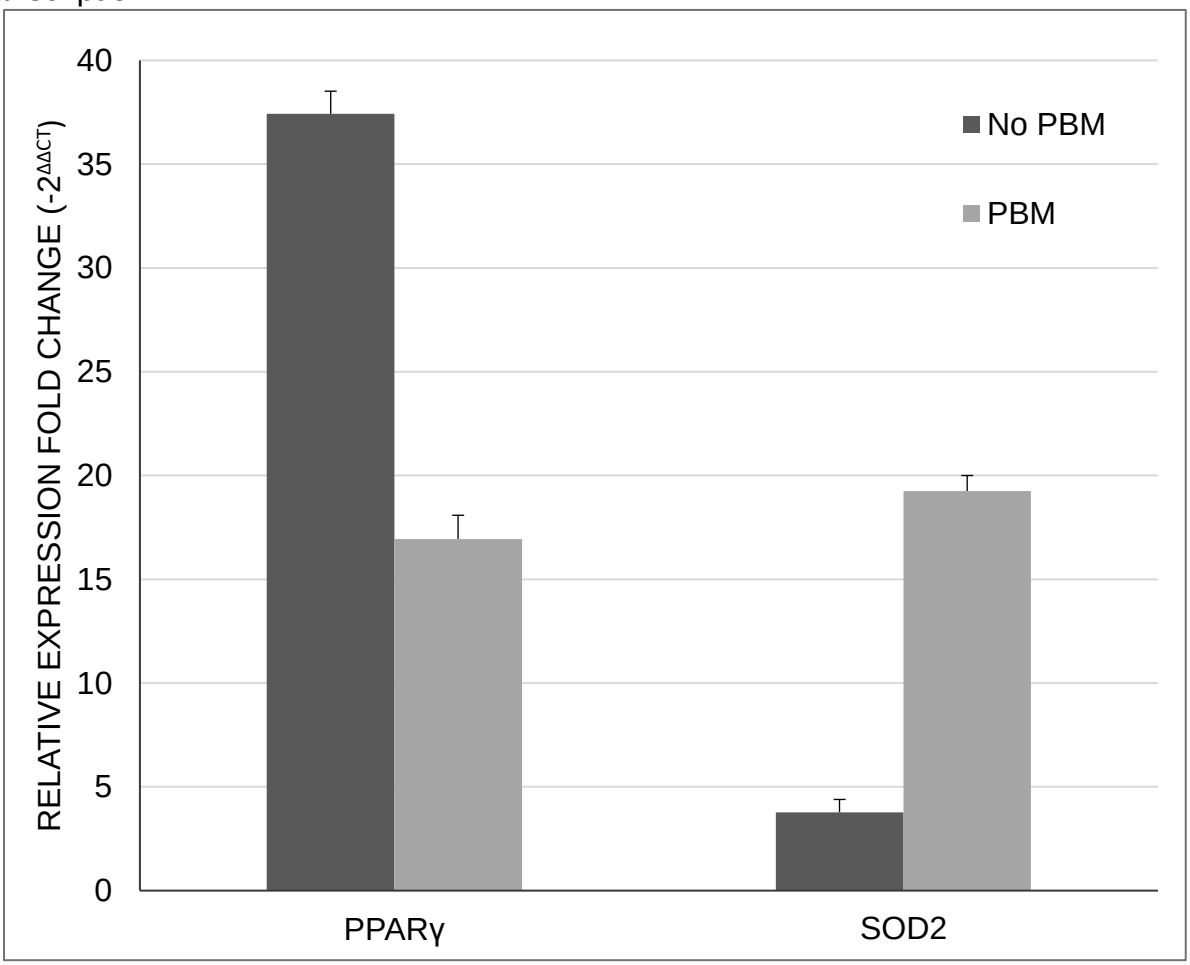

Figure 3. 6. *Relative expression of RNA production of adipogenic and ROS-sequestering genes. PBM group exposed to a fluence of 17.6J/cm^2 2 min/day for 10 days. Normalized to GAPDH, data presented as mean ± SEM, n=3.*

2.4 ATP and ROS Quantification

Since it is presumed that PBM targets CCO in mitochondria, ATP levels were quantified using luciferase luminescence. Each sample was prepared with the same cell density, and the levels of ATP were detected following PBM treatment. As shown in Figure 7, at the lowest fluence tested (8.8 J/cm^2), no significant difference was observed, which is consistent with the lack of adipogenesis. However, a higher fluence induced statistically significant difference in the ATP level.

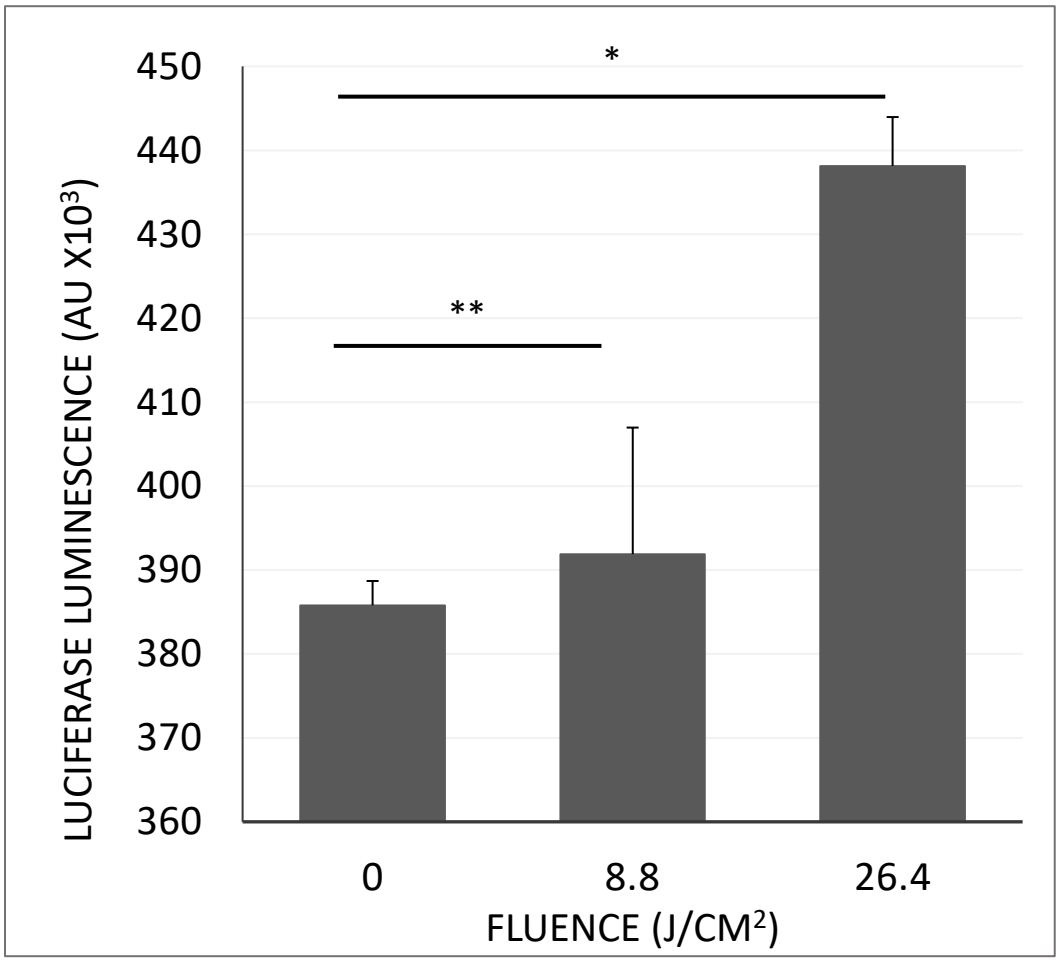

Figure 3. 7. *ATP quantification of MSCs determined by luciferase luminescence via CellTiter-Glo Assay (Promega). Cells irradiated for 2 minutes, incubated for 15 minutes, and then ATP was quantified using a plate reader. Data presented as mean ± SEM, n=5. * p < 0.05, ** p > 0.05*

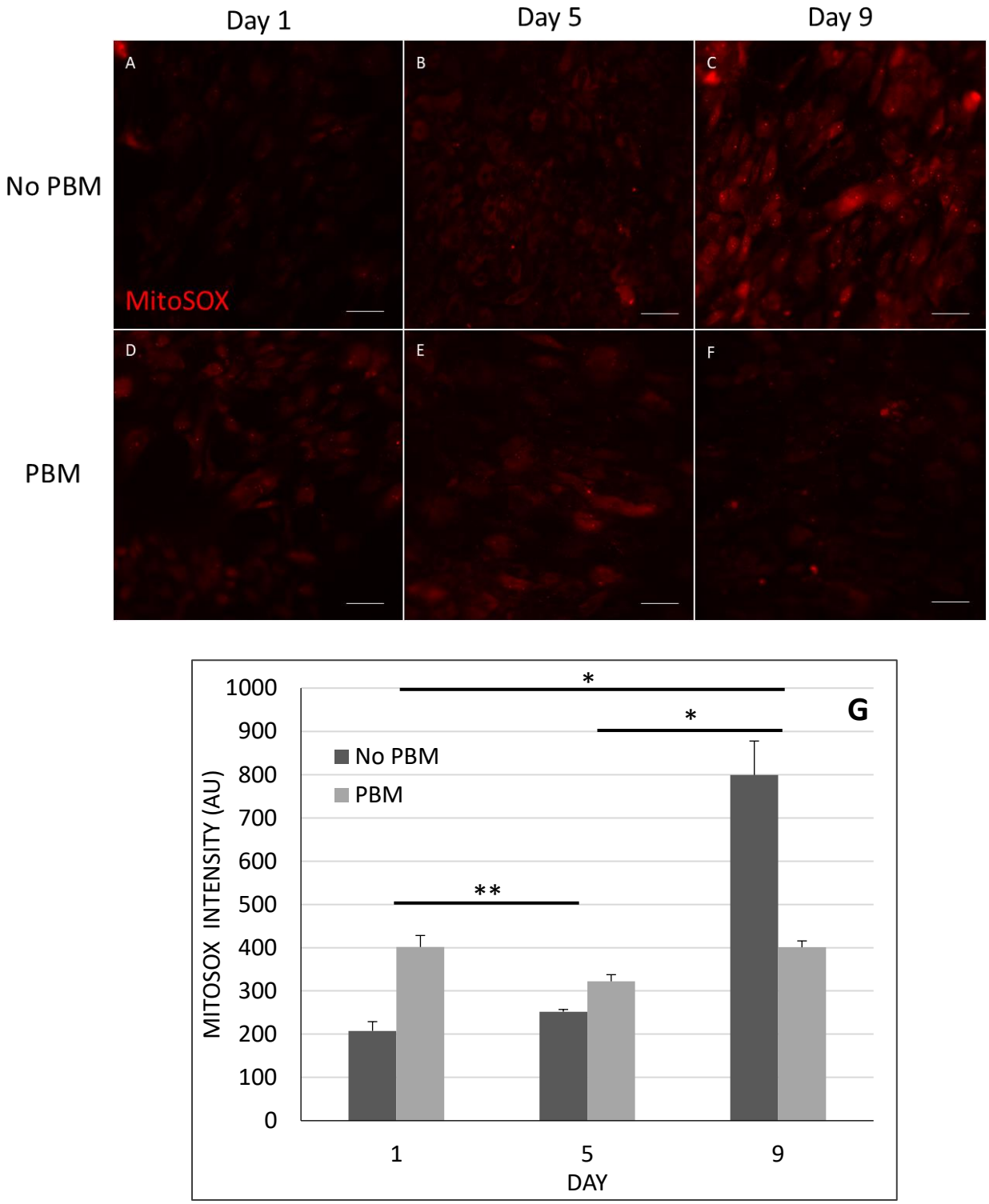

Figure 3. 8. *MitoSOX staining of MSCs during adipogenic differentiation taken at different days. During days 1, 5, and 9 without exposure MitoSOX staining begins lower, but increases as differentiation continues (A-C). Cells exposed to laser irradiation at a fluence of 17.6 J/cm^2 2 min/day every day show an overall lower amount of mitochondrial superoxide formation as differentiation proceeds (D-F). Scale bar = 50 µm. Quantification of MitoSOX fluorescence over differentiation shown in (G). Data presented as mean ± SEM, n=3. * p < 0.05, ** p > 0.05.*

Production of reactive oxygen species (ROS) was next observed during adipogenesis of both control and laser-irradiated groups. ROS levels have been previously determined to assist in adipogenesis of MSCs with levels increasing over time.[45] Mitochondrial superoxide levels were quantified using a specific fluorophore, MitoSOX. Fluorescent images show the superoxide level increased during normal adipogenesis, as expected (Fig. 8A to 8C). Conversely, in laser-irradiated treatment groups, the superoxide levels did not increase during adipogenic differentiation. Rather, the levels remained stable throughout the differentiation process (Fig. 8D to 8F), despite demonstrating a higher level initially in the early stage of adipogenesis when compared to the non-irradiated group (Fig. 8G). The superoxide level remained relatively unchanged over 9 days in response to PBM, but increased in normal adipogenesis as expected.[46]

2.5 Catalase Blocking

In order to confirm the effect of PBM on the overall levels of ROS, adipogenic differentiation of hMSCs was proceeded with the addition of the catalase enzyme-inhibitor 3-AT (2 mM). As 3-AT acts to reverse the effect of PBM by inhibiting the ROS-sequestering enzyme catalase to perform its function. The hypothesis was that addition of 3-AT would return adipogenesis to normal levels in PBM-treated hMSCs. Using the 17.6 J/cm^2 fluence, the production of lipid droplets was monitored as a function of time over 9 days (Fig. 9). The PBM- and 3-AT treated hMSCs were found to express the lipid droplets that are comparable to the control cells (e.g., no PBM treatment). There was no statistically significance difference, suggesting that PBM is indeed interfering with ROS-sequestering enzymes.

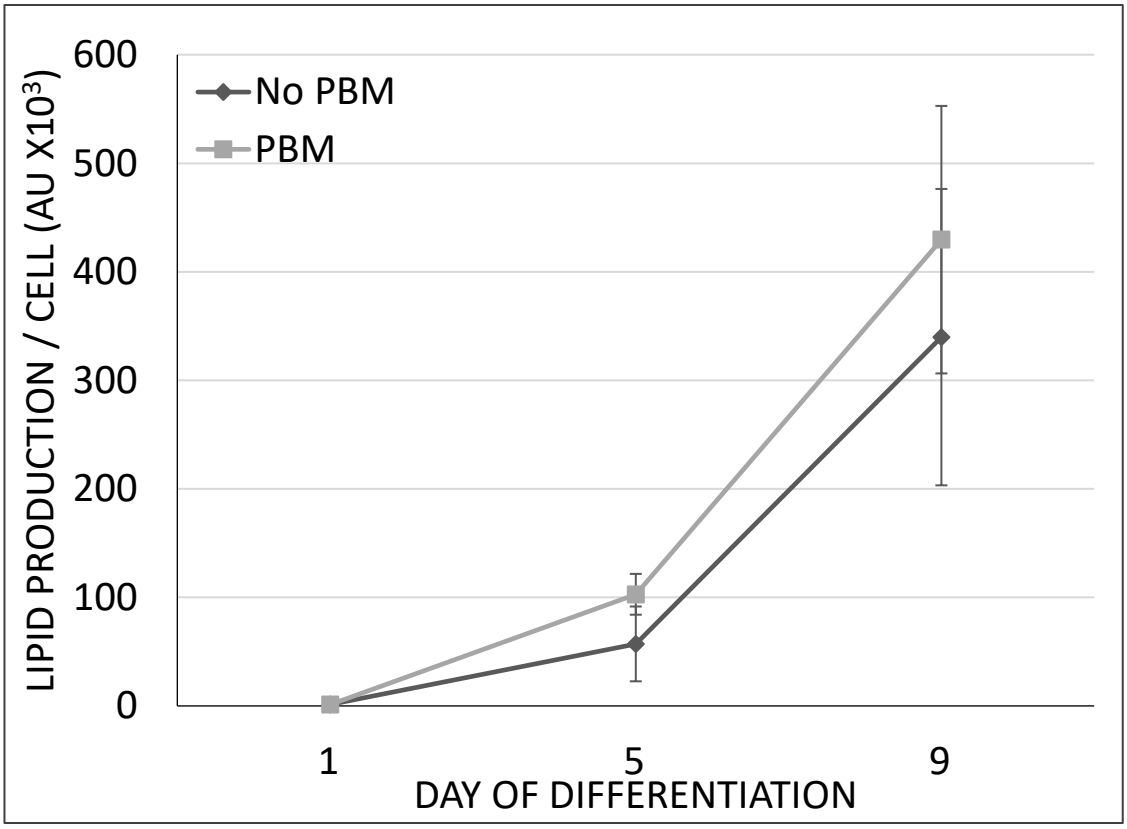

Figure 3. 9. *Comparison of lipid production determined by LipidTOX fluorescence intensity over 9 days of differentiation. hMSCs were exposed to 2 mM of the known catalase inhibitor 3-AT added in ADM media. Control group (no PBM) was also treated with the inhibitor, while the laser-irradiated (PBM) group was exposed to a fluence of 17.6 J/cm² 2 min/day every day. Data presented as mean ± SEM, n=3. No statistically significant difference was observed.*

Discussion

Obesity has rapidly emerged as one of the most important public health concerns with consequences ranging from diabetes, cardiovascular disease, and neoplasia. While diet and exercise are proven strategies for combating obesity, individuals still seek out other methods of fat removal. Methods such as liposuction and gastric band are expensive and invasive procedures requiring anesthesia and several days for recovery. Therefore, due to the cost and risks involved with surgery and recovery, great strides have recently been developed in the field of non-invasive fat-reducing techniques.

Photobiomodulation has previously been utilized as a method for fat reduction and body contouring, with several devices currently on the market. In one study, researchers exposed participant's waistlines with 635-680 nm laser light several times over the course of 4 weeks and found a significant reduction in waist girth.[47] Other studies have demonstrated fat reduction in hips, thighs, and arms due to treatment with PBM.[48-50] While the use of PBM to reduce fat and possibly mitigate the trend toward obesity has been documented, the mechanics behind PBM's effectiveness is less well understood. Originally, the fat-reducing capabilities of PBM was attributed to the formation of micropores on the adipocyte membrane, allowing the release of intracellular lipids.[51] However, this finding has been challenged by other studies that have failed to replicate the results.[52] Similarly, we demonstrated that hMSC-differentiated adipocytes exposed to PBM show no difference in the extracellular triglyceride levels compared to non-irradiated groups (see Fig. 5), suggesting the release of intracellular lipids may not be involved. Instead, we put forward a separate model for how light can influence fat production. This proposed model enhances activation of the mitochondria and its subsequent modulatory effects.

From the initial discovery of the multi-lineage potential of adult stem cells, modulation of their differentiation has taken many forms. What began as observing the effects of chemical induction quickly transformed into probing the influence of physical stimuli. Substrate properties, dynamic stretching, and 3-dimensional cell culture have all been examined regarding the differentiation of stem cells. Recently, a novel physical stimulation – that of the effect of light on biological tissues, or photobiomodulation – has

come into focus. PBM has been used previously in medicine demonstrating a variety of anti-inflammatory and wound healing effects.[14,15] In terms of stem cell differentiation, the coupling mechanisms of PBM may lead directly into the lineage potential of MSCs. Cytochrome c oxidase (CCO), the terminal enzyme of the electron transport chain, acts as the main contributor to the effect of PBM. In acting as a photo-acceptor, inhibitory nitric oxide (NO) dissociates from CCO, ultimately resulting in an enhanced flux through the electron transport chain. This mechanism provides three main outcomes; (1) an increase in ATP production; (2) a temporary increase in ROS; and (3) the downstream effects of NO release. Taken together these would likely affect the differentiation potential and lineage commitment of MSCs. While several groups have examined shorter wavelengths of NIR light on osteogenic differentiation,[28,29] we have yet to find confirmation of the effects of 1064 nm laser light on adipogenic differentiation. It should be noted here there emerged an alternate physical mechanism that was proposed by few research groups.[53] Their findings suggest localized heating of mitochondria or other organelles is possible, and that thermally-induced activation of mitochondria or temperature-sensitive ion channels should not readily be neglected.[30] Our laboratory is currently exploring high-resolution thermal imaging techniques to verify the thermal mechanism.

The first of the three effects of PBM – an increase in ATP production – follows the increase in mitochondrial respiration. Several groups have investigated the influence of light on ATP production, and have come to the similar conclusion of an overall increase in response to laser exposure.[54,55] Indeed, as determined and reported here, hMSCs also respond to light with increasing ATP levels in an energy-dependent manner. Interestingly,

a significant rise in ATP can be found as early as 15 min following PBM (see Fig. 7). A rise in mitochondrial activity and ATP levels may lead to a host of downstream effects. ATP is the primary energy source for cellular functions and its modulation opens the door for the activation of cellular processes. PBM has been shown to influence several cellular mechanisms including migration, proliferation, and wound healing, all implicated as ATP-dependent processes.[56-58] In stem cells, levels of ATP can influence and direct the cell's differentiation capability.[59] As cell metabolism and oxygen demands in undifferentiated MSCs are low, ATP levels are comparatively low as well.[60] As MSCs differentiate, their energy demands change and, depending on the cell type, switch from primarily glycolysis to oxidative phosphorylation.[61] It has been shown that preventing this switch retains the cell's stem-ness, while activating oxidative phosphorylation may inhibit the cell's ability to differentiate.[62]

Interestingly, PBM also was demonstrated to influence the nuclear size during differentiation. As previously described, the nucleus is remodeled over the course of lineage maturation into chemically-driven adipocytes. It became consistently smaller and more elongated in shape.[39] In contrast, PBM inhibited such changes of nuclei. Instead, the size of nuclei remained essentially constant over time (Fig. 4B). It is plausible then that PBM may have prevented or inhibited the morphologically-induced upregulation of adipogenic genes necessary for differentiation. As chromatin is organized within the nucleus, deliberate modifications of nuclear shape have been shown to modulate the subsequent activation or deactivation of relevant genes.[63,64] In adipogenesis, our previous work has demonstrated that such modification is brought about by dissociation of F-actins

from the nuclear membrane, as well as modulation of the structural nuclear envelope protein lamin A/C (LMNA).[65,66] Cytoskeletal involvement in the PBM-treated cells is evidenced by Houreld et al,[67] who showed the genetic regulation of several cell adhesion and cytoskeletal molecules are influenced by exposure to laser light. Future experiments identifying the effect of PBM on the cytoskeletal structure over differentiation into multiple different lineages would further advance the current understanding of PBM.

A natural byproduct of enhanced mitochondrial respiration is the production of mitochondrial superoxides.[68] These highly-charged molecules are detrimental to cell survival and can generate DNA damage and influence cell survival.[69] Because of its destructive potential, the cell retains several processes to sequester and eliminate ROS before irreversible cellular damage can be induced. Enzymes such as superoxide dismutase (SOD), catalase (CAT), and glutathione peroxidase (GPx) work together to limit the damage caused by high levels of ROS. More specifically, SOD and CAT work in tandem as part of a chain to reduce mitochondrial superoxide to the final product of oxygen and water.[70] When PBM is applied to hMSCs, we observed an immediate increase in ROS formation, shown by increased fluorescence of the mitochondrial superoxide indicator, MitoSOX. It can be inferred that this early increase, as well as that of ATP, is transient as the aforementioned enzymes work to reduce the levels of ROS to normal levels. Over the course of repeated daily PBM exposure, the cell begins to adapt by modulating levels of the superoxide-sequestering enzymes SOD and CAT. As shown in Figure 8, fluorescently-visualized superoxide levels change during PBM-exposed differentiation compared to control. Initially the levels of ROS are higher in the laser-

irradiated groups, but over time as the cell's strategy for combating ROS levels is implemented and the ROS levels remain relatively constant throughout the adipogenic differentiation.

ROS levels have also been shown to influence stem cell differentiation. As others have described in more detail, superoxide formation is an important factor in adipogenesis of MSCs.[26] As adipogenesis continues, ROS levels increase accordingly. The converse appears to be just as effective in that exogenous ROS has been utilized to enhance differentiation toward adipocytes and away from osteo- or chondro-genic lineages.[71,72] Therefore, it can be inferred that the continued irradiation from PBM over time – and the subsequent modulation of ROS-sequestering enzymes that arises as a result – causes an overall reduction in ROS levels. The reduction of superoxide levels is thought to hinder and slow the progression and differentiation efficiency.[73,74] In order to fully examine the mechanistic influence of PBM on superoxide levels, we attempted to disrupt the chain of reactions reducing superoxide to oxygen and water by blocking the activity of catalase (CAT). If the activity of SOD and CAT is modulated by PBM as suggested, blocking CAT should then serve to "rescue" adipogenesis to normal levels. This hypothesis was validated by the treatment of hMSCs with a competitive inhibitor of CAT (3-AT), which restored the lipid levels similar to that observed in normally differentiation stem cells without PBM. If the proposed mechanism of PBM is through a reduction in ROS levels during adipogenesis, PBM should serve to stimulate osteogenic differentiation. Indeed, this has been described by several groups examining the influence of PBM on osteogenesis.[29,75-76]

One of the goals of undertaking the current study was to examine the potential wavelength and lineage-dependency of the ability of PBM to affect stem cell differentiation. For example, several researchers have used shorter wavelengths of red and near-infrared light to direct osteogenic and chondrogenic differentiation. The shorter wavelength is beneficial in its specificity to the absorption spectrum of the CCO protein.[13] Similar to what has been examined here, researchers have implicated CCO activity, ATP increase, and ROS signaling as drivers of the altered differentiation capability brought about by the influence of laser light. In addition, these groups have implicated several signaling cascades which are modulated in response to the above changes. NF-κB,[77] Wnt/β-catenin,[78] and altered calcium signaling[79] have all been associated as contributors to the overall reaction of differentiating stem cells to PBM. Regarding adipogenesis specifically, few groups have examined the effect of PBM on differentiation capacity. In support of our findings here, Zhang et al., have also shown a reduction in adipogenic differentiation on stem cells exposed to laser light, potentially attributed to an alteration in ANT/Wnt/β-catenin signaling.[80]It has been suggested that longer wavelengths (> 900 nm) relies on activation of heat-gated ion channels brought on by heating of intracellular water.[81] Here, we attempted to mitigate the influence of heat by limiting bulk temperature change to 1 °C or less. However, further studies are warranted to investigate the cell-level resolution of temperature changes during application of PBM. Nevertheless, it appears that PBM could be selectively chosen to either hinder or facilitate the intended stem cell differentiation. Selection of the PBM parameters includes the wavelength, fluence, and also the lineage of intended stem cell differentiation. Much more work is warranted as the

coupling mechanisms of PBM may not be uniformly applicable but would have to tuned to the intracellular machineries that appear to interpret the PBM stimulation in divergent ways.

Conclusion

Here we have described a novel method to influence stem cell adipogenic differentiation using 1064 nm laser light. While the mechanisms behind PBM remain to be fully elucidated, we presented evidence of the influence of ATP generation and ROS modulation on the stem cell commitment to adipogenic lineage. Repeated irradiation by near-infrared laser light increases the mitochondrial activity, and as a result ATP and ROS levels are transiently increased. ATP levels directly influence several cellular processes including differentiation. As high ROS levels can damage cellular components, the cell's ROS-sequestering enzymes are modified, resulting in a better management of superoxide and an overall reduction in quantity. A reduction in ROS levels has previously been shown to reduce adipogenic differentiation as determined by lipid production. Furthermore, in an effort to demonstrate the influence of PBM on ROS levels, we blocked the mechanism of the superoxide-reducing agent catalase. Blocking CAT indeed restored the lipid levels to within the margin of error in comparison to the control group, suggesting no significant differences between the two. We postulate a multi-process mechanism of the PBM influence on stem cell differentiation that involves the cellular regulation of ATP and reactive oxygen species over time. It is not difficult to envision that both ATP and ROS are likely to impact the nuclear interactions. It is interesting to contemplate and perhaps speculate the potential PBM-induced signaling pathways that can modulate the nucleus' structure and function.

References

1. Minguell JJ, Erices A, Conget P. Mesenchymal stem cells. *Exp Biology Medicine Maywood N J*. 2001;226(6):507-520. doi:10.1177/153537020122600603

2. Chamberlain G, Fox J, Ashton B, Middleton J. Concise Review: Mesenchymal Stem Cells: Their Phenotype, Differentiation Capacity, Immunological Features, and Potential for Homing. *Stem Cells*. 2007;25(11):2739-2749. doi:10.1634/stemcells.2007-0197

3. Engler AJ, Sen S, Sweeney HL, Discher DE. Matrix Elasticity Directs Stem Cell Lineage Specification. *Cell*. 2006;126(4):677-689. doi:10.1016/j.cell.2006.06.044

4. Zhao W, Li X, Liu X, Zhang N, Wen X. Effects of substrate stiffness on adipogenic and osteogenic differentiation of human mesenchymal stem cells. *Mater Sci Eng C Mater Biological Appl*. 2014;40(Blood Cells 4 1978):316-323. doi:10.1016/j.msec.2014.03.048

5. Mao AS, Shin J-W, Mooney DJ. Effects of substrate stiffness and cell-cell contact on mesenchymal stem cell differentiation. *Biomaterials*. 2016;98(Curr. Opin. Pharm. 6 4 2006):184-191. doi:10.1016/j.biomaterials.2016.05.004

6. Kilian KA, Bugarija B, Lahn BT, Mrksich M. Geometric cues for directing the differentiation of mesenchymal stem cells. *P Natl Acad Sci Usa*. 2010;107(11):4872-4877. doi:10.1073/pnas.0903269107

7. Anders JJ, Lanzafame RJ, Arany PR. Low-Level Light/Laser Therapy Versus Photobiomodulation Therapy. *Photomed Laser Surg*. 2015;33(4):183-184. doi:10.1089/pho.2015.9848

8. Freitas LF de, Hamblin MR. Proposed Mechanisms of Photobiomodulation or Low-Level Light Therapy. *Ieee J Sel Top Quantum Electron Publ Ieee Lasers Electro-optics Soc*. 2016;22(3):348-364. doi:10.1109/jstqe.2016.2561201

9. Tasumi, M. Chapter 1: Introduction to Infrared Spectroscopy. In: ed Tasumi, M. Introduction to Experimental Infrared Spectroscopy: Fundamentals and Practical Methods. Hoboken, NJ: John Wiley and Sons; 2014: 33-59.

10. Fekrazad R, Asefi S, Allahdadi M, Kalhori KAM. Effect of Photobiomodulation on Mesenchymal Stem Cells. *Photomed Laser Surg*. 2016;34(11):533-542. doi:10.1089/pho.2015.4029

11. Hamblin MR. Mechanisms and Mitochondrial Redox Signaling in Photobiomodulation. *Photochem Photobiol*. 2018;94(2):199-212. doi:10.1111/php.12864

12. Linares SN, Beltrame T, Ferraresi C, Galdino GAM, Catai AM. Photobiomodulation effect on local hemoglobin concentration assessed by near-infrared spectroscopy in humans. *Laser Med Sci*. 2019:1-9. doi:10.1007/s10103-019-02861-x

13. Karu TI. Cellular and Molecular Mechanisms of Photobiomodulation (Low-Power Laser Therapy). *Ieee J Sel Top Quant*. 2014;20(2):143-148. doi:10.1109/jstqe.2013.2273411

14. Enwemeka CS, Parker JC, Dowdy DS, Harkness EE, Harkness LE, Woodruff LD. The Efficacy of Low-Power Lasers in Tissue Repair and Pain Control: A Meta-Analysis Study. *Photomed Laser Surg*. 2004;22(4):323-329. doi:10.1089/pho.2004.22.323

15. Amaroli A, Ravera S, Baldini F, Benedicenti S, Panfoli I, Vergani L. Photobiomodulation with 808-nm diode laser light promotes wound healing of human endothelial cells through increased reactive oxygen species production stimulating mitochondrial oxidative phosphorylation. *Laser Med Sci*. 2018;34(3):495-504. doi:10.1007/s10103-018-2623-5

16. Wang X, Tian F, Reddy DD, et al. Up-regulation of cerebral cytochrome-c-oxidase and hemodynamics by transcranial infrared laser stimulation: A broadband near-infrared spectroscopy study. *J Cereb Blood Flow Metabolism Official J Int Soc Cereb Blood Flow Metabolism*. 2017;37(12):3789-3802. doi:10.1177/0271678x17691783

17. Hamblin MR. Mechanisms and applications of the anti-inflammatory effects of photobiomodulation. *Aims Biophysics*. 2017;4(3):337-361. doi:10.3934/biophy.2017.3.337

18. Chrzanowskalightowlers ZMA, Turnbull DM, Lightowlers RN. A Microtiter Plate Assay for Cytochrome c Oxidase in Permeabilized Whole Cells. *Anal Biochem*. 1993;214(1):45-49. doi:10.1006/abio.1993.1454

19. Beard DA. A Biophysical Model of the Mitochondrial Respiratory System and Oxidative Phosphorylation. *Plos Comput Biol*. 2005;1(4):e36. doi:10.1371/journal.pcbi.0010036

20. Selivanov VA, Votyakova TV, Pivtoraiko VN, et al. Reactive oxygen species production by forward and reverse electron fluxes in the mitochondrial respiratory chain. *Plos Comput Biol*. 2011;7(3):e1001115. doi:10.1371/journal.pcbi.1001115

21. Sena LA, Chandel NS. Physiological roles of mitochondrial reactive oxygen species. *Mol Cell*. 2012;48(2):158-167. doi:10.1016/j.molcel.2012.09.025

22. Temple MD, Perrone GG, Dawes IW. Complex cellular responses to reactive oxygen species. *Trends Cell Biol*. 2005;15(6):319-326. doi:10.1016/j.tcb.2005.04.003

23. Powers SK, Duarte J, Kavazis AN, Talbert EE. Reactive oxygen species are signalling molecules for skeletal muscle adaptation. *Exp Physiol*. 2009;95(1):1-9. doi:10.1113/expphysiol.2009.050526

24. Shum LC, White NS, Mills BN, Bentley KL de M, Eliseev RA. Energy Metabolism in Mesenchymal Stem Cells During Osteogenic Differentiation. *Stem Cells Dev*. 2015;25(2):114-122. doi:10.1089/scd.2015.0193

25. Zhang Y, Marsboom G, Toth PT, Rehman J. Mitochondrial respiration regulates adipogenic differentiation of human mesenchymal stem cells. *Plos One*. 2013;8(10):e77077. doi:10.1371/journal.pone.0077077

26. Lin C-H, Li N-T, Cheng H-S, Yen M-L. Oxidative stress induces imbalance of adipogenic/osteoblastic lineage commitment in mesenchymal stem cells through decreasing SIRT1 functions. *J Cell Mol Med*. 2017;22(2):786-796. doi:10.1111/jcmm.13356

27. James AW. Review of Signaling Pathways Governing MSC Osteogenic and Adipogenic Differentiation. *Sci*. 2013;2013:1-17. doi:10.1155/2013/684736

28. Tani A, Chellini F, Giannelli M, Nosi D, Zecchi-Orlandini S, Sassoli C. Red (635 nm), Near-Infrared (808 nm) and Violet-Blue (405 nm) Photobiomodulation Potentiality on Human Osteoblasts and Mesenchymal Stromal Cells: A Morphological and Molecular In Vitro Study. *Int J Mol Sci*. 2018;19(7):1946. doi:10.3390/ijms19071946

29. Wang Y, Huang Y-Y, Wang Y, Lyu P, Hamblin MR. Photobiomodulation (blue and green light) encourages osteoblastic-differentiation of human adipose-derived stem cells: role of intracellular calcium and light-gated ion channels. *Sci Rep-uk*. 2016;6(1):33719. doi:10.1038/srep33719

30. Hamblin MR. Shining light on the head: Photobiomodulation for brain disorders. *Bba Clin*. 2016;6(N. Engl. J. Med. 273 1965):113-124. doi:10.1016/j.bbacli.2016.09.002

31. Ayuk SM, Abrahamse H, Houreld NN. The Role of Matrix Metalloproteinases in Diabetic Wound Healing in relation to Photobiomodulation. *J Diabetes Res*. 2016;2016:2897656. doi:10.1155/2016/2897656

32. Tian F, Hase SN, Gonzalez-Lima F, Liu H. Transcranial laser stimulation improves human cerebral oxygenation. *Laser Surg Med*. 2016;48(4):343-349. doi:10.1002/lsm.22471

33. Ramalho KM, Freitas PM de, Correa-Aranha AC, Bello-Silva MS, Lopes RM da G, Eduardo C de P. Lasers in esthetic dentistry: soft tissue photobiomodulation, hard tissue decontamination, and ceramics conditioning. *Case Reports Dent*. 2014;2014:927429. doi:10.1155/2014/927429

34. Zein R, Selting W, Hamblin MR. Review of light parameters and photobiomodulation efficacy: dive into complexity. *J Biomed Opt.* 2018;23:1–17. doi:10.1117/1.jbo.23.12.120901.

35. Wang X, Dmochowski JP, Zeng L, Kallioniemi E, Husain M, Gonzalez-Lima F, et al. Transcranial photobiomodulation with 1064-nm laser modulates brain electroencephalogram rhythms. *Proc Spie*. 2019;6:1. doi:10.1117/1.nph.6.2.025013.

36. Pruitt T, Wang X, Wu A, Kallioniemi E, Husain MM, Liu H. Transcranial Photobiomodulation (tPBM) With 1,064-nm Laser to Improve Cerebral Metabolism of the Human Brain In Vivo. *Laser Surg Med*. 2020. doi:10.1002/lsm.23232.

37. Gonzalez-Lima F, Rojas. Low-level light therapy of the eye and brain. *Eye Brain.* 2011;3:49–67. doi:10.2147/eb.s21391.

38. Titushkin I, Sun S, Paul A, Cho M. Control of adipogenesis by ezrin, radixin and moesin-dependent biomechanics remodeling. *J Biomech*. 2013;46(3):521-526. doi:10.1016/j.jbiomech.2012.09.027

39. McColloch A, Rabiei M, Rabbani P, Bowling A, Cho M. Correlation between Nuclear Morphology and Adipogenic Differentiation: Application of a Combined Experimental and Computational Modeling Approach. *Sci Rep-uk*. 2019;9(1):16381. doi:10.1038/s41598-019-52926-8

40. Sarrafzadeh O, Dehnavi A. Nucleus and cytoplasm segmentation in microscopic images using K-means clustering and region growing. *Advanced Biomedical Research.* 2015;4.

41. Walton PA, Pizzitelli M. Effects of peroxisomal catalase inhibition on mitochondrial function. *Front Physiol*. 2012;3:108. doi:10.3389/fphys.2012.00108

42. Livak KJ, Schmittgen TD. Analysis of Relative Gene Expression Data Using Real-Time Quantitative PCR and the 2−ΔΔC T Method. *Methods*. 2001;25(4):402-408. doi:10.1006/meth.2001.1262

43. Chen J, Shi Z-D, Ji X, et al. Enhanced osteogenesis of human mesenchymal stem cells by periodic heat shock in self-assembling peptide hydrogel. *Tissue Eng Part*. 2012;19(5-6):716-728. doi:10.1089/ten.tea.2012.0070

44. Ikuta K, Urakawa H, Kozawa E, et al. In vivo heat-stimulus-triggered osteogenesis. *Int J Hyperth Official J European Soc Hyperthermic Oncol North Am Hyperth Group*. 2014;31(1):58-66. doi:10.3109/02656736.2014.988662

45. Lee O-H, Kwon Y-I, Hong H-D, Park C-S, Lee B-Y, Kim Y-C. Production of Reactive Oxygen Species and Changes in Antioxidant Enzyme Activities during Differentiation of 3T3-L1 Adipocyte. *J Korean Soc Appl Bi*. 2009;52(1):70-75. doi:10.3839/jksabc.2009.012

46. Kanda Y, Hinata T, Kang SW, Watanabe Y. Reactive oxygen species mediate adipocyte differentiation in mesenchymal stem cells. *Life Sci*. 2011;89(7-8):250-258. doi:10.1016/j.lfs.2011.06.007

47. Caruso-Davis MK, Guillot TS, Podichetty VK, et al. Efficacy of low-level laser therapy for body contouring and spot fat reduction. *Obes Surg*. 2011;21(6):722-729. doi:10.1007/s11695-010-0126-y

48. McRae E, Boris J. Independent evaluation of low-level laser therapy at 635 nm for non-invasive body contouring of the waist, hips, and thighs. *Laser Surg Med*. 2013;45(1):1-7. doi:10.1002/lsm.22113

49. Jackson RF, Dedo DD, Roche GC, Turok DI, Maloney RJ. Low-level laser therapy as a non-invasive approach for body contouring: a randomized, controlled study. *Laser Surg Med*. 2009;41(10):799-809. doi:10.1002/lsm.20855

50. Jackson RF, Stern FA, Neira R, Ortiz-Neira CL, Maloney J. Application of Low-Level Laser Therapy for Noninvasive Body Contouring. *Laser Surg Med*. 2012;44(3):211-217. doi:10.1002/lsm.22007

51. Neira R, Arroyave J, Ramirez H, et al. Fat Liquefaction: Effect of Low-Level Laser Energy on Adipose Tissue. *Plast Reconstr Surg*. 2002;110(3):912-922. doi:10.1097/01.prs.0000019876.96703.ae

52. Medrado AP, Trindade E, Reis SRA, Andrade ZA. Action of low-level laser therapy on living fatty tissue of rats. *Laser Med Sci*. 2006;21(1):19-23. doi:10.1007/s10103-005-0367-5

53. Oron U, Ilic S, Taboada LD, Streeter J. Ga-As (808 nm) Laser Irradiation Enhances ATP Production in Human Neuronal Cells in Culture. *Photomed Laser Surg*. 2007;25(3):180-182. doi:10.1089/pho.2007.2064

54. Quirk BJ, Sannagowdara K, Buchmann EV, Jensen ES, Gregg DC, Whelan HT. Effect of near-infrared light on in vitro cellular ATP production of osteoblasts and fibroblasts and on fracture healing with intramedullary fixation. *J Clin Orthop Trauma*. 2016;7(4):234-241. doi:10.1016/j.jcot.2016.02.009

55. Ferraresi C, Kaippert B, Avci P, et al. Low-level Laser (Light) Therapy Increases Mitochondrial Membrane Potential and ATP Synthesis in C2C12 Myotubes with a Peak Response at 3-6 h. *Photochem Photobiol*. 2014;91(2):411-416. doi:10.1111/php.12397

56. Horssen R van, Janssen E, Peters W, et al. Modulation of cell motility by spatial repositioning of enzymatic ATP/ADP exchange capacity. *J Biological Chem*. 2008;284(3):1620-1627. doi:10.1074/jbc.m806974200

57. Lee DG, Bell SP. ATPase switches controlling DNA replication initiation. *Curr Opin Cell Biol*. 2000;12(3):280-285. doi:10.1016/s0955-0674(00)00089-2

58. Chiang B, Essick E, Ehringer W, et al. Enhancing skin wound healing by direct delivery of intracellular adenosine triphosphate. *Am J Surg*. 2007;193(2):213-218. doi:10.1016/j.amjsurg.2006.08.069

59. Birket MJ, Orr AL, Gerencser AA, et al. A reduction in ATP demand and mitochondrial activity with neural differentiation of human embryonic stem cells. *J Cell Sci*. 2011;124(Pt 3):348-358. doi:10.1242/jcs.072272

60. Ito K, Suda T. Metabolic requirements for the maintenance of self-renewing stem cells. *Nat Rev Mol Cell Biology*. 2014;15(4):243-256. doi:10.1038/nrm3772

61. Chen C-T, Shih Y-RV, Kuo TK, Lee OK, Wei Y-H. Coordinated changes of mitochondrial biogenesis and antioxidant enzymes during osteogenic differentiation of human mesenchymal stem cells. *Stem Cells Dayt Ohio*. 2008;26(4):960-968. doi:10.1634/stemcells.2007-0509

62. Buravkova LB, Rylova YV, Andreeva ER, et al. Low ATP level is sufficient to maintain the uncommitted state of multipotent mesenchymal stem cells. *Biochim Biophys Acta*. 2013;1830(10):4418-4425. doi:10.1016/j.bbagen.2013.05.029

63. Lanctôt C, Cheutin T, Cremer M, Cavalli G, Cremer T. Dynamic genome architecture in the nuclear space: regulation of gene expression in three dimensions. *Nat Rev Genet*. 2007;8(2):104-115. doi:10.1038/nrg2041

64. Nguyen HQ, Bosco G. Gene Positioning Effects on Expression in Eukaryotes. *Annu Rev Genet*. 2015;49(1):627-646. doi:10.1146/annurev-genet-112414-055008

65. Guelen L, Pagie L, Brasset E, et al. Domain organization of human chromosomes revealed by mapping of nuclear lamina interactions. *Nature*. 2008;453(7197):948-951. doi:10.1038/nature06947

66. Kosak ST, Scalzo D, Alworth SV, et al. Coordinate Gene Regulation during Hematopoiesis Is Related to Genomic Organization. *Plos Biol*. 2007;5(11):e309. doi:10.1371/journal.pbio.0050309

67. Houreld NN, Sekhejane PR, Abrahamse H. Irradiation at 830 nm stimulates nitric oxide production and inhibits pro-inflammatory cytokines in diabetic wounded fibroblast cells. *Laser Surg Med*. 2010;42(6):494-502. doi:10.1002/lsm.20812

68. Dröse S, Brandt U. Advances in Experimental Medicine and Biology. In: Vol 748. Advances in experimental medicine and biology. ; 2012:145-169. https://doi.org/10.1007/978-1-4614-3573-0_6

69. Schenk B, Fulda S. Reactive oxygen species regulate Smac mimetic/TNFα-induced necroptotic signaling and cell death. *Oncogene*. 2015;34(47):5796-5806. doi:10.1038/onc.2015.35

70. Ighodaro OM, Akinloye OA. First line defence antioxidants-superoxide dismutase (SOD), catalase (CAT) and glutathione peroxidase (GPX): Their fundamental role in the entire antioxidant defence grid. *Alexandria J Medicine*. 2018;54(4):287-293. doi:10.1016/j.ajme.2017.09.001

71. Higuchi M, Dusting GJ, Peshavariya H, et al. Differentiation of human adipose-derived stem cells into fat involves reactive oxygen species and Forkhead box O1 mediated upregulation of antioxidant enzymes. *Stem Cells Dev*. 2012;22(6):878-888. doi:10.1089/scd.2012.0306

72. Almeida M, Han L, Martin-Millan M, O'Brien CA, Manolagas SC. Oxidative Stress Antagonizes Wnt Signaling in Osteoblast Precursors by Diverting β-Catenin from T Cell Factor- to Forkhead Box O-mediated Transcription. *J Biol Chem*. 2007;282(37):27298-27305. doi:10.1074/jbc.m702811200

73. Imhoff BR, Hansen JM. Extracellular redox environments regulate adipocyte differentiation. *Differ Res Biological Divers*. 2010;80(1):31-39. doi:10.1016/j.diff.2010.04.005

74. Lee O-H, Kwon Y-I, Apostolidis E, Shetty K, Kim Y-C. Rhodiola-induced inhibition of adipogenesis involves antioxidant enzyme response associated with pentose phosphate pathway. *Phytotherapy Res Ptr*. 2011;25(1):106-115. doi:10.1002/ptr.3236

75. Yang D, Yi W, Wang E, Wang M. Effects of light-emitting diode irradiation on the osteogenesis of human umbilical cord mesenchymal stem cells in vitro. *Sci Rep-uk*. 2016;6(1):37370. doi:10.1038/srep37370

76. Fekrazad R, Asefi S, Eslaminejad MB, Taghiar L, Bordbar S, Hamblin MR. Photobiomodulation with single and combination laser wavelengths on bone marrow mesenchymal stem cells: proliferation and differentiation to bone or cartilage. *Laser Med Sci*. 2018;34(1):115-126. doi:10.1007/s10103-018-2620-8

77. Chen AC-H, Arany PR, Huang Y-Y, et al. Low-level laser therapy activates NF-kB via generation of reactive oxygen species in mouse embryonic fibroblasts. *Plos One*. 2011;6(7):e22453. doi:10.1371/journal.pone.0022453

78. Kim JE, Woo YJ, Sohn KM, Jeong KH, Kang H. Wnt/β-catenin and ERK pathway activation: A possible mechanism of photobiomodulation therapy with light-emitting diodes that regulate the proliferation of human outer root sheath cells. *Laser Surg Med*. 2017;49(10):940-947. doi:10.1002/lsm.22736

79. Amaroli A, Benedicenti A, Ferrando S, et al. Photobiomodulation by Infrared Diode-Laser: Effects on Intracellular Calcium Concentration and Nitric Oxide Production of Paramecium. *Photochem Photobiol*. 2016;92(6):854-862. doi:10.1111/php.12644

80. Zhang R-F, Wang Q, Zhang A-A, et al. Low-level laser irradiation promotes the differentiation of bone marrow stromal cells into osteoblasts through the APN/Wnt/β-catenin pathway. *Eur Rev Med Pharmaco*. 2018;22(9):2860-2868. doi:10.26355/eurrev_201805_14988

81. Wang Y, Huang Y-Y, Wang Y, Lyu P, Hamblin MR. Photobiomodulation of human adipose-derived stem cells using 810nm and 980nm lasers operates via different mechanisms of action. *Biochim Biophys Acta*. 2016;1861(2):441-449. doi:10.1016/j.bbagen.2016.10.008

CHAPTER 4:

Photobiomodulation with NIR Laser Light Reduces Lipid Levels and Restores Glucose Transport Function of Hypertrophic Adipocytes in an *in vitro* Model of Obesity

Andrew McColloch, Hanli Liu, and Michael Cho

In Preparation for Publication

Abstract

Adipocyte hypertrophy, caused by the swelling of cells due to increased lipid volume, has been implicated in the progression of obesity-induced complications. Hypertrophic adipocytes cause release of free fatty acids and inflammatory cytokines, promote hypoxia and fibrosis, and limit insulin sensitivity. Photobiomodulation (PBM), or the influence of light on biological tissues, has previously been demonstrated to reduce lipid quantity in stem cells undergoing adipogenesis. Here, we characterize the effect of PBM on an *in vitro* hypertrophic obesity model and its influence on reduction of lipids and restoration of normal adipocyte function. Adipose-derived stem cells (ADSCs) were induced to hypertrophic adipocytes with the addition of palmitic acid (PA). Hypertrophy was confirmed with fluorescent imaging of lipid content, and functional changes were assessed using the fluorescent glucose analog 2-NBDG. Glucose transport into the cell was diminished and expression of glucose transporter GLUT4 was downregulated. The irradiated group was exposed to 1064 nm columnated laser at a fluence of 17.6 J/cm^2 every day for 7 days following addition of PA. When exposed to irradiation, lipid levels in hypertrophic adipocytes were decreased and levels of GLUT4 protein was restored. Functionally, irradiated adipocytes showed enhanced glucose transport compared to non-irradiated cells.

Key Terms: Adipose tissue, Diabetes, Fluorescent microscopy, Functional restoration, GLUT4, 2-NBDG, Reactive oxygen species (ROS), Mitochondria, Electron transport chain

Introduction

Obesity and metabolic disease have asserted themselves as a major concern for public health with complications resulting from heart disease to diabetes[21]. While a general treatment of diet and exercise exists for most, several individuals with genetic or additional complications still seek out other methods of fat removal. Surgical methods such as gastric band or liposuction are invasive and expensive procedures with the potential for additional complications. Consequently, great strides have been made in developing fat-reducing techniques that do not require invasive procedures.

Obesity carries with it a dysfunction in adipocyte physiology, characterized by hyperplasia (cell number increase) and hypertrophy (cell size increase)[18]. Several of the downstream effects of obesity – inflammation, insulin resistance, etc. – can be attributed to the abnormal cell size and function of hypertrophic adipocytes[31]. These dysregulated adipocytes cause the release of free fatty acids (FFAs) and pro-inflammatory cytokines, promote hypoxia, and reduce insulin sensitivity[36]. Additionally, it has been shown that hypertrophic adipocytes result in an increase in the level of reactive oxygen species (ROS)[8]. ROS are short-lived, volatile molecules with the potential to damage DNA and disrupt intracellular signaling[4].

One of the major functions of adipocyte is energy storage. To achieve this, glucose sequestration from the blood is initiated by insulin release, where it is then transformed into lipid, a more stable energy molecule. Although fatty tissue is not responsible for most of the body's insulin-stimulated glucose removal, its disfunction has been shown to lead

to whole body insulin resistance and progression to type 2 diabetes (DM2)[2, 6]. GLUT4 is the primary protein responsible for glucose transport in adipocytes and has been shown to be deteriorated in an oxidative and inflammatory microenvironment[12]. In obesity and type 2 diabetes, adipose levels of the transporter GLUT4 are diminished while expression in skeletal muscle remains stable[22]. Additionally, the ability for cells to take up glucose is inhibited due to an acquired resistance to insulin, brought about by dysregulation in GLUT4 trafficking[20]. Over time, this resistance increases to the DM2 disease state.

Recently, photobiomodulation (PBM) has been demonstrated to influence a wide range of cellular processes[19]. Commonly believed to be caused by activation of the photon-acceptor cytochrome c oxidase (CCO), PBM has been shown to increase cellular metabolism, enhance calcium signaling, and improve diabetic wound healing[1, 34, 39]. Previously, we have demonstrated the capability of PBM with NIR light to reduce the lipid content in mesenchymal stem cells undergoing adipogenic differentiation. This can be attributed to the activation of several cellular factors such as increased ATP production, and enhanced expression of ROS-sequestering enzymes[17].

PBM has been utilized *in vivo* for fat reduction and body contouring[5]. However, the mechanism behind this process remains to be fully understood. Additionally, the influence of PBM on hypertrophic adipocytes has, to our knowledge, not been tested *in vitro*. Given the capabilities of PBM to reduce lipid content, diminish ROS, and lower inflammation, it is therefore reasonable to speculate that PBM will improve the condition of hypertrophic adipocytes. Here, we attempt to discern the effect of PBM using NIR light on adipose-

derived stem cells (ADSCs) induced to dysfunctional, hypertrophic adipocytes similar to an obese condition.

Materials and Methods

Cell culture and Differentiation

Human adipose-derived stem cells (ADSCs) were purchased from Lonza and expanded on tissue culture plates in growth medium until 70-80% confluence. Once confluent, ADSCs were separated from the culture plates with 0.5% Trypsin-EDTA and seeded onto round glass coverslips in 24-well plates at a seeding density of 2.5×10^4 cells/cm^2.

24 hours following seeding, adipogenic differentiation of ADSCs was begun following a well-established protocol[35]. Briefly, growth medium was replaced with adipogenic differentiation (AD) medium containing: Dulbecco's Modified Eagle Medium (DMEM), 15% fetal bovine serum (FBS), 1% antibiotics/antimycotics (penicillin, streptomycin, and ampicillin), 1 µM dexamethasone, 200 µM indomethacin, 10 µg/mL insulin, and 0.5 mM 3-isobutyl-1-methylxanthine (IBMX). AD media was changed every other day throughout the course of the differentiation.

Generation of hypertrophic adipocytes

In order to mimic a chronic obesity environment *in vitro*, differentiating ADSCs were induced to a hypertrophic phenotype. To achieve this, differentiating cells were challenged with hypertrophic induction media containing AD media supplemented with 500 µM palmitic acid (PA) as previously described[20]. Briefly, palmitate was dissolved in pure ethanol and diluted in FFA-free BSA for 10 minutes at 55 °C. Stock BSA-PA was

further diluted in AD medium to achieve a final concentration of 500 µM. Differentiating ADSCs were challenged with PA following 7 days of normal adipogenic induction, and continued to be challenged through 15 days.

Fluorescence Microscopy and Immunohistochemistry

To confirm and characterize the degree to which addition of palmitic acid induced hypertrophy, lipid quantity and droplet size were observed over differentiation. Lipid content was observed via fluorescence of LipidTOX Green dye (Thermofisher), and quantified using a proprietary code previously described[29]. Lipid content and droplet size were compared between ADSCs undergoing normal differentiation and those challenged with PA medium.

In addition to lipid quantity, levels of the glucose transporter GLUT4 were observed using immunofluorescence over time during differentiation and induction towards hypertrophy. Briefly, cells were fixed in 4% paraformaldehyde, permeabilized using 0.2% Triton X-100, and blocked with 3% bovine serum albumin (BSA). Samples were then incubated with GLUT4 antibodies produced in mouse overnight at 4 °C. Cells were then washed with PBS and incubated with Alexa-Fluo 555-conjugated goat-anti-mouse secondary antibodies for 1 hour. Primary and secondary antibodies were diluted in phosphate buffered saline (PBS) at ratios of 1:100 and 1:500, respectively.

Glucose Uptake Assay

As a marker of insulin resistance, the ability of differentiating adipocytes to take up glucose was monitored over differentiation and hypertrophic induction. On several specified days during differentiation, ADSCs were rinsed of AD or PA medium using PBS and were incubated in growth media containing nuclear stain NucBlue (Thermofisher), 100 ng insulin, and 10 µM of fluorescent glucose analog 2-(*N*-(7-Nitrobenz-2-oxa-1,3-diazol-4-yl)Amino)2-Deoxyglucose (2-NBDG, Thermofisher) for 60 minutes. Following incubation, cells were washed with PBS and imaged under fluorescent microscopy.

Laser set up and exposure

Before laser exposure, cells were induced to adipocyte differentiation in 24-well plates for 7 days. Following initial differentiation, cells were then induced to hypertrophy with PA medium and transferred from 24-well plates to 35 mm culture dishes to better handle individual irradiation of samples. The 1064 nm NIR laser (Cell Gen Therapeutics, Dallas, TX; model CG-5000) was set up as previously described[28]. Briefly, 35 mm dishes were removed from the incubator and set on a white Styrofoam stage 5 cm directly under the laser aperture. The entirety of the glass coverslip containing the cells was exposed to a fluence of 17.6 J/cm^2 over 2 minutes. Following irradiation, culture dishes were quickly returned to the incubator. Laser exposure began after 7 days of differentiation and continued every day through 15 days.

Statistical analysis

All experiments were run in triplicate and data are presented as mean ± SEM. Differences between groups were compared using a student's T-test, with significance indicated as a

p-value < 0.05. In experiments with more than two conditions, an analysis of variance (ANOVA) was performed with a post-hoc Tukey test to investigate significance among groups. All statistical tests were performed in Excel (Microsoft, Redmond, WA).

Results

Adipocyte Differentiation and Hypertrophic Induction

Human ADSCs were induced to adipocytes using the adipogenic reagents in AD medium described above. Successful adipocyte lineage induction was determined by the presence of lipids as observed using LipidTOX fluorescent lipid dye (FIG1). Cells were exposed to AD media for 7 days, following which samples were removed and tested as baseline values. The remaining samples were then challenged with AD-PA medium to generate hypertrophy.

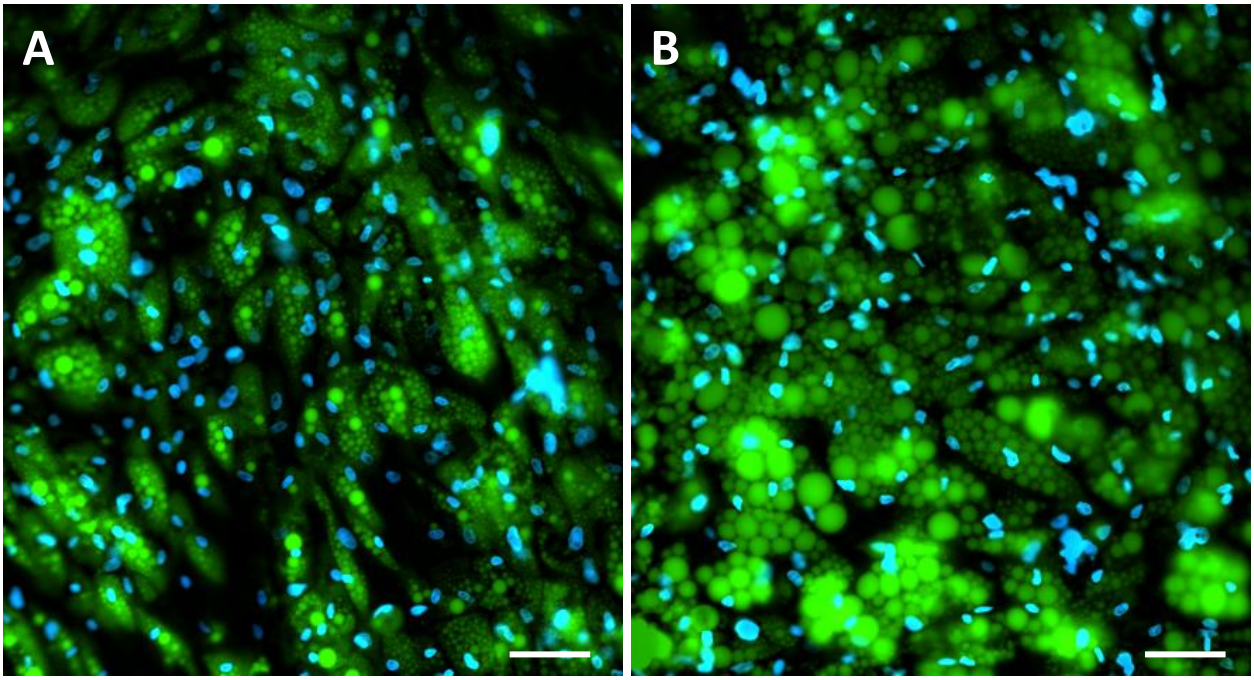

Figure 4. 1. *Adipose-derived stem cells 15 days after being induced toward adipocytes. ADSCs challenged with 500 µM Palmitic Acid displayed greater lipid quantity and larger droplets (B) compared to control (A). Images taken at 20X. Scale bar = 50 µm.*

Hypertrophic adipocytes were differentiated from normal adipocytes in terms of lipid content and lipid droplet size. Hypertrophic adipocytes displayed larger sized lipid droplets (FIG1) as well as significantly greater amounts of total lipid compared to normal (FIG2). Together these constitute a successful generation of hypertrophic cells, which were further tested for functionality differences.

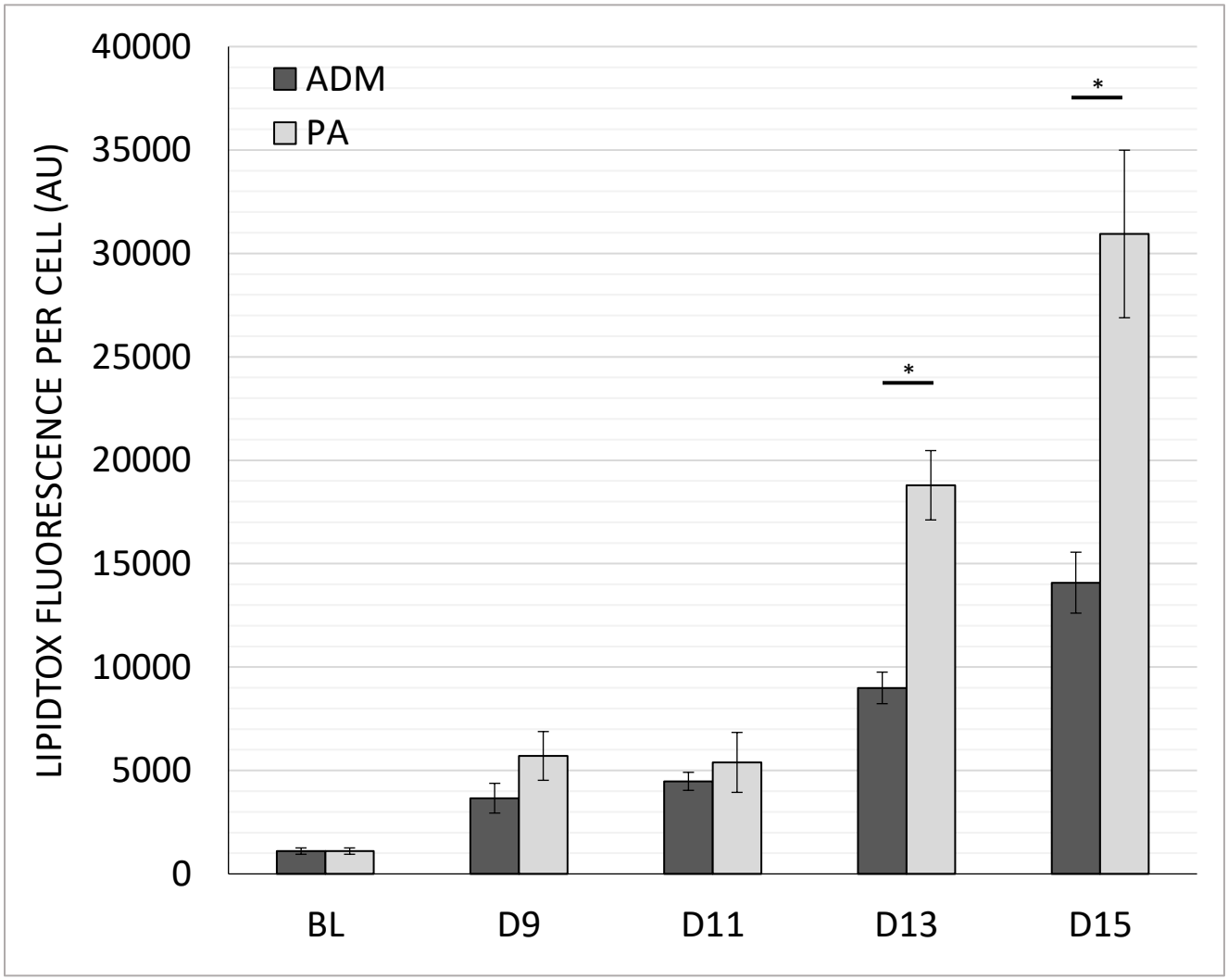

Figure 4. 2. *Lipid content of ADSCs undergoing adipogenic differentiation under normal (ADM) and hypertrophic (PA) conditions. ADSCs exposed to palmitic acid demonstrated significantly greater amounts of lipid during later differentiation stages. Mean ± SEM, n=3.*

** indicates p value < 0.05*

To characterize the effect of hypertrophy on adipocyte functionality, the degree to which cells uptake glucose was observed via the fluorescent glucose analog, 2-NBDG. While similar in trend, cells induced to hypertrophy demonstrated a significant reduction in 2-NBDG fluorescence, correlating to a reduced amount of glucose uptake (FIG3).

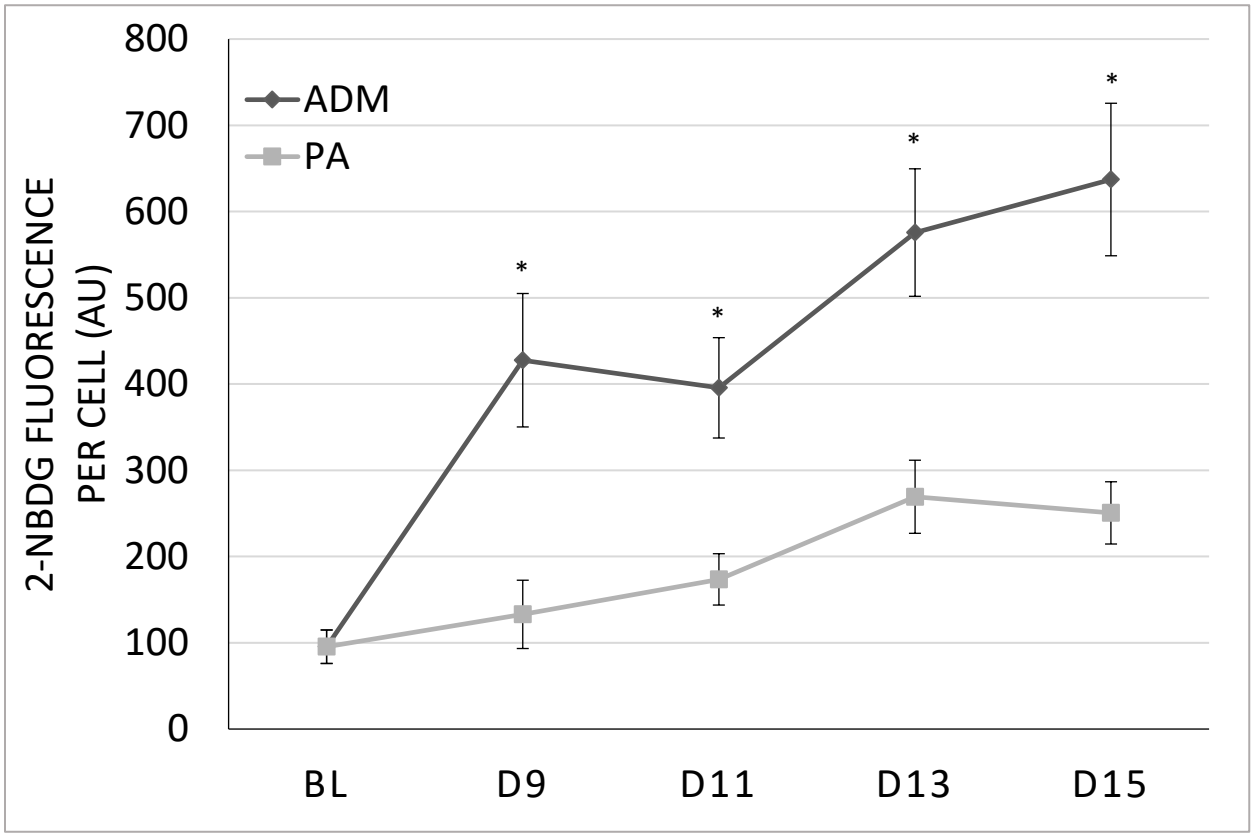

Figure 4. 3. *Fluorescent quantification of glucose analog 2-NBDG corresponding to levels of glucose differentiation ADSCs uptake. Glucose uptake increases during differentiation for both normal and hypertrophic groups. However, ADSCs exposed to palmitic acid demonstrate lower glucose uptake at all points over differentiation. Mean ± SEM, n=3.*

** Indicates p value < 0.05*

To further investigate this, the expression and distribution of glucose transporter GLUT4 was quantified. In both normal and hypertrophic conditions, GLUT4 was mostly distributed in the cell nucleus throughout differentiation. However, as differentiation continued,

GLUT4 expression increased in normal differentiation, while instead decreasing in adipocytes induced to hypertrophy (FIG4).

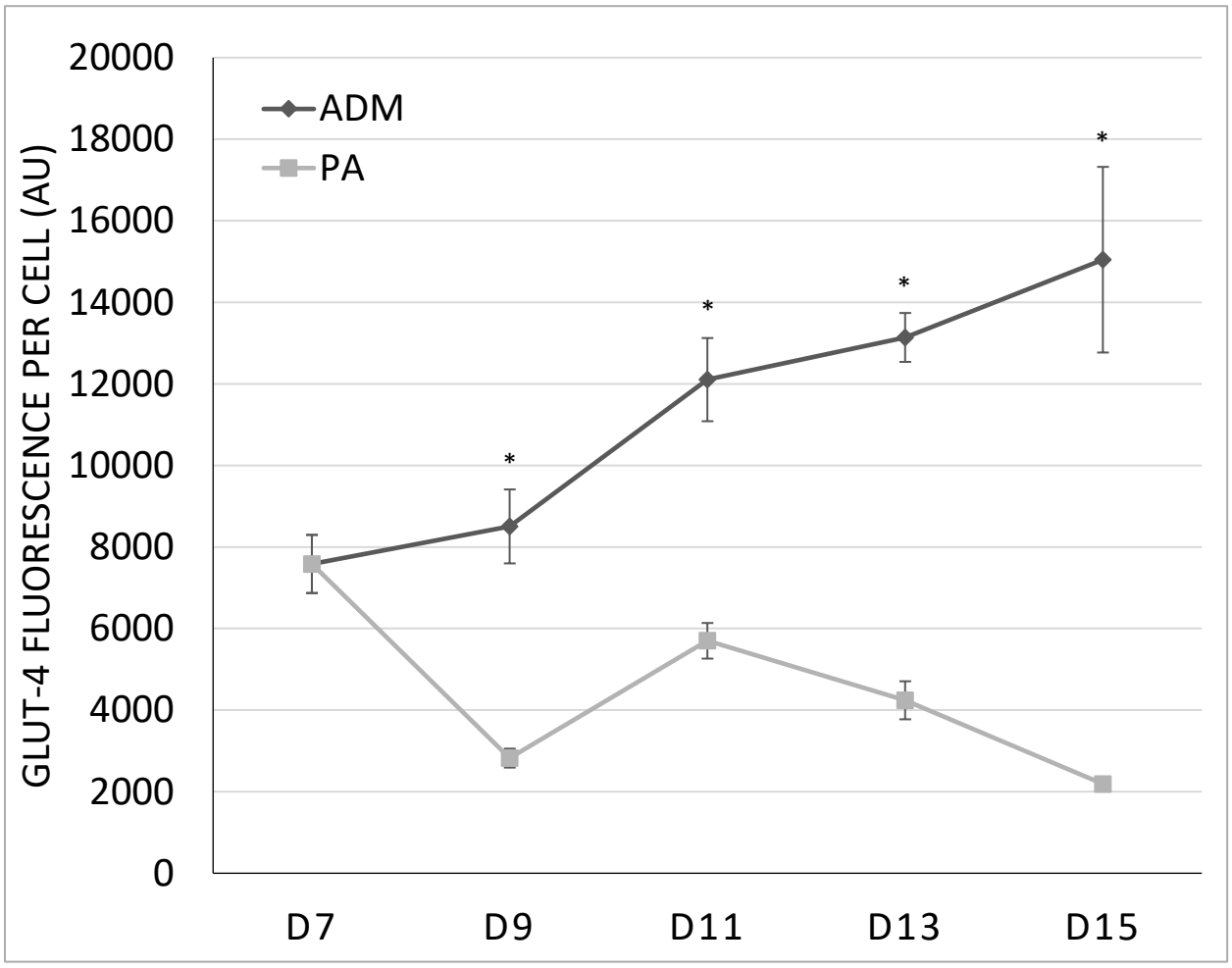

Figure 4. 4. *Fluorescent quantification of the major adipocyte glucose transporter GLUT4. Normal differentiation shows an increase in GLUT4 expression, while cells induced to hypertrophy show a decreasing trend. Mean ± SEM, n=3.*

** indicates p value < 0.05*

Laser set up and exposure

As we have previously described the influence of PBM on reducing the amount of lipids in differentiating adipocytes, here we further investigated the application of 1064 nm laser irradiation on hypertrophic cells. Figure 5 shows lipid droplets at day 15 of differentiation between ADM, PA, and PA-PBM groups. Total lipid content was diminished in cells

exposed to laser light (FIG6). Fluorescence levels of LipidTOX dye increased 12.8X in normal ADM between days 7 and 15. In the hypertrophic group, this increase was markedly greater at a level of 28.1X. As expected, the hypertrophic cells exposed to PBM decreased lipid content, though not as much as non-hypertrophic cells, finishing with a relative increase of 16.6X.

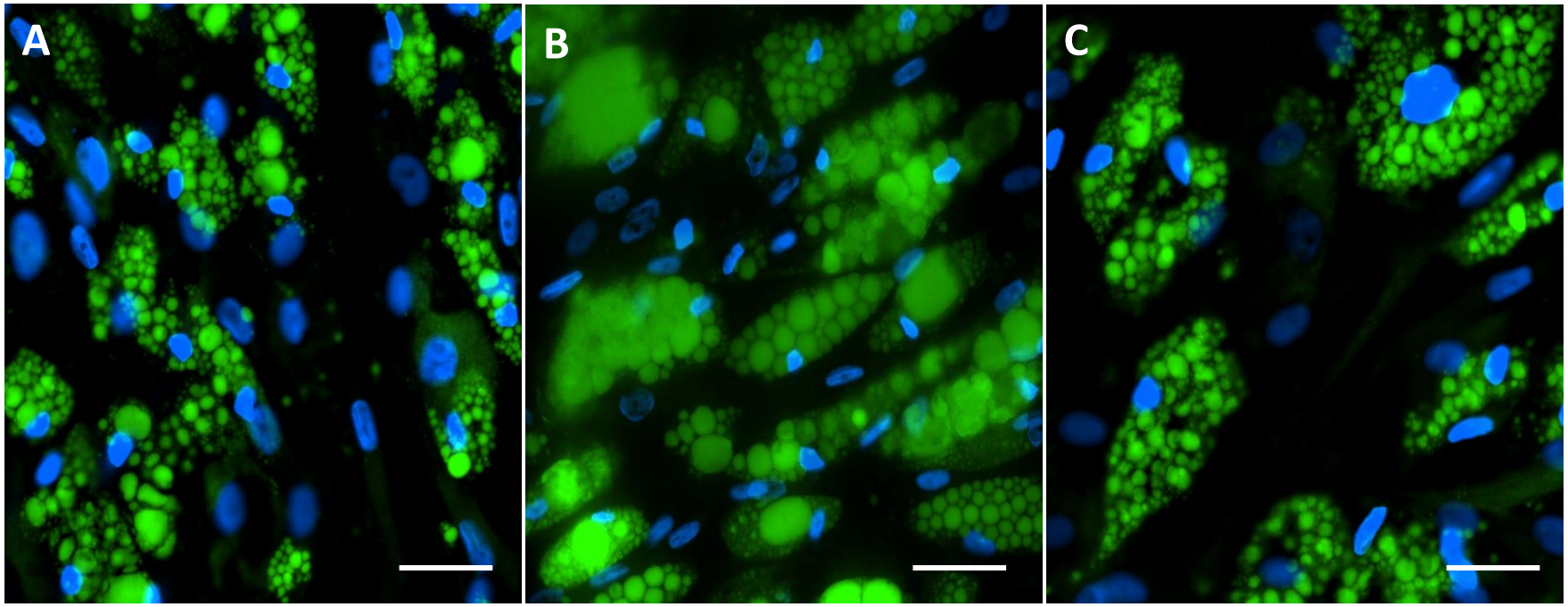

Figure 4. 5. *Adipose-derived stem cells 15 days after being induced toward adipocytes (A). ADSCs induced to hypertrophy using 500 µM Palmitic Acid (B). ADSCs induced to hypertrophy and exposed to 17.6 J/cm^2 PBM for 7 days (C). Images taken at 40X. Scale bar = 25 µm.*

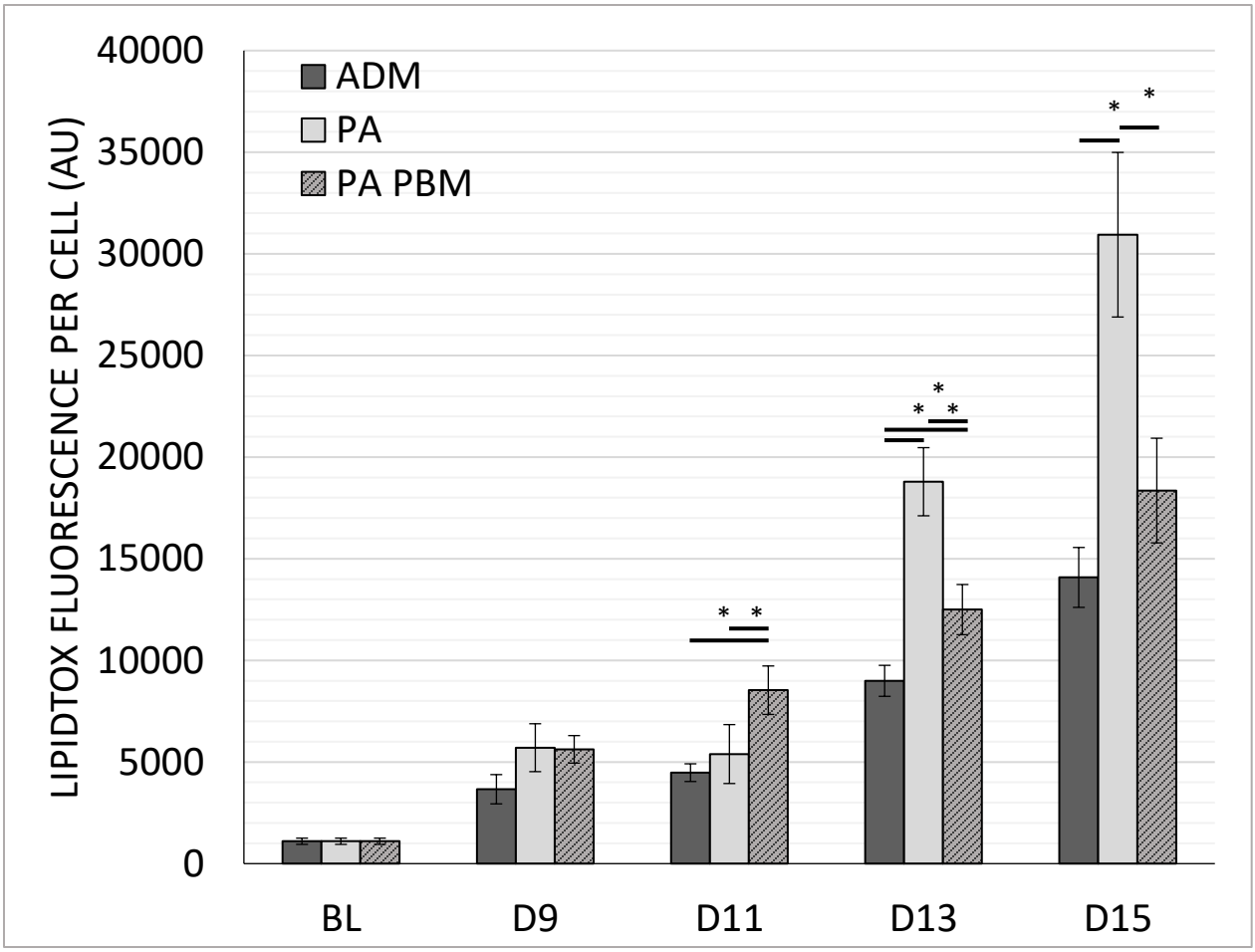

Figure 4. 6*. Lipid content of ADSCs undergoing adipogenic differentiation. Hypertrophic ADSCs (PA) display significantly greater amounts of lipid compared to normal (ADM) and laser irradiated (PA-PBM) groups. Hypertrophic cells exposed to laser (PA-PBM) produced slightly more lipid than ADM, and significantly less than PA. Mean ± SEM, n=3.*

** Indicates p value < 0.05*

Functional changes in cellular mechanisms were also investigated when exposed to PBM. 2-NBDG fluorescence was increased in both ADM and PA groups, though this increase was significant less in the hypertrophic cells, with relative increases at day 15 of 6.6X and 2.6X, respectively. Interestingly, application of PBM significantly restored fluorescence levels of 2-NBDG compared to hypertrophic cells alone, with a relative increase of 3.6X from baseline (FIG7).

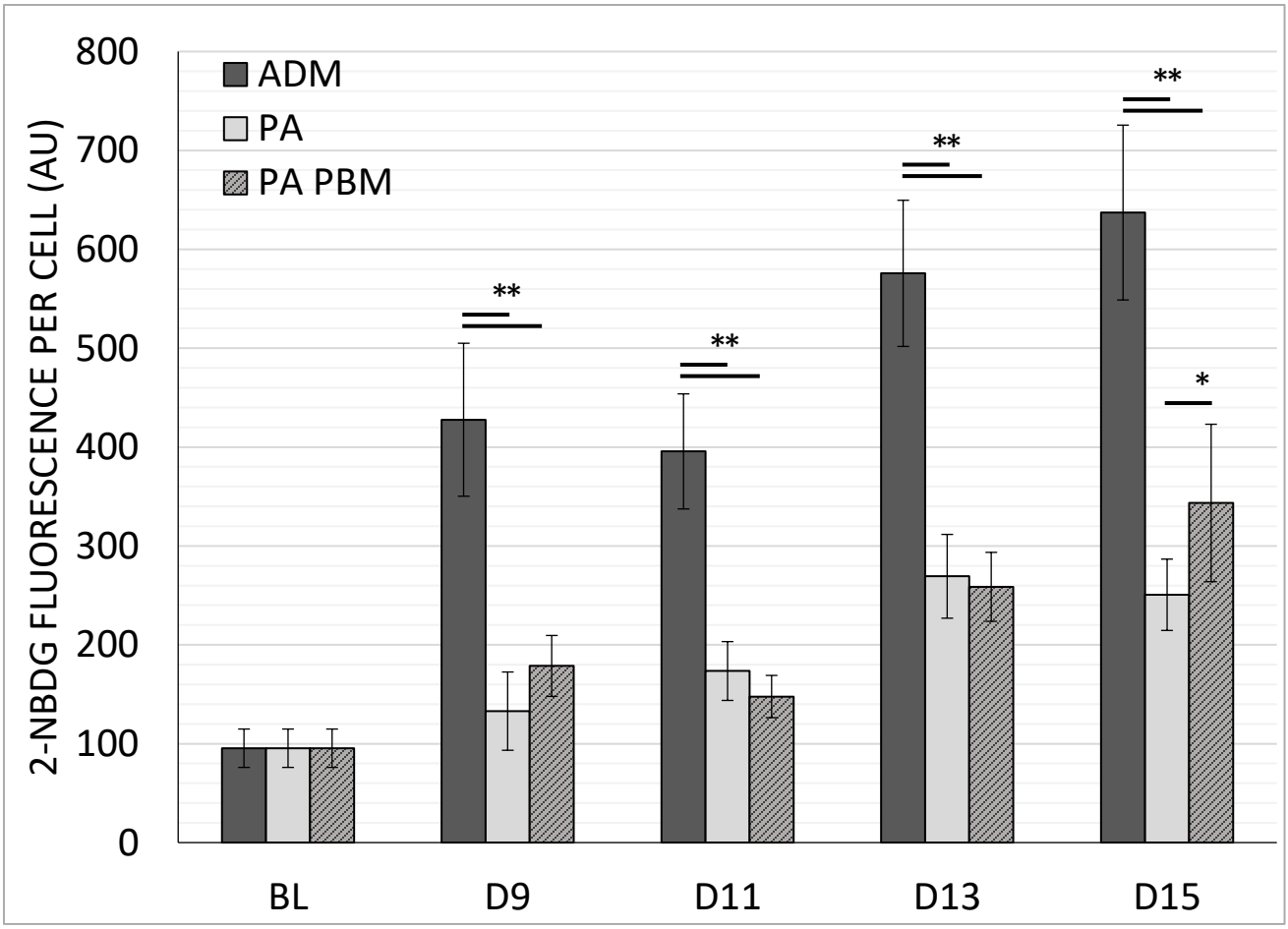

Figure 4. 7. *2-NBDG fluorescence comparing glucose uptake at baseline (BL) through to end-stage (D15) adipogenic differentiation. Application of PBM shows an overall trend similar to hypertrophic cells. At the final day, glucose fluorescence in PA PBM was significantly greater than PA, although still less than that of normal differentiation. Mean ± SEM, n=3.*

** Indicates p value < 0.05.*

Further functional changes with PBM were shown with altered levels of glucose transporter GLUT4. As before shown before, GLUT4 fluorescence increased 2-fold from baseline in normal ADM. In hypertrophic cells, this level decreased to less than half of baseline. Hypertrophic cells exposed to PBM however, demonstrated levels of GLUT4 similar to that of baseline, suggesting a form of functional restoration caused by PBM (FIG8).

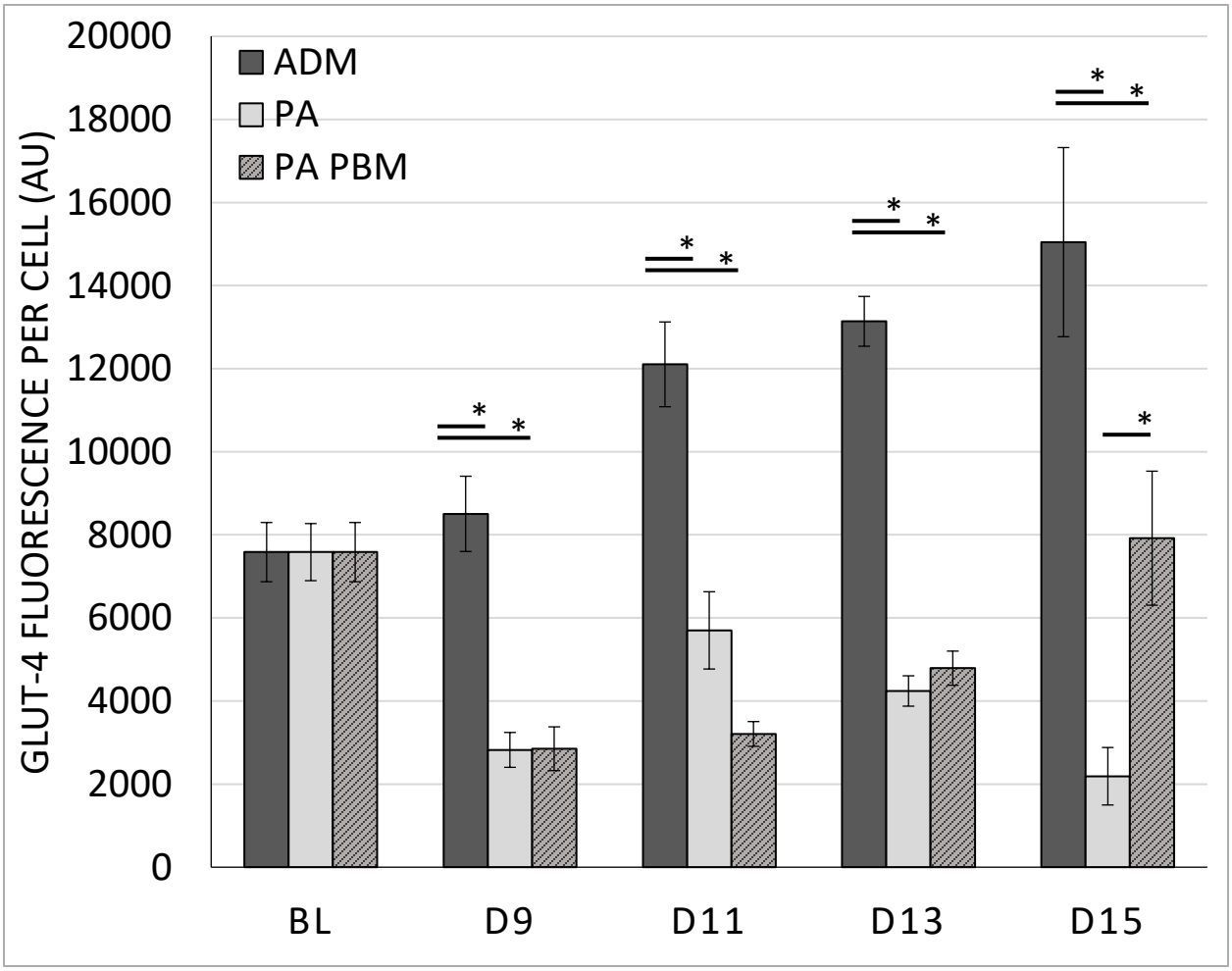

Figure 4. 8. *Fluorescence quantification of GLUT4 levels in ADSCs undergoing adipogenic differentiation. Normal adipogenesis (ADM) show an increase in GLUT4 levels over time, while cells induced to hypertrophy (PA) show a decrease in protein expression. Hypertrophic cells exposed to laser irradiation (PA PBM) show an initial decrease, followed by an increase and return to baseline values. Mean ± SEM, n=3.*

** Indicates p value < 0.05.*

Discussion

Dysfunctional cellular physiology alters not only the tissue in which it is part, but the body as a whole. Adipocyte physiology specifically has implications on energy storage and glucose management[33]. In obesity, adipocyte dysregulation comes about in two ways: hyperplasia and hypertrophy. Hypertrophic adipocytes are those swollen with excess lipid

and consequently, these enlarged cells produce several deleterious effects such as hypoxia, inflammation, and insulin resistance which together can lead toward the progression of metabolic disease and diabetes[24]. Adult onset diabetes (DM2), is caused by a dysregulation in insulin signaling, often exacerbated from complications with obesity[26]. Hypertrophic adipocytes have been shown to be directly correlated to metabolic disease and BMI[14]. At a cellular level, the obesity microenvironment is one of low oxygen concentration and high levels reactive oxygen species[9]. We have previously demonstrated the effect of photobiomodulation on reducing lipid content in differentiating adipocytes[28]. Several researchers have also shown PBM as an effective method for reducing fat content and body contouring *in vivo*[5]. However, it remains to be seen how this approach factors to hypertrophic adipocytes at a cellular level. The mechanisms of PBM are well situated to oppose the microenvironment induced by enlarged adipocytes. Here, we attempt to characterize the degree to which PBM effects adipocytes swollen with excess fat and potentially restores normal adipocyte function.

Photobiomodulation has previously been shown to reduce inflammation *in vitro* through a mitochondrial mechanism[13]. PBM acts primarily by increasing flux through the electron transport chain, leading to several downstream effects such as improved cell survival, protein synthesis, and cell proliferation[7]. Researchers investigating PBM have shown a reduction in levels of pro-inflammatory cytokines in various inflammatory environments. Yamaura et al artificially induced inflammation by addition of exogenous TNFα and discovered mRNA levels of inflammatory proteins TNFα, IL-1β, and IL-8 were mitigated by application of 810 nm laser light[40]. Several groups have investigated the response of

PBM to a diabetic wound environment and have shown a reduction in TNF and macrophage M1 inflammatory factors, as well as improvement in the wound healing model[16, 30].

In order to investigate the influence of PBM on adipocyte physiology, a functional model must first be characterized. To do this, stem cells derived from adipose tissue were induced to adipose cells using a well-established chemical method[35]. Subsequently, hypertrophic adipocytes, those which mimic the *in vivo* obesity environment, were generated with the addition of palmitate, a free fatty acid. Upon addition, the cells swelled with excess lipid and formed much larger droplets (FIGS1&2). One of the main complications that may arise from hypertrophic cells is hypoxia[15]. In obesity, vascularization is low, and adipocytes can swell to up to 100 μm in size, past the limit of oxygen diffusion[10]. This in turn causes an upregulation in inflammatory cytokines and ROS[3]. Oxidative stress has been linked to insulin resistance through activation of several stress-induced factors such as c-Jun N-terminal kinase, nuclear factor kappa β (NF-κβ), and isoforms of protein kinase C (PKC)[27]. Conversely, transient increases in ROS are produced in response to insulin and play a role in mediating insulin signaling[23]. PBM's effect on ROS generation has been demonstrated previously by several groups. At the time of exposure, a transient burst of ROS is produced as oxidative phosphorylation is increased and electrons leak out of the system. This is followed over time with an upregulation in antioxidant enzyme gene transcription and an overall lowering of ROS load[17].

Further characterization of adipocyte functionality was examined in ability to take up glucose. Glucose transport across the adipocyte membrane is primarily mediated by the transport protein GLUT4. The GLUT4 transporter is mostly regulated to adipocytes and striated muscle cells (skeletal and cardiac)[25]. In normal conditions, GLUT4 is located intracellularly, in vesicles at or near the cell nucleus. In response to high levels of glucose, insulin – released from pancreatic beta-cells – triggers GLUT4 vesicles to fuse with the cell membrane, allowing facilitated diffusion of glucose into the cell[11]. In hypertrophic adipocytes, this trafficking of GLUT4 vesicles is inhibited. Kim et al (2015), demonstrate that lipid-overloaded adipocytes exhibit defects in GLUT4 shuttling to the plasma membrane, resulting in impaired glucose uptake to the cell[20]. This phenomenon was shown to occur regardless of the state of inflammation. Here, we show GLUT4 expression is downregulated in hypertrophic cells (FIG4). Taken together, a downregulation along with a defect in trafficking sum to a significant reduction in glucose transport into the cell. Indeed, shown here we demonstrate enlarged adipocytes show over 2.5-fold less glucose transported into the cell via fluorescence measurements of glucose analog 2-NBDG (FIG3).

As photobiomodulation has previously been shown to reduce lipid content in stem cells undergoing adipogenesis, it stands to reason it may assist in mitigating the complications from hypertrophic adipocytes. Visually, lipid droplets appeared smaller, more closely resembling that of non-hypertrophic cells (FIG5). Quantified fat content in ADSCs exposed to palmitic acid and PBM reduced significantly compared to those without irradiation. At the final day of differentiation (D15), PA-PBM showed no statistical

difference than normal, non-hypertrophic differentiation (ADM) (FIG6). Lipid levels increased 28-fold from baseline in the hypertrophic group, compared to 12.8- and 16.6-fold in ADM and PBM groups, respectively. This accounts for a significant reduction in lipid content and appears to suggest a conformational restoration of hypertrophic adipocytes.

Along with this reduction in lipid content we show a slight return to normal glucose transport. While glucose uptake in control cells far exceeded both groups exposed to palmitic acid, those exposed to PBM show an upregulation from non-treated cells (FIG7). Accompanied with this, we see a significant increase in GLUT4 fluorescence in the PBM-treated group compared to hypertrophic (FIG8). This can potentially be due to an increase in cellular metabolism leading to greater protein levels. It has been documented that PBM increases protein content in cells during exposure[38]. Interestingly, this increase follows only after an initial decrease, something also seen with the untreated cells, though not observed by the control group. This suggests some level of time delay in the mechanism of PBM. Most studies with PBM involve bursts of irradiation over time, often spanning multiple days or weeks. Possibly, the cellular mechanisms with which PBM is influencing requires consistent activation. In our previous research, we demonstrated daily PBM increases ROS signaling at the onset of irradiation. However, after successive days of treatment, the cells respond by manufacturing greater levels of ROS-sequestering enzymes and thus contribute to an overall lower ROS load[28]. The same pattern appears to occur here with GLUT4 – an initial decrease due to induction of hypertrophy, followed

by a steady upregulation caused by activation of multiple cellular processes including genomic transcription and protein translation.

The main mechanism by which PBM operates is hypothesized to be at the site of the mitochondria. As cytochrome c oxidase accepts a photon and removes inhibitory nitric oxide, its activity is increased allowing enhanced flux through the electron transport chain. In obesity and DM2, mitochondrial function is downregulated showing a marked decrease in electron transport chain activity[32]. As described previously, ATP levels in differentiating adipocytes are increased in cells exposed to PBM. Several groups have shown similar conclusions in enhancing mitochondrial activity[1, 37]. For hypertrophic adipocytes, an increase in cellular respiration and ATP would counteract the downregulation shown in obesity.

There are various limitations to this study, which can be addressed in future experiments. Firstly, the model of obesity generated is in two dimensions. While hypoxia and oxygen diffusion are important factors in the progression to insulin resistance, the degree of impact hypertrophy has on oxygen diffusion in monolayer culture is negligible. PBM works through upregulation in oxidative phosphorylation therefore its effectiveness in a hypoxic environment requires investigation. Further studies in truly hypoxic environments or three-dimensional modeling are warranted. Secondly, it would be beneficial to have additional protein quantification such as insulin receptors and the proteins activated in response to insulin which assist in trafficking GLUT4 to the plasma membrane such as Akt and its substrate, AS160. Thirdly, as PBM demonstrates a time-delay characteristic of action, the

duration of the experiment may need to be extended to show the full degree of influence. Finally, future work in true *in vivo* mouse models of obesity would be a great benefit to show the systemic applicability of PBM on obesity.

In conclusion, we show photobiomodulation demonstrates some degree of success in restoring normal cellular activity in dysfunctional hypertrophic adipocytes. Previously, we have shown PBM to reduce lipid content in stem cells undergoing adipogenesis through mechanisms involving enhanced ATP production and transcription of ROS-eliminating enzymes. Here, we postulate the same mechanism applied to hypertrophic adipocytes as a method to mitigate the complications of obesity. We show a marked decrease in lipid production and droplet size in adipocytes exposed to irradiation. Additionally, glucose and GLUT4 levels trend upward after an initial time delay, showing a significant increase in both compared to cells not exposed to laser. Continuation of this work involving 3-dimensional cell culture or *in vivo* experiments is warranted to further investigate the mechanism of laser application for treatment of obesity complications.

References

1. Amaroli A., S. Ravera, S. Parker, I. Panfoli, A. Benedicenti and S. Benedicenti. An 808-nm Diode Laser with a Flat-Top Handpiece Positively Photobiomodulates Mitochondria Activities. Photomedicine and Laser Surgery 34: 564–571, 2016.

2. Attie A. D. and P. E. Scherer. Adipocyte metabolism and obesity. Journal of Lipid Research 50: S395–S399, 2009.

3. Bondia-Pons I., L. Ryan and J. A. Martinez. Oxidative stress and inflammation interactions in human obesity. Journal of Physiology and Biochemistry 68: 701–711, 2012.

4. Brieger K., S. Schiavone, F. J. M. Jr. and K.-H. Krause. Reactive oxygen species: from health to disease. Swiss Medical Weekly 142: 2012.

5. Caruso-Davis M. K., T. S. Guillot, V. K. Podichetty, N. Mashtalir, N. V. Dhurandhar, O. Dubuisson, Y. Yu and F. L. Greenway. Efficacy of low-level laser therapy for body contouring and spot fat reduction. Obesity surgery 21: 722–729, 2011.

6. Ferranti S. d. and D. Mozaffarian. The Perfect Storm: Obesity, Adipocyte Dysfunction, and Metabolic Consequences. Clinical Chemistry 54: 945–955, 2008.

7. Freitas L. F. d. and M. R. Hamblin. Proposed Mechanisms of Photobiomodulation or Low-Level Light Therapy. IEEE journal of selected topics in quantum electronics: a publication of the IEEE Lasers and Electro-optics Society 22: 348–364, 2016.

8. Furukawa S., T. Fujita, M. Shimabukuro, M. Iwaki, Y. Yamada, Y. Nakajima, O. Nakayama, M. Makishima, M. Matsuda and I. Shimomura. Increased oxidative stress in obesity and its impact on metabolic syndrome. Journal of Clinical Investigation 114: 1752–1761, 2004.

9. Fuster J. J., N. Ouchi, N. Gokce and K. Walsh. Obesity-Induced Changes in Adipose Tissue Microenvironment and Their Impact on Cardiovascular Disease. Circulation Research 118: 1786–1807, 2016.

10. Goossens G. H. and E. E. Blaak. Adipose Tissue Dysfunction and Impaired Metabolic Health in Human Obesity: A Matter of Oxygen? Frontiers in Endocrinology 6: 55, 2015.

11. Govers R. Molecular mechanisms of GLUT4 regulation in adipocytes. Diabetes & Metabolism 40: 400–410, 2014.

12. Graham T. and B. Kahn. Tissue-specific Alterations of Glucose Transport and Molecular Mechanisms of Intertissue Communication in Obesity and Type 2 Diabetes. Hormone and Metabolic Research 39: 717–721, 2007.

13. Hamblin M. R. Mechanisms and applications of the anti-inflammatory effects of photobiomodulation. AIMS biophysics 4: 337–361, 2017.

14. Harmelen V. v., T. Skurk, K. Röhrig, Y.-M. Lee, M. Halbleib, I. Aprath-Husmann and H. Hauner. Effect of BMI and age on adipose tissue cellularity and differentiation capacity in women. International Journal of Obesity 27: 0802314, 2003.

15. Hodson L., S. M. Humphreys, F. Karpe and K. N. Frayn. Metabolic Signatures of Human Adipose Tissue Hypoxia in Obesity. Diabetes 62: 1417–1425, 2013.

16. Houreld N. N., P. R. Sekhejane and H. Abrahamse. Irradiation at 830 nm stimulates nitric oxide production and inhibits pro-inflammatory cytokines in diabetic wounded fibroblast cells. Lasers in surgery and medicine 42: 494–502, 2010.

17. Janzadeh A., F. Nasirinezhad, M. Masoumipoor, S. B. Jameie and P. hayat. Photobiomodulation therapy reduces apoptotic factors and increases glutathione levels in a neuropathic pain model. Lasers in Medical Science 31: 1863–1869, 2016.

18. Jo J., O. Gavrilova, S. Pack, W. Jou, S. Mullen, A. E. Sumner, S. W. Cushman and V. Periwal. Hypertrophy and/or Hyperplasia: Dynamics of Adipose Tissue Growth. PLoS Computational Biology 5: e1000324, 2009.

19. Karu T. Mitochondrial Mechanisms of Photobiomodulation in Context of New Data About Multiple Roles of ATP. Photomedicine and Laser Surgery 28: 159–160, 2010.

20. Kim J., J. Huh, J. Sohn, S. Choe, Y. Lee, C. Lim, A. Jo, S. Park, W. Han and J. Kim. Lipid-Overloaded Enlarged Adipocytes Provoke Insulin Resistance Independent of Inflammation. Molecular and Cellular Biology 35: 1686–1699, 2015.

21. Kopelman P. G. Obesity as a medical problem. Nature 404: 635–643, 2000.

22. Kouidhi S., R. Berrhouma, K. Rouissi, S. Jarboui, M.-S. Clerget-Froidevaux, I. Seugnet, F. Bchir, B. Demeneix, H. Guissouma and A. B. Elgaaied. Human

subcutaneous adipose tissue Glut 4 mRNA expression in obesity and type 2 diabetes. Acta Diabetologica 50: 227–232, 2013.

23. Krieger-Brauer H. I. and H. Kather. Human Fat Cells Possess a Plasma Membrane-bound H2O2-generating System That is Activated by Insulin via a Mechanism Bypassing the Receptor Kinase. The Journal of Clinical Investigation 89: 1006–1013, 1992.

24. Laforest S., J. Labrecque, A. Michaud, K. Cianflone and A. Tchernof. Adipocyte size as a determinant of metabolic disease and adipose tissue dysfunction. Critical Reviews in Clinical Laboratory Sciences 52: 301–313, 2015.

25. Leto D. and A. R. Saltiel. Regulation of glucose transport by insulin: traffic control of GLUT4. Nature Reviews Molecular Cell Biology 13: 383–396, 2012.

26. Maggio C. A. and F. X. Pi-Sunyer. Obesity and type 2 diabetes. Endocrinology and Metabolism Clinics of North America 32: 805–822, 2003.

27. Matsuda M. and I. Shimomura. Increased oxidative stress in obesity: Implications for metabolic syndrome, diabetes, hypertension, dyslipidemia, atherosclerosis, and cancer. Obesity Research & Clinical Practice 7: e330–e341, 2013.

28. McColloch A., C. Liebman, H. Liu and M. Cho. Altered Adipogenesis of Human Mesenchymal Stem Cells by Photobiomodulation using 1064 nm Laser Light. Lasers in Surgery and Medicine (In Review) 2020.

29. McColloch A., M. Rabiei, P. Rabbani, A. Bowling and M. Cho. Correlation between Nuclear Morphology and Adipogenic Differentiation: Application of a Combined Experimental and Computational Modeling Approach. Scientific Reports 9: 16381, 2019.

30. Meireles G. C. S., J. N. Santos, P. O. Chagas, A. P. Moura and A. L. B. Pinheiro. Effectiveness of Laser Photobiomodulation at 660 or 780 Nanometers on the Repair of Third-Degree Burns in Diabetic Rats. Photomedicine and Laser Surgery 26: 47–54, 2008.

31. Muir L. A., C. K. Neeley, K. A. Meyer, N. A. Baker, A. M. Brosius, A. R. Washabaugh, O. A. Varban, J. F. Finks, B. F. Zamarron, C. G. Flesher, J. S. Chang, J. B. DelProposto, L. Geletka, G. Martinez-Santibanez, N. Kaciroti, C. N. Lumeng and R. W. O'Rourke. Adipose tissue fibrosis, hypertrophy, and hyperplasia: Correlations with diabetes in human obesity. Obesity 24: 597–605, 2016.

32. Ritov V. B., E. V. Menshikova, J. He, R. E. Ferrell, B. H. Goodpaster and D. E. Kelley. Deficiency of Subsarcolemmal Mitochondria in Obesity and Type 2 Diabetes. Diabetes 54: 8–14, 2004.

33. Rosen E. D. and B. M. Spiegelman. Adipocytes as regulators of energy balance and glucose homeostasis. Nature 444: 847–853, 2006.

34. Ruh A. C., L. Frigo, M. F. X. B. Cavalcanti, P. Svidnicki, V. N. Vicari, R. A. B. Lopes-Martins, E. C. P. L. Junior, N. D. Isla, F. Diomede, O. Trubiani and G. M. Favero. Laser photobiomodulation in pressure ulcer healing of human diabetic patients: gene expression analysis of inflammatory biochemical markers. Lasers in Medical Science 33: 165–171, 2018.

35. Scott M. A., V. T. Nguyen, B. Levi and A. W. James. Current Methods of Adipogenic Differentiation of Mesenchymal Stem Cells. Stem Cells and Development 20: 1793–1804, 2011.

36. Shoelson S. E., L. Herrero and A. Naaz. Obesity, Inflammation, and Insulin Resistance. Gastroenterology 132: 2169–2180, 2007.

37. Silveira P. C. L., G. K. Ferreira, R. P. Zaccaron, V. Glaser, A. P. Remor, C. Mendes, R. A. Pinho and A. Latini. Effects of photobiomodulation on mitochondria of brain, muscle, and C6 astroglioma cells. Medical Engineering & Physics 71: 108–113, 2019.

38. Sperandio F. F., A. Simões, L. Corrêa, A. C. C. Aranha, F. S. Giudice, M. R. Hamblin and S. C. O. M. Sousa. Low-level laser irradiation promotes the proliferation and maturation of keratinocytes during epithelial wound repair. Journal of Biophotonics 8: 795–803, 2015.

39. Wang Y., Y.-Y. Huang, Y. Wang, P. Lyu and M. R. Hamblin. Photobiomodulation (blue and green light) encourages osteoblastic-differentiation of human adipose-derived stem cells: role of intracellular calcium and light-gated ion channels. Scientific reports 6: 33719, 2016.

40. Yamaura M., M. Yao, I. Yaroslavsky, R. Cohen, M. Smotrich and I. E. Kochevar. Low level light effects on inflammatory cytokine production by rheumatoid arthritis synoviocytes. Lasers in Surgery and Medicine 41: 282–290, 2009.

CHAPTER 5:
GENERAL CONCLUSIONS

As stem cells undergo differentiation, they progress through several morphological and functional changes. These changes occur in both the cytoskeletal structure, as well as in the nucleus. In order to bring about these changes, researchers have employed several strategies including chemical and physical factors. Initially, stem cells were differentiated by a means of specific reagents including growth factors, antioxidants, hormones, and other biochemical agents to induce cells to a specific lineage. As research continued, however, it was discovered that stem cells directly respond to their physical microenvironment which in turn affects differentiation efficiency or lineage potential. Since this discovery, several physical factors have been studied including substrate stiffness[1], dynamic stretching[2], cell shape[3], and cell-cell contacts[4]. Even more recently it has been a focus of researchers to investigate the role these physical factors play on the nucleus[5,6]. The nucleus contains the cell's genetic code, which must be manipulated for gene activation as distinct lineages require unique cellular mechanisms.

In chapter 2, it was shown that during adipogenic differentiation of stem cells, the nucleus undergoes significant reorganization. This is demonstrated as a reduction in nuclear area and increase in aspect ratio. Differentiation appeared to occur in stages, with nuclear shape change occurring prior to the majority of lipid production (see Fig 2.3). This finding is consistent with other researchers which describe adipogenesis as occurring in two distinct phases: (1) lineage commitment to pre-adipocytes; and (2) adipocyte maturation[7]. Along with a reduction in nuclear size, we also observe a change in overall morphology

of nucleus as adipogenesis continues. Differentiation brings about an increase in the aspect ratio (e.g., reciprocal decrease in roundness) of the nucleus. We compared the timing of the nuclear shape change with that of the expression of the nuclear structural protein lamin A/C and found an inverse relationship. Lamin A/C (LMNA) is the major structural component of the nuclear envelope and was also shown to undergo reorganization during differentiation[8,9]. LMNA redistributed to the nuclear periphery and increased in fluorescence and mRNA expression. As a director of nuclear shape and chromosome positioning, LMNA (and thus nuclear mechanical properties) cannot be understated as a factor in stem cell differentiation. Furthermore, chapter 2 also investigated the physical confinement of stem cells as a factor in differentiation. Inducing shape change in the nucleus was performed by microcontact printing of pattered substrates (see Fig 2.4). Upon seeding, undifferentiated stem cells displayed nuclei with aspect ratios similar to that of mature adipocytes. However, despite this change adipogenesis was impeded compared to normal. Additional experiments with actin stabilizing agent jasplakinolide showed similar reduction in adipocyte maturity. Together, these findings suggest that the modulation of nuclear morphology comes about as a result of genetic regulation induced by the differentiation factors. In other words, it appears the nuclear shape is a result of lineage commitment, rather than requirement for adipogenic differentiation.

Furthermore, while the stiffness of the stem cell nuclear membrane undergoing adipogenesis has not been documented experimentally, it can potentially be calculated mathematically. To this end, a two-dimensional model was generated with the

assumptions that (1) actin filaments keep the nuclear membrane under tension; and (2) these forces generated from the actins are dissipating over time due to the significant cytoskeletal rearrangement that occurs during adipogenesis. Using the experimental data together with known mechanical forces found in literature, an approximation of nuclear membrane stiffness during adipogenesis can be estimated. It was discovered that the mechanical properties of the nuclear membrane are in the range of 0.0055 ± 0.0005 N/m, or approximately an order of magnitude less than cytoskeletal actin filaments (see Fig 2.7). Additionally, the rate of actin reorganization during adipogenic differentiation, and its effect on nuclear membrane mechanics, can be assessed computationally. It was discovered that a fourth-order rate equation most closely followed the experimental results, indicating a rapid reorganization of actin filaments in early adipogenesis followed by a slowing down over time (see Fig. 2.7).

While the simulation was successful in aligning with experimental data and providing insight into alterations of nuclear membrane tension over adipogenesis, it is not without its limitations. Firstly, the number of actin elements connecting the cytoplasm to the nuclear membrane had to be determined empirically. Although simulation of biological systems can lead to complex models, it would require often impractical computational times. Numerous techniques such as coarse-graining and scaling have been developed to address this challenge and reduce computational time. In coarse-graining, the goal is to simplify the model to include only what is necessary to capture the phenomena of interest. In this work, it was found that at least 16 actin filaments and 250 bodies representing the material inside the nucleus were needed to match the experimental data.

While other cellular and nuclear behaviors may be gleaned by increasing these parameters, validation by the experimental results was the criteria to optimize the computational cost. Secondly, this simulation was modeled in 2-dimensions to be consistent with the experimental image analysis also conducted in 2D monolayer culture. Future experiments and modeling would benefit from 3D systems which more closely relate to *in vivo* conditions. Providing the internuclear structures (i.e. beads) with a Z-direction to reorganize into will potentially provide new insights into overall nuclear shape over adipogenesis. This however does come with the caveat of increasing modeling complexity and reducing computational speed. Future work regarding 3D systems will require a balance between revealing biological observations and increasing model complexity.

The proteins responsible for joining the actin cytoskeleton to the nucleus are the SUN and KASH domains of the Linkers of Nucleoskeleton and Cytoskeleton (LINC) complexes. SUN proteins are localized to the inter nuclear membrane which connect to the nuclear lamina and chromosomes. KASH proteins span the outer nuclear membrane and connect SUN proteins to cytoskeletal elements such as actin[10]. Conceivably, the next iteration of the simulation can incorporate the bi-layered characteristic of the nuclear membrane along with the inclusion of LINC complexes each in their appropriate layer. The current model demonstrated results of nuclear reorganization consistent with experimental data. Perhaps with inclusion of LINC complexes as separate rigid bodies and providing a range of connections with actin will further drill down the appropriate number of actin binding domains. Future improvements might also include computational

techniques to accommodate the position-dependent tension at the nuclear envelope. Although the current model does consider the fluctuating nuclear tension, it was averaged over the nucleus. This strategy minimized the computational time but still was able to capture the restructuring and reorganizing the nuclear biomechanics.

The physical differentiation factors investigated in chapter 2 (cell confinement, nuclear shape, and cytoskeletal polymerization) resulted in a lower degree of adipogenic differentiation, as determined by less lipid production. Adipose tissue in the body has a complicated purpose of energy storage, endocrine signaling, and a mediator of the inflammatory response[11,12]. However, what adipose is most commonly known for is its excess in obesity. Obesity has situated itself as one of the most important public health concerns with downstream effects including diabetes, heart disease, and neoplasia[13]. Therefore, accruing less lipid by means of physical stimuli is worth investigating. While the above examples demonstrate less lipid production, they have been heavily investigated and are not practical *in vivo*. Consequently, researchers have begun to examine novel, non-invasive physical factors to influence lipid production and stem cell differentiation. One such physical cue is photobiomodulation (PBM), or the influence of light irradiation on biological tissues.

Photobiomodulation has already been utilized as a method for fat reduction and body contouring, however few have investigated the cellular mechanisms by which fat reduction may be acheived[14]. Chapter 3 examines the effect of PBM on stem cells while undergoing adipogenesis, via irradiation with a near infrared laser at 1064 nm. It was

demonstrated that PBM increased ATP production and modulated levels of reactive oxygen species (ROS) and ROS eliminating enzymes. Levels of ATP have been shown to influence a cell's differentiation capability[15]. However, the most prominent factor of PBM's effect on adipogenesis appears to be the change in ROS properties. PBM works by enhancing mitochondrial respiration and as a result produces a rise in mitochondrial superoxides[16]. Due to the destructive potential of high levels of ROS, the cell employs several methods of elimination such as the antioxidant enzymes superoxide dismutase (SOD) and catalase (CAT). SOD and CAT work together to reduce mitochondrial superoxide to oxygen and water[17]. In terms of adipogenesis, levels of ROS are an important factor in differentiation. ROS levels increase during normal adipogenesis, and inhibition of ROS formation subsequently inhibits differentiation[18]. In PBM-treated cells, superoxide levels are transiently higher than control due to the increased mitochondrial respiration. However, as time continues, ROS levels in the irradiated group remain stable in comparison to normally differentiated cells without laser exposure (see Fig. 3.8). It can be inferred that over the course of daily exposure, the cells are likely to adapt to high levels of ROS by increasing the levels of antioxidant enzymes. This was further supported by SOD mRNA levels significantly increasing in laser-treated stem cells. Furthermore, treatment of stem cells with the catalase-blocking agent 3-Amino-1,2,4-triazole (3-AT) negated the effect of PBM and restored lipid levels to that of non-irradiated differentiation (see Fig. 3.9). Altogether, a potential mechanism for the fat-reducing characteristics of the novel physical factor PBM on differentiating adipocytes has been described. As lipid levels and pre-adipocyte differentiation have implications in the progression of obesity,

PBM may prove to be a viable method of fat reduction *in vivo*. Demonstration of such fat reduction by PBM using animal models would further establish the proposed mechanism.

While preemptive treatment of obesity with photobiomodulation may prove effective in mitigating lipid production, it does little for the individuals already effected by the disease's complications. Obesity is characterized by excess lipids, which carries with it a dysfunction in adipocyte physiology in the form of cell number increase (hyperplasia) and cell size increase (hypertrophy)[19]. Chief among these as a mediator in the progression to chronic obesity outcomes such as insulin resistance and diabetes, is cellular hypertrophy[20]. The consequences of adipocyte hypertrophy – high lipid volume, oxidative stress, and inflammation – have all been directly regulated by the actions of photobiomodulation. As PBM has been shown to be an effective method for reducing fat content *in vivo*, as well as the promising *in vitro* results from chapter 3, a hypertrophic cell model was developed using stem cells, and the ability of PBM to restore the morphology and function of dysregulated hypertrophic adipocytes was determined.

In chapter 4, hypertrophic adipocytes were generated from stem cells through adipogenic induction followed by addition of palmitic acid. Lipid content significantly increased, and cells swelled with large lipid droplets (see Fig. 4.1). Functionally, hypertrophic adipocytes demonstrated a significantly reduced expression of the primary insulin-sensitive glucose transporter GLUT4 (see Fig. 4.4). GLUT4 has previously shown to be dysfunctional in hypertrophic and obese environments, with a diminished expression and altered trafficking to the plasma membrane from insulin stimulation[21,22]. This in turn causes a

decrease in glucose uptake to the cells, as quantified by levels of fluorescent glucose marker 2-(*N*-(7-Nitrobenz-2-oxa-1,3-diazol-4-yl)Amino)2-Deoxyglucose (2-NBDG) (see Fig. 4.3). In order for PBM to prove effective in the treatment of hypertrophic adipocytes, it must succeed in restoring the form as well as function of the cells. Hypertrophic cells treated with PBM showed significantly less lipid production than those without. At day 15 of differentiation, there was no significant difference between laser-treated hypertrophic cells and normal adipogenesis. Functionally, GLUT4 expression and 2-NBDG fluorescence increased compared to hypertrophic controls, however both remained lower than cells not induced to hypertrophy. As the main mechanism of action for PBM is through enhanced mitochondrial activity, lipid and protein production are subsequently altered. In obesity, mitochondrial activity is downregulated as lipids are accumulated[23]. In addition, the processing of proteins is inhibited due to chronic endoplasmic reticulum stress from elevated oxidative stress and nutritional excess, leading to a decrease in GLUT4 production[22]. In chapter 3, PBM has been shown to effectively enhance ATP, and other groups described an upregulation in mitochondrial activity[24,25]. The ability of PBM to modulate the ROS environment and reduce oxidative stress was demonstrated as well. Here, the results indicate an upregulation in GLUT4 protein expression, leading to an increased level of glucose uptake. Interestingly, the effects of PBM described in this work occur after a time delay. Most studies with PBM utilize bursts of exposure over multiple days to weeks. It is possible the cellular mechanisms PBM is coupled to require consistent activation. Potentially, the upregulation in GLUT4 only occurs following an upregulation of antioxidant enzymes, which as described in chapter 3, does not occur immediately.

In conclusion, this work set out to investigate modulating stem cell adipogenesis through novel physical methods and to examine the influence of these methods on the nuclear mechanics and lipid physiology. In Aim 1, the alterations in the nuclear morphology of stem cells during adipogenesis were quantitatively established. It was determined that nuclear organization is significantly modified throughout differentiation, and suggested to be driven by alterations in nuclear envelope protein, lamin A/C. Aim 2 determined the influence of the novel physical factor photobiomodulation using 1064 nm laser light on adipogenic differentiation. Here it was shown that PBM significantly altered adipogenesis by reducing lipid content through a mechanism of enhanced mitochondrial processing and modulation of ROS enzymes. Finally, Aim 3 further investigated PBM on the major disruptor of adipocyte function in obesity: cellular hypertrophy. It was found that PBM had some moderate influence on restoration of form and function of hypertrophic adipocytes by reducing lipid content and upregulating GLUT4 expression and glucose uptake.

In the future, studies involving PBM should more directly focus on actin arrangement and nuclear shape. Chapter 3 begins to describe the influence of PBM on nuclear shape in that the reduction of area does not occur to the degree of non-irradiated cells. It was described in chapter 2 that this morphological change precedes adipocyte maturation. Therefore, inhibition of this change – and therefore adipogenesis – by PBM deserves further investigation. Secondly, quantification of additional proteins involved in obesity and/or type 2 diabetes would be beneficial to study. Insulin receptors and the proteins activated in response to insulin, which assist in GLUT4 trafficking to the plasma membrane, are of interest in determining the correct mechanism of action of PBM on

hypertrophic adipocytes. Finally, future work involving *in vivo* animal models of obesity would be a great advantage in determining the systemic application of PBM.

References

1. Zhao, W., Xiaowei L., Xiaoyan L., Ning Z., and Xuejun W. 2014. "Effects of substrate stiffness on adipogenic and osteogenic differentiation of human mesenchymal stem cells." *Materials science & engineering. C, Materials for biological applications* 40: 316–23. doi:10.1016/j.msec.2014.03.048.

2. Huang Y., Zheng L., Gong X., et al. 2012. “Effect of Cyclic Strain on Cardiomyogenic Differentiation of Rat Bone Marrow Derived Mesenchymal Stem Cells.” *Plos One*. 7: e34960.

3. Gao, L., McBeath, R. & Chen, C. S. “Stem cell shape regulates a chondrogenic versus myogenic fate through rac1 and n-cadherin.” *Stem Cells.* **28**, 564–572, DOI: 10.1002/stem.308 (2010).

4. Mao A.S., Shin J-W., Mooney D.J. 2016. “Effects of substrate stiffness and cell-cell contact on mesenchymal stem cell differentiation.” *Biomaterials*. 98:184–91.

5. Heo S-J., Driscoll T.P., Thorpe S.D., et al. 2016. “Differentiation alters stem cell nuclear architecture, mechanics, and mechano-sensitivity.” *Elife*. 5: e18207.

6. Driscoll T.P., Cosgrove B.D., Heo S-J., Shurden Z.E., Mauck R.L. 2015. “Cytoskeletal to Nuclear Strain Transfer Regulates YAP Signaling in Mesenchymal Stem Cells.” *Biophysical Journal*. 108: 2783–93.

7. Birket, M. J. et al. 2011. “A reduction in ATP demand and mitochondrial activity with neural differentiation of human embryonic stem cells.” *Journal of cell science* 124, 348–358.

8. Caruso-Davis, M. K. et al. 2011. “Efficacy of low-level laser therapy for body contouring and spot fat reduction.” *Obesity surgery* 21, 722–729.

9. Constantinescu, D., Gray, H. L., Sammak, P. J., Schatten, G. P. & Csoka, A. B. 2006. “Lamin A/C Expression Is a Marker of Mouse and Human Embryonic Stem Cell Differentiation.” *STEM CELLS* 24, 177–185.

10. Sosa, B. A., Kutay, U., & Schwartz, T. U. 2013. “Structural insights into LINC complexes.” *Current opinion in structural biology*, 23(2), 285-291.

11. Fantuzzi, G. 2005. “Adipose tissue, adipokines, and inflammation.” *Journal of Allergy and Clinical Immunology* 115, 911–919.

12. Hamblin, M. R. 2018. “Mechanisms and Mitochondrial Redox Signaling in Photobiomodulation.” *Photochemistry and Photobiology* 94, 199–212.

13. Ighodaro, O. M. & Akinloye, O. A. 2018. “First line defence antioxidants-superoxide dismutase (SOD), catalase (CAT) and glutathione peroxidase (GPX): Their fundamental role in the entire antioxidant defence grid.” *Alexandria Journal of Medicine* 54, 287–293.

14. Jo, J. et al. 2009. “Hypertrophy and/or Hyperplasia: Dynamics of Adipose Tissue Growth.” *PLoS Computational Biology* 5, e1000324.

15. Kershaw, E. E. & Flier, J. S. 2004. “Adipose Tissue as an Endocrine Organ.” *The Journal of Clinical Endocrinology & Metabolism* 89, 2548–2556.

16. Kim, J. et al. 2015. “Lipid-Overloaded Enlarged Adipocytes Provoke Insulin Resistance Independent of Inflammation.” *Molecular and Cellular Biology* 35, 1686–1699.

17. Kopelman, P. G. 2000. “Obesity as a medical problem.” *Nature* 404, 635–643.

18. Kouidhi, S. et al. 2013. “Human subcutaneous adipose tissue Glut 4 mRNA expression in obesity and type 2 diabetes.” *Acta Diabetologica* 50, 227–232.

19. Laforest, S., Labrecque, J., Michaud, A., Cianflone, K. & Tchernof, A. 2015. “Adipocyte size as a determinant of metabolic disease and adipose tissue dysfunction.” *Critical Reviews in Clinical Laboratory Sciences* 52, 301–313.

20. Lin, C.-H., Li, N.-T., Cheng, H.-S. & Yen, M.-L. 2017. Oxidative stress induces imbalance of adipogenic/osteoblastic lineage commitment in mesenchymal stem cells through decreasing SIRT1 functions. *Journal of cellular and molecular medicine* 22, 786–796.

21. Moreno-Navarrete, J. & Fernández-Real, J., M.E. Symonds (Ed.) 2012. “Adipocyte Differentiation” In: *Adipose Tissue Biology*. 17–38 (2012).

22. Ritov, V. B. et al. 2004. “Deficiency of Subsarcolemmal Mitochondria in Obesity and Type 2 Diabetes.” *Diabetes* 54, 8–14.

23. Verstraeten, V. L. R. M. et al. 2011. “Reorganization of the nuclear lamina and cytoskeleton in adipogenesis.” *Histochemistry and Cell Biology* 135, 251–261.

24. Amaroli A., S. Ravera, S. Parker, I. Panfoli, A. Benedicenti and S. Benedicenti. 2016. “An 808-nm Diode Laser with a Flat-Top Handpiece Positively Photobiomodulates Mitochondria Activities.” *Photomedicine and Laser Surgery* 34: 564–571.

25. Silveira P. C. L., G. K. Ferreira, R. P. Zaccaron, V., et al. 2019. “Effects of photobiomodulation on mitochondria of brain, muscle, and C6 astroglioma cells.” *Medical Engineering & Physics* 71: 108–113, 2019.